Dynamics of resonant low-frequency waves over a schematized fringing coral reef

MSc Thesis written by

Camila Gaido

TU Delft

Cover Image: Coral reef from French Polynesia. Source: https://coral.org/coral-reefs-101/coral-reef-ecology/types-of-coral-reef-formations/

Dynamics of resonant low-frequency waves over a schematized fringing coral reef

by

C. Gaido

to obtain the degree of Master of Science
at the Delft University of Technology,
to be defended publicly on Tuesday December 10, 2019 at 2:00 PM.

Student number:	4744586	
Project duration:	February, 2019 – November, 2019	
Thesis committee:	Dr. Marion Tissier ,	TU Delft
	Prof.dr.ir Ad Reniers	TU Delft
	Dr.ir Jeremy Bricker,	TU Delft
	Ir. Stuart Pearson,	TU Delft/Deltares

TU Delft

Preface

I was able to finish this thesis due to the help of several people along the way.

To my friends and more. Irene, Tina, and Gil, thanks for feeding me, supporting me, and giving me love during the thesis. Thanks Gil for all the thesis related and programming free consultancy. Susana, thank you for all our third-floor walks, all our "Narnia" talks, and for always believing in me. Jorgito and Luis, our funny lunches, especially during the lonely summer, made my thesis-life much better. Tessa and Laurie, thanks for being my favorites Dutch girls, and always hugging me. Also, I want to thanks Akshay, Bas, Jochem, and Jo for making the thesis room environment so chill and for all your moral support and technical help.

To my family. Ma and Pa, thanks for your constant love and support, even when you didn't agree with my decisions. Thanks to my brothers, you are cool people. Thank you Flo for making me laugh and Vale for being interested in what I was studying.

To my Committee. Thanks Marion for all the support, inspiration, brainstorming, patience, time, more time, extra time, nice talks, and good moments spent during these (this) months. Thanks Stuart for your contagious enthusiasm about the topic, your patience with my English, and for your constructive opinions. Thanks Ad for always having that new idea that changed the course of my analysis, and made me wonder about so many more things I could learn. Thanks Jeremy, for showing another perspective to the topic and for helping me when I needed it.

It was a pleasure to work and spend time with all of you.

C. Gaido
Delft, December 2019

Summary

Low-lying islands are highly vulnerable to wave-induced flooding, with low-frequency waves (frequency <0.04 Hz) being one of the main drivers. The impact of these inundations can increase due to wave resonance over coral reefs, which has been observed in the range of low-frequency waves. This study aims to understand the reef resonance phenomenon along with processes that could limit its resonant amplification over wave height and wave run-up.

A numerical experiment was carried out based on a 1D SWASH numerical model. A cross-shore profile of a schematized fringing coral reef was built, and resonance was forced over this bathymetry for the first two resonant modes and two water depths. The offshore forcing was designed as a simplified wave climate, with small amplitude regular low-frequency waves.

Resonance was found to occur in a bandwidth of periods for each resonant mode, generating two resonant amplification peaks (one for each resonant mode). The periods leading to the maximum resonant amplification inside each resonant bandwidth are the modeled resonant periods, which were found to be longer than the theoretical resonant periods (based on reef flat width and water depth). The resonant amplification over wave height and run-up were found to be more significant for the fundamental mode than for the first mode, decreasing for both resonant modes when increasing the water depth. Moreover, for the wave conditions modeled in this experiment, the relative resonant amplification was found to be stronger for smaller wave heights than larger wave heights.

Reef wave resonance presented a build-up behavior, needing a minimum number of waves to reach a maximum resonant amplification, which varied depending on the wave period, wave height, and water depth. Resonant amplification was found to increase for a larger amount of trapped wave energy over the reef and lower friction dissipation. Frictional dissipation was found to be the most effective process to counteract wave resonant amplification. Thus, increasing coral reef bottom friction is essential for enhancing low-lying island coastal safety.

Contents

List of Figures

List of Tables

List of symbols

Symbol	Units	Description
A_H	-	Relative amplification of the wave height at the beach toe with respect to incident offshore wave height
A_{N°	-	Ratio between individual wave height and maximum wave height
A_R	-	Relative amplification of the maximum run-up with respect to incident offshore wave height
A_{Shoal}	-	Relative amplification of the wave height with respect to the expected wave shoaling
As	-	Wave asymmetry
c	m/s	Wave celerity
d_{off}	m	Offshore water depth
d_r	m	Reef flat water depth
F	J/m/s	Energy flux
g	m/s^2	Gravity (9.81 m/s^2)
$H_{beachtoe}$	m	Wave height at the beach toe
H_{off}	m	Incident offshore wave height
H_{m0}	m	Significant wave height (spectrum analysis)
H_s	m	Significant wave height (time-series analysis)
H_{s-in}	m	Incident significant wave height (time-series analysis)
$H_{s-shoal}$	m	Expected significant wave height due to wave shoaling
K_{sh}	-	Shoaling coefficient
L	s	Wavelength
L_1^*	s	First resonant theoretical wavelength
L_1	s	First resonant modeled wavelength
n	$s/m^{1/3}$	Manning friction coefficient
R_{max}	m	Maximum wave run-up
$R_{2\%}$	m	Wave run-up value exceeded by 2% of the incoming waves
$R_{10\%}$	m	Wave run-up value exceeded by 10% of the incoming waves
Sk	-	Wave skewness
T_1^*	s	First resonant theoretical period
T	s	Wave period
T_1^*	s	First resonant theoretical period
T_0	s	Fundamental resonant modeled period
T_1	s	First resonant modeled period
T_p	s	Peak period
U	m/s	Depth average velocity
W	m	Reef width
x	m	Horizontal position on the modeled profile
ΔAs	-	Difference in asymmetry between outgoing and incoming waves
$\Delta\mathscr{F}$	J/m/s	Difference between incoming and outgoing energy flux
ΔR	m	Wave run-up resolution
Δx	t	Time step
Δx	m	Grid resolution
η	m	Water surface elevation
σ	-	Courant number

1 Introduction

1.1. Motivation

Low-lying islands with elevations of less than a few meters above mean sea level are highly vulnerable to flooding(Woodroffe 2008). This risk in safety is expected to increase due to climate change effect on sea-level rise and wave climate (Storlazzi et al. 2018, Cheriton et al. 2016). Low-lying islands, compared to traditional beaches, have a fringing coral reef preceding their beaches. Fringing coral reef can act as a coastal flooding defense, because they can dissipate a large amount of wave energy, reducing the wave heights reaching the coastline. However, under certain hydrodynamic conditions fringing coral reef can also enhance flooding due to their impact on reef wave dynamics. An example for such enhance flooding has been observed under storm conditions due to typhoons(Roeber and Bricker (2015), Péquignet et al. (2009), Shimozono et al. (2015)).

The coral roughness and the fringing reefs particular bathymetry determine reef hydrodynamics. Fringing coral reefs are characterized by a sharp frontal slope, a shallow water reef flat, and considerable bottom roughness. These features strongly induce wave energy dissipation, mainly due to wave breaking and bottom friction. The limited water depth over the reef platform leads to dissipation of high-frequency waves (frequency > 0.04 Hz) and dominance of low-frequency waves (frequency < 0.04 Hz) (Cheriton et al. 2016). Low-frequency waves can be seen as flooding drivers in low-lying islands due to their relevant contribution to over-wash and run-up (Nwogu and Demirbilek (2010),Cheriton et al. (2016)).

Inundations on low-lying islands can increase due to long waves resonant amplification on the reef flat (Gawehn et al. 2016). The resonant phenomenon has been observed during flooding such as the ones caused by the tropical storm Man-Yi in Guam (Péquignet et al. 2009) and the typhoon Haiyan at the Samar Island in the Philippines (Shimozono et al. 2015). The main characteristics influencing reef resonance and its corresponding amplification are offshore wave conditions (wave height and wave period), offshore water level, reef flat water depth, reef geometry (flat width, fore reef, and beach slope), and coral roughness (bottom friction dissipation). Theoretically, resonance can occur when the incoming offshore wave frequency matches one of the reef natural frequencies. This matching of frequencies will form standing waves with a node at the reef crest (Buckley et al. 2018). The eigenmodes (also known as natural frequencies), are mainly determined by the reef flat width and water depth. Narrower reefs and larger water depths increase resonant frequencies.

The impact of resonating waves on flooding depends on the resonant amplification, which can occur under the condition of an energetic resonant forcing (Péquignet et al. 2009). Thus, a forcing matching a natural frequency, but without enough energy, is not expected to generate a strong resonant amplification. The study of Pomeroy et al. (2012) showed that the magnitude of amplification is also friction-dependent, and it can be significantly reduced due to frictional dissipation. According to Pearson et al. (2017), resonance is more probable under conditions with considerable low-frequency wave energy or higher water level. Both conditions can be found during storms, however, it is also important to understand if resonance can happen under swell conditions. Pomeroy et al. (2012) found that resonance under mild conditions was only possible with minimal bottom friction. According to Péquignet et al. (2009), the resonant frequencies can increase with a rise in

the water level, allowing a larger wave frequency range to resonate. Thus, under the scenario of sea-level rise and coral reef degradation, resonance over reefs may become relevant under mild wave climate conditions.

Resonant waves can also develop non-linear wave shapes (Gawehn et al. 2016), which are expected to be more dangerous than sinusoidal waves (Didenkulova et al. 2007). However, the increase of coastal flooding due to non-linear wave shapes has not been studied over coral reefs. Non-linearity could generate a larger run-up amplification, or on the contrary reduce resonant amplification due to wave breaking dissipation, and/or non-linear transference of energy to other frequencies.

The resonance mechanism of low-frequency waves over coral reefs has not been thoroughly investigated. A better understanding of the environmental conditions triggering/counteracting wave resonant amplification and their impact on reef hydrodynamics is needed. Understanding the conditions and the hydrodynamics transformations over the reef flat is essential to comprehend the impact of resonance on coastal flooding hazards.

1.2. Research objectives

1.2.1. Problem definition

Resonance of low-frequency waves over fringing coral reefs can generate massive flooding on low-lying islands. The probability of this phenomenon is expected to increase due to sea-level rise. Additionally, resonant waves can present non-linear wave shapes that can increase/reduce the resonant amplification and, consequently, the flooding impact. Thus, understanding processes that can enhance or counteract the resonant amplification is essential for assessing coastal flooding hazard on reef-lined coasts.

1.2.2. Research question

What are the main processes limiting the resonant amplification of long waves and the associated run-up over a schematized fringing coral reef?

Hypotheses: Resonant amplification is expected to be more effective when energetic long waves reach the reef flat. However, nonlinear wave shapes and energy dissipation are more likely to develop for the largest long waves, which could limit the amplification factor. Thus, perhaps the highest wave will not result in the maximum wave height and run-up amplification.

Research sub-questions

- For a certain water level, what are the characteristics (period and wave height) of a regular long wave leading to a maximum wave height/run-up amplification?
- How do long waves transform over the reef flat under resonant conditions? Which non-linear wave shapes are present under resonance? Does this have a significant impact on wave height/run-up amplification?
- How long does it take for resonant behavior to be built up in order to generate a maximum wave height/run-up amplification over the reef?
- What is the effect of friction on wave height/run-up resonant amplification over the reef?

1.3. Thesis outline

Chapter 1 outlines the motivation, problem definition, and research questions of this thesis. Chapter 2 gives the necessary background to have a general understatement of reef hydrodynamics and wave resonance, and Chapter 3 reviews the methodology to force resonance over fringing reefs and shows the validation of the numerical wave model (SWASH) used to do so. Chapter 4 presents the results of this resonance study, and Chapter 5 discusses the limitations and findings of this study. Chapter 6 presents the main conclusions and gives some recommendations for future research. The appendices include complementary information about the modeled reef profile (A), the SWASH code (B) and more detailed results (C).

2

Background

Coral reefs are marine ecosystems formed by layers of calcium carbonate skeletons. These structures can be found mainly along with land formations characterized by shallow and warm water. Coral reefs can be classified into three types: fringing reefs (grow near coastlines of islands or continents), barrier reefs (located offshore and parallel to the coastline), and coral atolls (grow rings above a sinking volcano in the ocean). This thesis focuses on fringing reefs connected to low lying islands.

Fringing coral reefs can be differentiated from sandy beaches by their rougher bed and their particular bathymetry (Van Dongeren et al. 2013). A general reef profile consists of a sharp frontal slope that, which leads to a reef crest, followed by a reef flat (figure 2.1). According to Quataert et al. (2015), an average fore reef slope is steeper than 1:20, and the width of the reef platform ranges between 50 and 1000 m. Moreover, the reef flat experiences shallow water conditions, and it can even be exposed during low tide. The reef platform in the shore direction ends on a beach slope connecting with a low lying island. A low elevation characterizes these islands, commonly of only a few meters above mean sea level. Due to this elevation condition, low-lying islands are highly vulnerable to flooding (Woodroffe 2008) and to the impacts of climate change on sea-level rise and wave climate (Storlazzi et al. 2018).

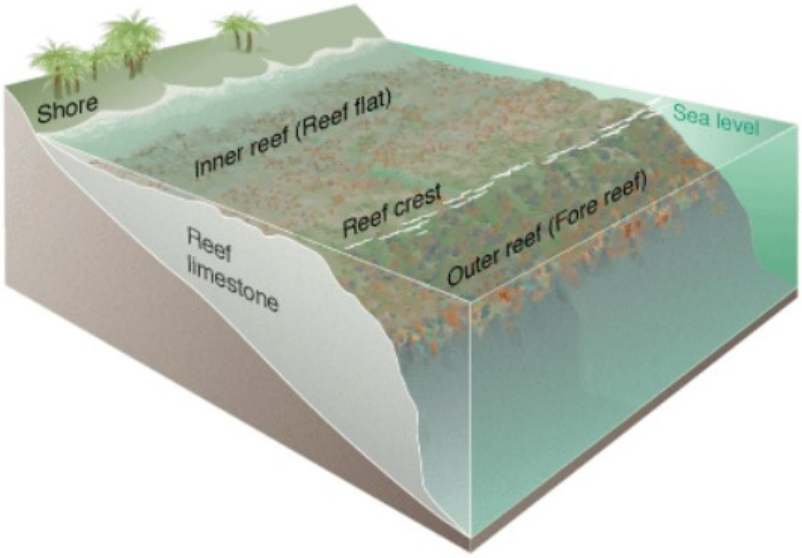

Figure 2.1: Fringing reef coral bathymetry diagram(USC).

Fringing coral reef systems provide coastal protection against erosion and flooding of low-lying islands coastlines during moderate storms, because in average they can dissipate 97% of the wave energy Ferrario

et al. (2014). However, fringing coral reefs can also lead to an enhancement of flooding during storm conditions, such as a typhoon, due to their impact on wave dynamics (Roeber and Bricker 2015, Péquignet et al. 2009, Shimozono et al. 2015). This flooding is mainly caused by wave-driven water level variability, which has a final impact on the run-up at the coastline. Wave run-up can be defined as the last expression of wave transformation while propagating shoreward. In other words, wave run-up is the instantaneous variation of the shoreline compared to the still water level(Buckley et al. 2018). Even though the definition of run-up seems simple, its value is not easy to predict. This prediction complexity can increase in fringed coral reefs environments, where model conditions and assumptions for sandy coasts may not apply due to the steep slopes and high roughness (Buckley et al. 2018). Thus, a better understanding of coral reef hydrodynamics is essential to asses coastal flooding impact on reef-lined coasts.

2.1. Coral reef hydrodynamics

2.1.1. General

Coral reef features such as the abrupt fore reef slope, the shallow water conditions on the reef flat, and the large coral roughness, lead to strong wave dissipation. This dissipation mainly affects high-frequency waves, and leads to a dominance of low-frequency wave over the reef. High-frequency wave energy reduces towards the coast due to wave breaking, bottom friction dissipation, and non-linear energy transfer to lower frequencies. On the contrary, low-frequency wave energy has been found to be minimum at the reef crest, increasing as waves propagate landward(Nwogu and Demirbilek 2010). Thus, low-frequency waves are important contributors on the resultant wave run-up and, consequently, one of the main flooding drivers on low-lying islands.

At the reef crest, according to Shimozono et al. (2015), the incoming offshore wave energy is considerably dissipated around the peak frequency due to wave breaking and non-linearly transferred to lower frequencies. The amount of energy dissipated/transferred is strongly dependent on the reef flat water level, which is modulated by the tide (Hardy and Young 1996). During low tide, high-frequency wave energy on the reef flat is limited by bottom friction, and due to a high rate of wave breaking at the fore reef slope. Under larger water levels, waves start breaking at the reef crest, allowing waves to propagate further towards the coast than with smaller water depths (Masselink et al. 2019). Thus, the wave energy reaching the shoreline is larger for higher water depths.

Wave breaking leads to an increase in the mean water level, also known as wave setup. This rising of the mean water level can increase wave run-up by allowing larger waves to reach the shoreline (Buckley et al. 2018). Wave setup reduces with increasing water depths (Cheriton et al. 2016), but its magnitude difference between low and high tide is not big enough to reach the same water level under both tide conditions. Thus, even when accounting for wave setup, shoreline wave energy is larger during high tide (Péquignet et al. 2011).

2.1.2. Low-frequency waves

Coral reef long waves can be generated mainly by two mechanisms: (1) Bound long waves and (2) Breakpoint-forced long waves. Mechanism (1) consists of a release of the long wave bound to the offshore wave group (Figure 2.2) due to high-frequency waves breaking. Mechanism (2) generates low-frequency waves through wave breakpoint oscillations due to incident waves amplitude variations (Symonds et al. 1982). The dominant mechanism on a reef depends on the fore reef slope (Péquignet et al. 2011). According to Masselink et al. (2019) the mechanism (1) is dominant for slopes flatter than 1/20, whereas breakpoint-forced long waves mechanism becomes more important for slopes steeper than 1/10. Furthermore, the same study concludes that mechanism (2) is the most effective. Additionally, this mechanism generates more energetic low-frequency waves on reefs with a fore reef slope steeper than 1/6.

After generation, low-frequency waves can go through several transformations over the reef flat. These waves can be dissipated due to bottom friction, wave breaking, and non-linear energy transfer to other frequencies. Additionally, low-frequency waves can experience changes in their wave shape due to non-linear wave steepening, and they can even form undular and or turbulent bores. According to Cheriton et al. (2016), wave non-linearity increases with decreasing reef flat water depth. Two reflectors limit the reef flat, the reef

crest, and the beach (Figure 2.2). Incoming long waves can be reflected in both locations, and they can form a standing wave pattern over the reef (Nwogu and Demirbilek 2010). Outgoing long waves can be partially reflected at the reef crest, changing their direction towards the coast. This double reflection, of incoming waves at the beach and outgoing waves at the reef crest, can lead to wave energy being trapped over the reef.

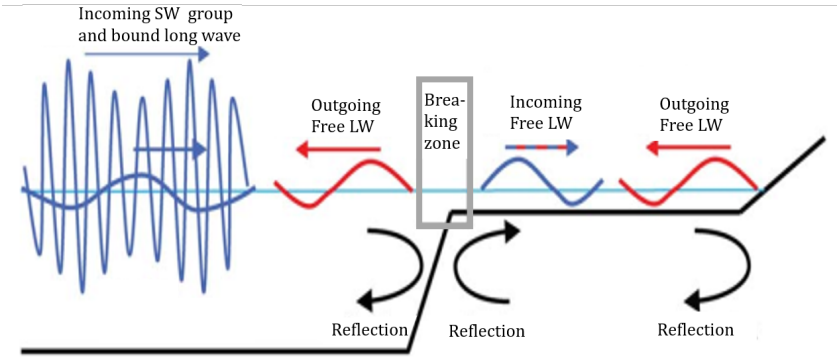

Figure 2.2: Scheme of wave generation processes and reflection in a fringing coral reef. Modified from (Buckley et al. 2018).

Low-frequency waves can be classified into two groups depending on their frequency: infra-gravity waves, with a frequency in the range of 0.004-0.04 Hz, and very low-frequency waves with a frequency varying between 0.001-0.004 Hz. The amplitude of both low-frequency waves is rather small under mild wave conditions, increasing with higher offshore waves and larger water levels (Péquignet et al. 2009).

Gawehn et al. (2016) conducted a classification of very low-frequency wave motions over the fringing reef on Roi-Namur Island in the Republic of the Marshall Islands (Figure 2.3). Water levels and wave data analysis, measured during five months at a cross-reef transect, lead to the conclusion that very low-frequency waves can develop four different wave classes: resonant, (non-resonant) standing, progressive-growing, and progressive-dissipative waves. From these four behaviors, resonant waves are the ones that can have a stronger impact on coastal safety. Resonant long waves over the reef platform can lead to an increase of wave run-up and coastal flooding (Nwogu and Demirbilek (2010), Péquignet et al. (2009)). According to Gawehn et al. (2016) study, resonant situations are not unlikely to occur, being a 3.6% of the five months data, and can happen under both mild and storm conditions.

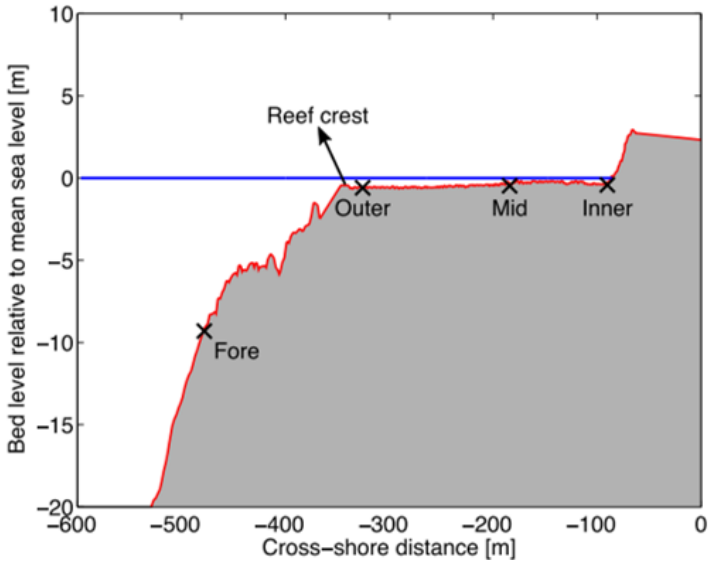

Figure 2.3: Bathymetric profile of the cross reef transect (Gawehn et al. 2016).

2.2. Resonance

2.2.1. Resonance in basins

Wave resonance in basins develops when the forcing frequency matches one of the basin natural frequencies. Resonant waves can present different standing wave patterns, differentiating between each other in the number of nodes developed over the basin (Figure 2.4). For example, for an open-ended basin, the fundamental mode ($n = 0$) has a one node standing wave pattern, while the first resonant mode presents two nodes standing wave pattern ($n = 1$).

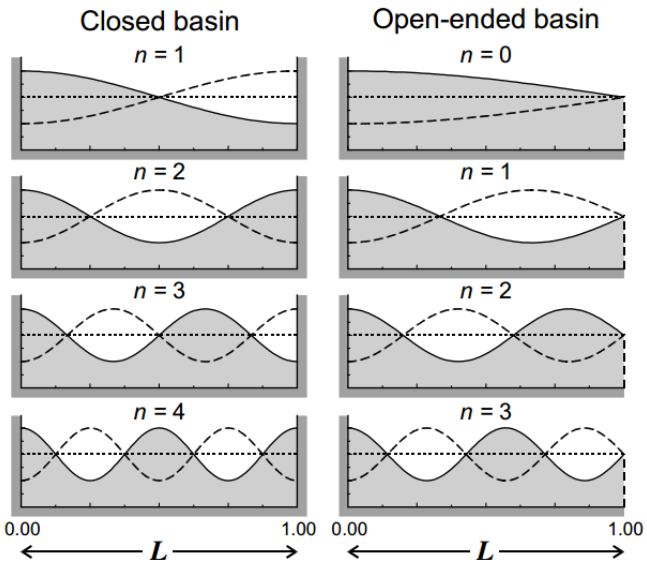

Figure 2.4: First four eigen modes, or natural frequencies, in rectangular closed and open-ended basins. Source: (Rabinovich 2009).

The natural resonant frequencies, are determined by the basin geometry and the water depth. For an open basin of length W with a uniform water depth d, these natural resonant periods can be estimated with the Merian formula as:

$$T_n = \frac{4W}{(2n+1)\sqrt{gd}}, \quad n = 0, 1, 2, 3, \ldots \tag{2.1}$$

An example of an open-ended basin is a harbor, which has natural periods in the order of low-frequency waves. Resonance in harbors lead to strong water level amplifications that can damage structures and vessels. For the case of a harbor, the long waves resonant amplification factor can be estimated as (Rabinovich 2009):

$$H(f)^2 = \frac{1}{\left(1 - f/f_0\right)^2 + Q^{-2}\left(1 - f/f_0\right)^2} \tag{2.2}$$

where,

$H(f)^2$ = resonant amplification factor for wave frequency f

f = frequency of the incoming long wave

f_0 = resonant frequency of the harbor

$Q^{-1} = (dE/dt)/2\pi fE$

Q is a quality factor that plays a double role by indicating the time decay rate of the energy (E) in the system, and by measuring the increase of wave heights due to resonance. A higher Q value indicates a slower energy decay and larger wave height amplification.

2.2.2. Beach resonance

Edge waves are low-frequency waves trapped in the nearshore that can experience resonance over a beach, which due to the frequency range and trapped wave condition, could have similarities to the behavior of resonant low-frequency waves over reefs. Guza and Davis (1974) theoretically demonstrated that normally incident waves experiencing a total reflection can excite edge waves under certain frequencies, generating this excitation a resonant wave amplification. According to (Guza and Bowen 1976), edge waves can resonate over a range of frequencies for a specific wavenumber. This resonant bandwidth is centered and maximum at the natural frequency, which also shows a maximum initial growth. Moreover, the wave edge excitation is larger for the fundamental resonant mode, which also shows the most rapid growth (Guza and Bowen 1977). Theoretically, the edge wave amplitude is three times larger than the incoming offshore wave amplitude(Guza and Bowen 1976).

The resonant edge wave amplitude has an initial exponential growth rate behavior. This rate reduces as the wave amplitude grows, reaching zero at the final equilibrium state. This limitation of the maximum amplification, or finite amplitude, is mainly due to three processes (Guza and Bowen 1976). The first process is frictional dissipation, which for a constant forcing, limits the resonant wave amplitude growth. The second process is further non-linear interactions, which refers to a loss of edge wave energy due to energy radiation to the far field (at double edge wave frequency) or non-linear energy transfer to other edge wave modes. Finally, the third cause of finite resonant wave amplitude is the demodulation from the resonant natural period, which is amplitude-dependent at a fixed wave number. The detuning from the resonant period occurs because the natural frequency increases with increasing wave height, as larger trapped edge waves travel faster than the ones with smaller wave heights. Thus, the forcing can cease being inside the resonant bandwidth as the wave height increases, because the edge wave dispersion relation is amplitude dependent.

The Guza and Bowen (1976) study, which is valid for moderately non-linear waves, showed that the last two processes are the most, and equally important, for limiting the wave amplitude growth. For a case without wave energy radiation, the natural frequency and edge wave amplitude will rise until the lower end of the resonant band. On the other hand, if the change of natural frequency is not considered, radiation limits the wave amplitude if it can balances exactly the incident wave forcing. If the radiation is stronger than the forcing the wave amplitude will slowly decay, which decreases with decreasing wave amplitude. For a frictionless case, the radiated energy flux must balance the loss of edge wave energy.

2.2.3. Resonance over fringing coral reefs

Fringing coral reefs can be seen as a semi-enclosed basin, where the natural resonant frequencies depend mainly on the reef flat width and water depth. These resonant periods, for most fringing reefs, are in the order of tens of minutes(Péquignet et al. 2009). An upper limit for natural frequencies can be obtained for a narrow reef with large water depth (Equation 2.1). For example, a 50 m reef flat width with 3.8 m water depth (maximum water depth found according to Quataert et al. (2015)) has natural frequencies lower than 0.03 Hz.

Resonance over fringing coral reefs can occur under two main conditions. The first requirement is that the standing low-frequency waves have a node at the reef crest (Buckley et al. 2018). The natural frequency needed to have this specific node location, can be estimated with:

$$f_{node} = \frac{1}{4}(2n-1)\left(\int_0^{x_{shoreline}} \frac{1}{\sqrt{gh(x)}}dx\right)^{-1} \tag{2.3}$$

where,

$x_{shoreline}$ = point of reflection at the shoreline

n = number of nodes from the reflection point

$h(x)$ = still water depth + wave setup

This formula differs from 2.1 due to its consideration of non-constant water depths, which is mainly due to varying wave setup. Furthermore, this expression considers the reef flat width as the distance between the reef crest ($x = 0$) and the shoreline ($x_{shoreline}$).

The second requirement needed for resonance to occur is to have a significant amount of low-frequency energy trapped over the reef flat (Péquignet et al. 2009). Under these two conditions, resonant amplification will arise since incoming offshore waves will be in phase with re-reflected incoming trapped waves (figure 2.2).

The wave energy over the reef flat increases with higher low-frequency waves. This amplitude is directly dependent on the incident offshore wave height and water level. Furthermore, the duration of the offshore forcing and its groupiness characteristics can also have an impact on the long waves amplitude, and consequently, on the amount of energy over the reef flat. Gawehn et al. (2016) found some short time occurrence of wave resonance, and a positive correlation between the low frequency energy over the reef flat and the incident wave groupiness factor. However, this study was carried out in a specific location, and the findings could be site related. The amount of wave energy at the reef flat is depth limited (Cheriton et al. 2016) and can be reduced due to wave dissipation, such as wave breaking and bottom friction (Van Dongeren et al. 2013). According to Buckley et al. (2018), coral roughness can dissipate wave energy of different frequencies, with the low-frequencies being the most affected. Moreover, bottom friction dissipation limits the magnitude of resonant run-up amplification (Pomeroy et al. 2012).

Resonant low-frequency waves can occur under different eigenmodes, and the fundamental mode is expected to amplify more than higher modes(Nwogu and Demirbilek 2010). The conditions under which the different resonant modes could resonate differ depending on the reef characteristics. The fundamental mode, which occurs when the wavelength is close to four times the reef width, will most probable resonate in narrow reefs with larger water depths (Shimozono et al. 2015), whereas higher modes can resonate with lower water depth conditions. The reef flat width determines which type of low-frequency waves are more likely to resonate. Infra-gravity resonance is dominant over a reef flat narrower than 300 m (Shimozono et al. 2015), whereas very low-frequency waves are dominant on reef flats widths between 250 and 500 m (Pearson et al. 2017). Resonant very low-frequency waves were found to induce large water level oscillations amplitudes, between 0.14 and 0.83 m, on a reef flat 270 m wide (Gawehn et al. 2016). No resonance of low-frequency waves was found on reef platforms wider than 500 m.

Additionally to the wave resonance, Shimozono et al. (2015) found in his experiments an amplification of the run-up over the beach. This resonant run-up was shown by comparing the run-up spectrum (S_R) with the wave spectrum at the toe beach ($S_{beachtoe}$). The ratio of $S_R/S_{beachtoe}$ showed significant peaks at specific frequencies. This resonant behavior is dependent on the beach slope, and not the reef platform width as for waves resonance. The same study showed that this resonant run-up occurs in the long waves frequency range, over milder beach slopes.

Wave resonance is more probable to occur under conditions with considerable low-frequency wave energy and/or large water depths (Pearson et al. 2017). This rise in water level reduces dissipation due to bottom friction and increases the resonant frequencies, allowing to resonate a wider wave frequency range (Péquignet et al. 2009). Thus, under the scenario of sea-level rise wave resonance over coral reefs may become more likely to happen, even under mild wave conditions.

Flooding can also increase due to non-linear wave shapes, such as bore-like wave shape. Bores form due to non-linear wave steepening and are more likely to occur over wide reefs with steep slope beaches (Shimozono et al. 2015). Steeper waves are more dangerous for flooding than regular waves, because non-linear waves have greater velocities, and they can reach larger inland distances (Didenkulova et al. 2007). Additionally, the bore-like wave shape acts as a shock force, having a larger impact on structures than sinusoidal waves. These non-linear wave shapes have also been observed in resonant low-frequency waves (Gawehn et al. 2016). Non-linearity could enhance or counteract resonance, leading respectively to a larger resonant run-up amplification or to a stronger wave energy dissipation. A continuous wave steepening could even lead to wave breaking and non-resonant conditions.

3

Methodology

3.1. Numerical modeling

A numerical wave model can be used to better understand resonance conditions, wave transformations, and shoreline impacts. There are mainly two types of wave models: (1) phase-averaged models and (2) phase-resolving models. Model (1) is based on the energy equation and calculates the sea surface statistics, while model (2) is based on momentum and mass conservation, and computes the sea surface elevation. The phase resolving model is the most appropriate for this research due to the complex reef hydrodynamics. An example is XBeach-Non hydrostatic model, which has been successfully used in several studies to represent wave dynamics over a coral reef (Quataert et al. 2015, Pearson et al. 2017, Pomeroy et al. 2012).

Another option of phase resolving model is SWASH, which is a public code for simulating surface wave transformations and rapidly varied flows in coastal waters developed by Zijlema et al. (2011). SWASH is governed by the non-linear shallow water equations, including non-hydrostatic pressure, and its main difference with the previous model is that it can resolve the vertical velocity (u) profile, whereas XBeach-Non hydrostatic uses a depth averaged velocity. SWASH can correctly simulate complex nearshore processes (such as wave breaking, non-linear interaction, wave run-up, and wave-induced circulation) and represent hydraulic jumps and bores (Zijlema et al. 2011). Moreover, Zijlema (2012) demonstrate the capabilities of SWASH for predicting the wave dynamics over a fringing coral reef. These dynamics included wave breaking, bottom friction, wave-induced setup, run-up, and generation/propagation of low-frequency waves.

SWASH was chosen in this study due to the characteristics mentioned above. As a starting point, a validation of SWASH was carried out using laboratory experiments data. After this step, the research questions were analyzed through a horizontal one dimensional (1D) SWASH model, where resonance was force over a schematized cross-shore fringing coral reef profile. This model setup neglects processes such as wave directional spreading and 2D effects.

3.2. Model validation

SWASH was validated with laboratory data from Demirbilek et al. (2007), an experiment where resonance was observed. The reef bathymetry and the location of the nine wave gauges installed during this laboratory experiment can be seen in Figure 3.1.

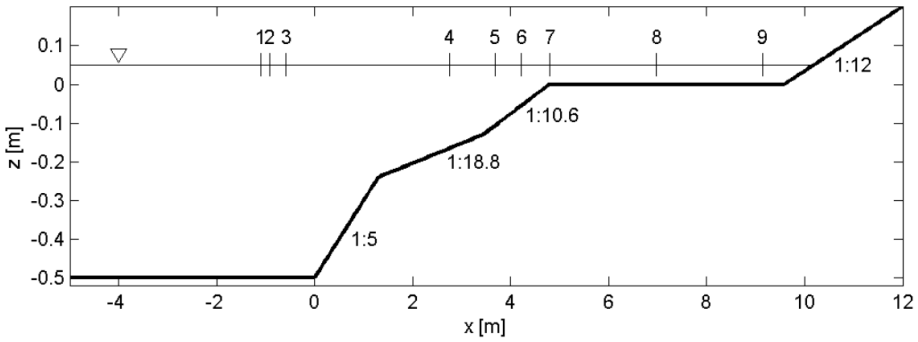

Figure 3.1: Reef profile and location of wave gauges of Demirbilek et al. (2007) laboratory test. Source:Zijlema (2012).

In this laboratory experiment several tests were carried out for different input conditions, from which four tests (Table 3.1) were selected to validate the predictive capabilities of SWASH over a coral reef. This selection was based on Zijlema (2012), where the same tests were used to prove that SWASH in its depth-averaged model was able to accurately predict the bulk wave properties over a fringing coral reef.

Table 3.1: Input conditions of Demirbilek et al. (2007) tests used for SWASH validation.

Test N°	H_{m0} (cm)	T_P (s)	d_r (cm)
18	8.5	2.00	5.1
27	5.5	1.25	1.6
38	8.4	2.00	0.0
48	7.5	1.5	3.1

3.2.1. General validation

SWASH capability for modeling over reefs was analyzed by comparing the model results with the laboratory gauge measurements. Due to measurement errors, gauge 4 was excluded from the validation (Zijlema 2012). The comparison was made for three common wave parameters: significant wave height (H_{m0}), wave setup, and wave run-up. The latter was analyzed through three statistics, maximum run-up (R_{max}), run-up value exceeded by 2% of the incoming waves ($R_{2\%}$), and run-up value exceeded by 10% of the incoming waves ($R_{10\%}$).

The model was tested for a horizontal 1D model with a uniform grid resolution of Δx = 5 cm, an initial time step of Δt = 0.005 s, and two vertical layers (velocity profile resolution). To account for friction, a Manning coefficient of $n = 0.01\ s/m^{1/3}$ was assumed. This friction value represents a smooth material such as the plastic used to build the reef profile in this experiment (Demirbilek et al. (2007), Zijlema (2012)). The model was built with a weakly reflective offshore boundary condition and without any at the onshore side (sufficient beach length to avoid overtopping).

Figure 3.2 shows a comparison of the significant wave height (H_{mo}) cross-shore evolution between the model results and laboratory measurements. In general, for every test, the largest differences were observed for the first instrument seawards of the reef crest (gauge 6). In this area, plunging breaking waves were observed during the experiment (Demirbilek et al. 2007), which could explain the deviations from measurements, as SWASH cannot describe plunging waves due to its consideration of mono-value surface elevation. Over the reef flat SWASH shows a good agreement with the four tests, presenting a stronger variability for the largest d_r (Test 18). Wave setup (Figure 3.3) appears to be slightly overestimated in almost every location and test. However, the setup cross-shore evolution sign was predicted correctly by SWASH. The run-up calculations and statistics (Figure 3.4) have a more erratic behavior depending on the test. Nevertheless, the R_{max} shows to have an overall stronger agreement with laboratory data in all cases, which is the relevant run-up statistic for this thesis.

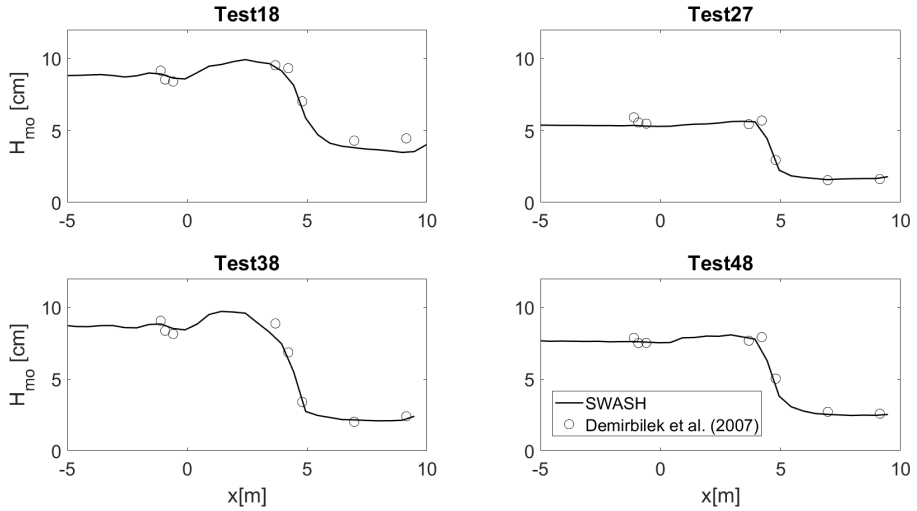

Figure 3.2: Comparison between SWASH computed significant wave height H_{m0} (solid line) and Demirbilek et al. (2007) measurements (circles) for tests N° 18,27,38 and 48.

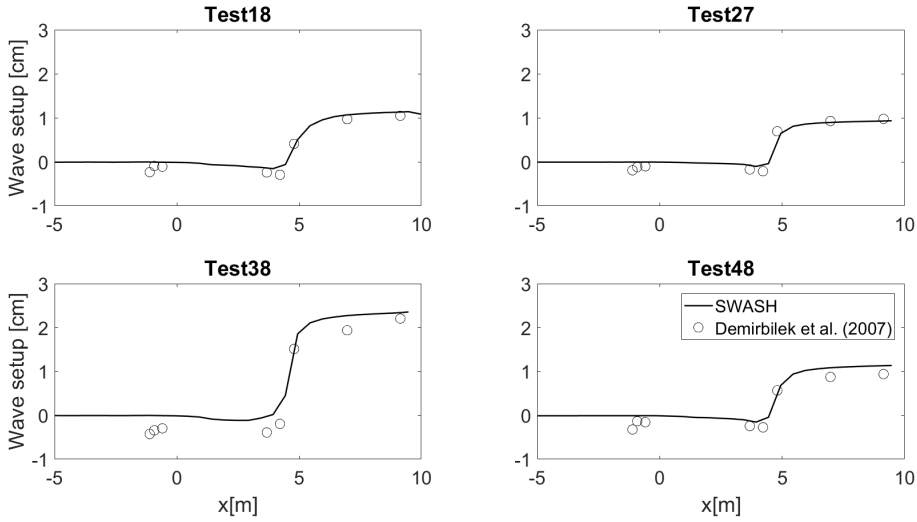

Figure 3.3: Comparison between SWASH computed wave setup (solid line) and Demirbilek et al. (2007) measurements (circles) for tests N° 18,27,38 and 48.

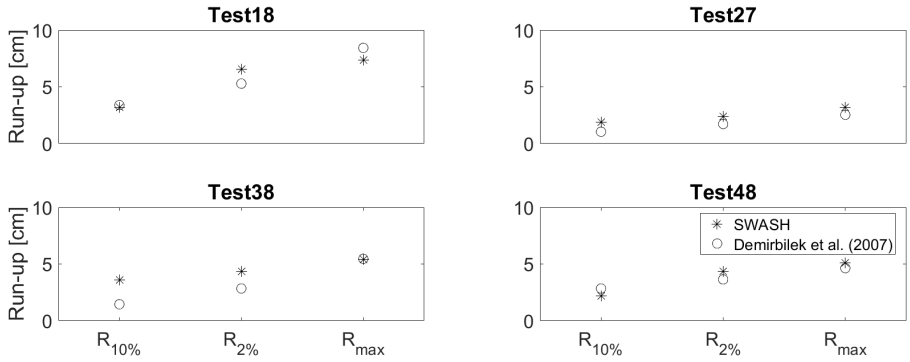

Figure 3.4: Comparison of statistic runup (R_{max},$R_{2\%}$,$R_{10\%}$ (solid line) between SWASH calculations (stars) and Demirbilek et al. (2007) measurements (circles) for tests N° 18,27,38 and 48.

To evaluate the general SWASH predictive skill for H_{mo} and wave setup, the bias and scatter index (SI) were used and computed as:

$$\text{Bias} = \frac{1}{N}\sum_{i=1}^{N}\left(X^i_{\text{SWASH}} - X^i_{\text{obs}}\right) \tag{3.1}$$

$$\text{SI} = \frac{\sqrt{\frac{1}{N}\sum_{i=1}^{N}\left(X^i_{\text{SWASH}} - X^i_{\text{obs}}\right)^2}}{\frac{1}{N}\sum_{i=1}^{N} X^i_{\text{obs}}} \tag{3.2}$$

Table 3.2 shows a good agreement between SWASH results and Demirbilek et al. (2007) measurements. The maximum bias is found to be less than 7 mm (gauge 6) for the significant wave height and lower than 2 mm for the wave setup. For the SI, an 18% is the maximum error for both H_{mo} (gauge 9) and wave setup (gauge 7), with an acceptable mean error of less than 8% and 15%, respectively. This error is expected to be influenced by the imposed conditions and/or measurement errors, which did not show a good fit since the beginning of the run (offshore gauges comparison). An adjustment to the imposed conditions could help to reach a closer agreement between SWASH and laboratory test results.

Table 3.2: Statistical measures of SWASH performance for predicting H_{m0} and wave setup for different locations.

Gauge N°	Bias H_{m0} (cm)	SI H_{m0}	Bias setup (cm)	SI setup
1	-0.32	0.04	-	-
2	0.13	0.03	-	-
3	0.12	0.03	-	-
5	-0.08	0.06	-	-
6	-0.63	0.09	-	-
7	-0.34	0.08	-0.09	0.18
8	-0.14	0.11	0.15	0.17
9	-0.31	0.18	0.09	0.1

3.2.2. Grid size influence

To understand the impact of Δx value (uniform grid) on SWASH performance, the reef was modeled with the same characteristics as in Subsection 3.2.1 but for a finer grid with Δx = 1 cm. In order to compare, the root mean square errors ($RMSE$) for different wave parameters were computed (Table 3.3). For both grid sizes, coarser and finer, SWASH can model hydrodynamics over coral reef with acceptable $RMSE$. The influence Δx over $RMSE$ varies per parameter. The coarser grid leads to a smaller $RMSE_{run-up}$, while the higher resolution reduces $RMSE_{Hm0}$. The wave setup error remains stable for both grid sizes. The finer grid is more time consuming and does not perform better for every parameter. Thus a positive effect, in this case, was not found.

Table 3.3: Root mean square errors ($RMSE$) for different wave parameters and grid resolutions.

Δx (cm)	$RMSE_{Hm0}$(cm)	$RMSE_{setup}$ (s)	$RMSE_{run-up}$ (cm)
5	0.41	0.2	1
1	0.29	0.21	1.26

3.2.3. Vertical layers influence

The influence of vertical resolution on reef modeling was studied by varying the numbers of vertical layers (1,2,6 and 12), with the corresponding adjustment of the breaking parameters according to Smit et al. (2014). The rest of the model characteristics remained as in Subsection 3.2.1. Due to considerable computational time needed for this variation, the experiment was carried out only for Test 18. Table 3.4 presents how the model agreement varies depending on the analyzed parameter for different vertical resolutions. For example, by comparing the $RMSE$, the two vertical layers model performed better for H_{mo}, and depth average showed a more satisfactory fit for setup and run-up calculations. Thus, as for the grid size variation, a positive impact of increasing vertical layers, in this case, can not be easily detected.

Table 3.4: RMSE for Test 18 computed with different number of vertical layers.

N° of vertical layers	$RMSE_{H_{mo}}(cm)$	$RMSE_{setup}(cm)$	$RMSE_{runup}(cm)$
1	0.69	0.12	0.79
2	0.51	0.13	0.96
6	0.81	0.14	0.91
12	0.84	0.17	2.01

3.2.4. Resonance validation

Resonance of the fundamental mode was also predicted by SWASH. Figure 3.5 shows that the fundamental mode of resonance, modeled and measured, is in good agreement with theory (2.1) for every case. Nevertheless, the wave spectrum magnitude around the peak frequency is not computed adequately by SWASH for test 18. This considerable difference remained even with higher grid and vertical resolutions.

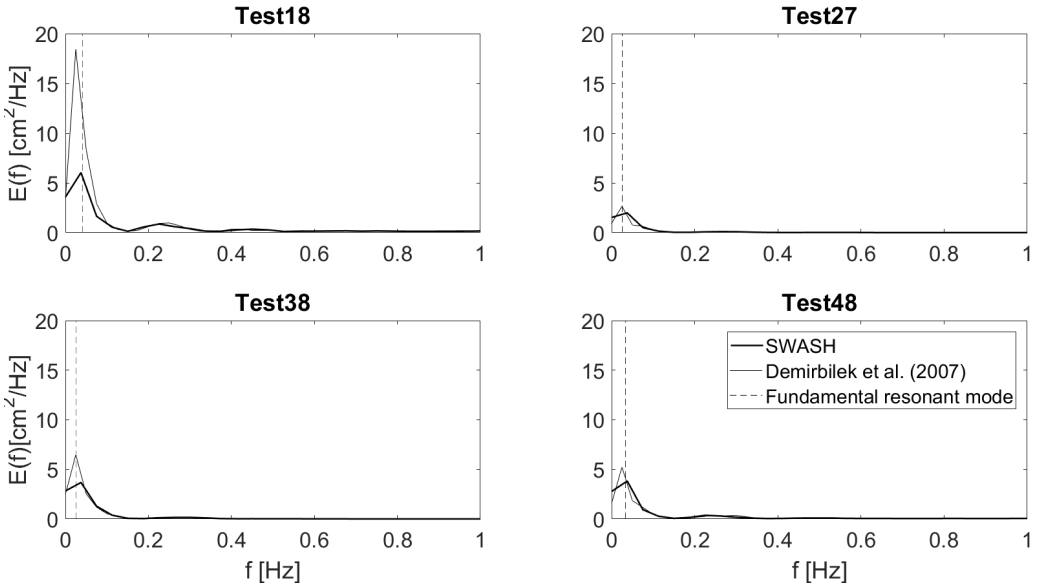

Figure 3.5: Comparison between gauge 9 SWASH computed wave spectrum (thick line) and Demirbilek et al. (2007) measurements (thin line) for tests N° 18,27,38 and 48 Dashed line indicates the first resonant mode (2.1).

3.3. Numerical experiments

3.3.1. Model setup

The schematized fringing coral reef profile used for the numerical modeling was taken as a simplified version of the reef profile analyzed in Gawehn et al. (2016) (Figure 2.3), over which low-frequency wave resonance with non-linear wave shape was observed (Gawehn et al. 2016). The reef profile built for the model (Figure 3.6), is characterized by a 1:6 fore reef slope, followed by a 270 m wide reef flat (width is in the range of maximum resonance for low-frequency waves, according to Pearson et al. (2017)). The reef flat is delimited by two features, the reef crest (x = 0 m) offshore and the beach toe (x = 270 m) onshore. After the latter, the reef structure ends with a 1:6 beach slope.

In order to better understand the offshore hydrodynamics conditions needed for waves to resonate over the reef, and its impacts in reef hydrodynamics resonance was studied for a simplified wave climate. This wave climate consisted in small amplitude regular low-frequency waves, which could have a wavelength longer than 20 km. Thus, to fulfill SWASH requirement of linear wave theory at the wavemaker boundary, the reef profile (Figure 3.6) was extended with a slope of 1/3 until reaching a bed level of -440 m at x = -2000 (Appendix A, Figure A.1). Moreover, at the most offshore modeled position (x = -2000) a weakly reflective boundary condition was set, which is effective in absorbing waves inside the low-frequency band, while onshore the beach acted as a boundary condition. The beach was designed large enough to avoid overtopping and water level reaching the grid limits, with a total beach height of 15 m over the reef flat.

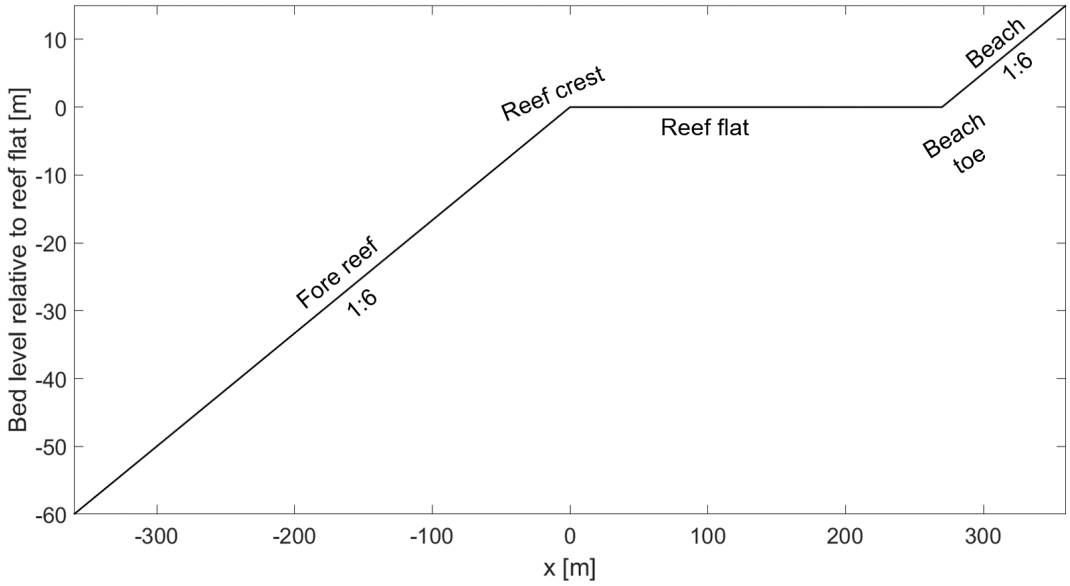

Figure 3.6: Schematized fringing coral reef profile built for numerical modeling experiments.

Table 3.5 shows the SWASH model setup used for these numerical experiments. A uniform grid, the only option for a 1D SWASH model, with a resolution of Δx = 10 cm, was chosen to characterize wave run-up. Due to the large order difference between offshore water depth (minimum of 440 m) and grid resolution (10 cm), the model could only be stable for one vertical layer. However, this minimum vertical resolution is not expected to have a relevant impact on long wave dynamics. The time resolution (Δt), was changed automatically by SWASH to fulfill a Courant number ($\sigma = u\Delta t\ /\Delta x$) smaller than 0.5 starting from Δt = 5 ms. This σ limitation is recommended by SWASH user manual for wave non-linearity and wave interactions with steep slopes, such as this case. To ensure stationary signals, a duration of four hours by run was chosen. A low friction coral reef ($n = 0.01 s/m^{1/3}$) was considered to avoid the influence of friction on resonant amplification and wave transformations. The breaking parameter command option was activated in every case, with the default values, to account for wave breaking and its impact on wave shape.

Table 3.5: Reef numerical model setup - SWASH.

Characteristic	Symbol	Value
Grid resolution	Δx	0.1 m
Vertical layers	N°	1
Courant number	σ	< 0.5
Run duration	t	4 h
Friction coefficient	n (Manning)	0.01 $s/m^{1/3}$

3.3.2. Small amplitude resonant regular long waves experiment

The goal of this numerical experiment is to generate and understand simplified scenarios of resonance under the first two resonant modes. Therefore, resonance will be forced over a fringing reef with monochromatic long waves, which will vary in wave period and wave amplitude. Moreover, resonance will be forced and studied under two reef flat water depths (d_r = 0.8 m, and d_r = 1.6 m). The results of this numerical modeling will be analyzed, and the reef resonant hydrodynamics characteristics will be investigated by searching the long wave frequency and amplitude that generates the maximum resonant amplification on the wave height at the beach toe ($H_{beachtoe}$), and the maximum run-up (R_{max}) .

Several steps needs to be followed to obtain the experiment objective:

1. The first two theoretical reef natural periods, fundamental T_0^* and first mode T_1^*, will be estimated from

Equation 2.3 for both d_r.

2. The model will be run with theoretical resonant regular long waves with an incident wave height of H_{off} = 1 cm. This small amplitude (H_{off}/d_r < 1.5%) was chosen to avoid a possible influence of non-linear effects on resonance.

3. Following runs will be carried out with wave periods neighboring the theoretical resonant ones until finding a maximum ($H_{beachtoe}$), and (R_{max}) for the two first resonant modes. The offshore wave height will be kept at 1 cm.

4. The two modeled eigenmodes leading to these maxima will be defined as modeled resonant periods. They will be named as T_0 and T_1 for the ones close or equal to T_0^* and T_1^*, respectively.

5. The influence of wave amplitude on the resonant amplification ratio will be studied for these two frequencies by varying H_{off} between 0.1 and 1.5 cm.

6. Resonant amplification ratios will be computed to compare resonant $H_{beachtoe}$ and R_{max} values with respect to H_{off} ($A_H = H_{beachtoe}/H_{off}$, and $A_R = R_{max}/H_{off}$).

These steps can be divided as two consecutive experiments. The first experiment has the objective of finding the modeled resonant periods for the first two modes (step 1 to 4), and the second experiment has the objective of understanding offshore wave height (H_{off}) influence on resonant amplification (step 5 to 6). The steps to be followed in each experiment can be visualize in Figure 3.7.

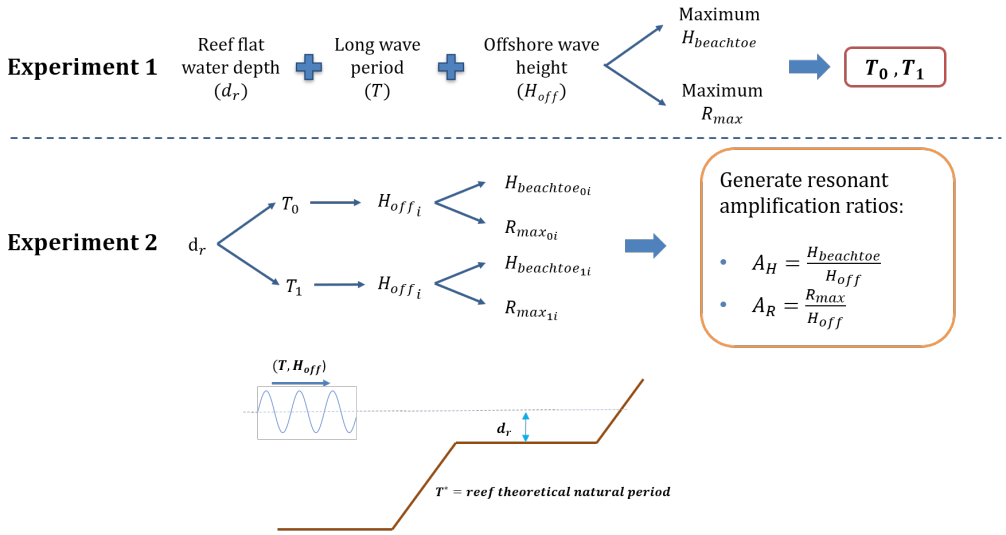

Figure 3.7: Methodology followed in this study to force resonance over a schematized fringing reef.

3.3.3. Data analysis

The methods and formulas used to analyze the results of the different SWASH runs are highlighted in this section.

Splitting incoming and outgoing wave

The surface elevation η and the depth average velocity U were split based on the method of Guza et al. (1985):

$$\eta^{\pm} = \frac{1}{2}(\eta \pm U\sqrt{\frac{d}{g}}) \tag{3.3}$$

$$U^{\pm} = \frac{1}{2}(U \pm \eta\sqrt{\frac{g}{d}}) \tag{3.4}$$

This methodology works under the assumptions of linear wave theory, shallow water, and cross-shore wave propagation. It can be applied for long waves with a small amplitude.

Wave nonlinearity

The analysis of non-linear wave shape was carried out through the parameters of wave skewness (Sk) and wave asymmetry (As), which were computed with the third-moment of the surface elevation (η) based on Cheriton et al. (2016) study:

$$Sk = \frac{\langle \eta^3 \rangle}{\langle \eta^2 \rangle^{3/2}} \tag{3.5}$$

$$As = \frac{\langle \mathscr{H}^3(\eta) \rangle}{\langle \eta^2 \rangle^{3/2}} \tag{3.6}$$

where $\mathscr{H}$ corresponds to the Hilbert transformation.

Energy fluxes

The average incoming and outgoing wave energy E and energy fluxes F were calculated based on Sheremet et al. (2002), which assumes shallow water and cross-shore propagation:

$$\begin{aligned} E^{\pm}(f,x) = \frac{1}{4}\big[&Co_{\eta\eta}(f,x) + (d/g)Co_{UU}(f,x) \\ &\pm(2\sqrt{d/g})Co_{\eta U}(f,x)\big] \end{aligned} \tag{3.7}$$

$$F^{\pm}(f,x) = E^{\pm}(f,x)\sqrt{gd} \tag{3.8}$$

where, $Co_{\eta U}$ is the $\eta - U$ cospectrum and $Co_{\eta\eta}$ Co_{UU} are η and U autospectra, respectively.

The time evolution of the incoming and outgoing energy fluxes F were calculated based on Madsen et al. (1997), which can be applied for regular and irregular waves in shallow water conditions:

$$F^{\pm}(t,x) = \rho U^{\pm}(t,x)\left(g\eta^{\pm}(t,x)d(t,x) + \frac{1}{2}U^{\pm 2}(t,x)d(t,x)\right) \tag{3.9}$$

where, $\eta^{\pm}$ and $U^{\pm}$ were obtain from equations 3.3 and 3.4 respectively.

4

Results & Analysis

The SWASH numerical modeling experiment results and analysis are presented in this chapter. This experiment focuses on forcing small amplitude regular long waves resonance over fringing coral reefs, in order to understand the basics of low-frequency wave resonance and the corresponding resonant amplification over reefs. The resonant amplification was analyzed for the first two resonant modes, and for different incident offshore wave heights (H_{off}). To normalize the influence of (H_{off}) on resonant amplification two ratios were built. The first resonant amplification ratio A_H shows how much larger is the wave height at the beach toe (x = 270 m) compared to H_{off}, and the second ratio A_R reflects the ratio between the maximum beach run-up and H_{off}:

$$A_H = H_{beachtoe} / H_{off} \tag{4.1}$$

$$A_R = R_{max} / H_{off} \tag{4.2}$$

After presenting the experiment results, an analysis was carried out for different processes that could influence the wave height and run-up resonant amplification. These processes are:

- Influence of wave period on resonant amplification
- Influence of wave height on resonant amplification
- Resonant build-up behavior
- Influence of reef energy balance on resonant amplification

4.1. Numerical modeling results

The results were divided into two experiments. The first experiment was carried out to find the first two modeled resonant modes (fundamental resonant period T_0, and first resonant period T_1) for a fixed H_{off}, and understand how the wave height at the beach toe ($H_{beachtoe}$) and maximum run-up (R_{max}) vary for different wave periods. In the following experiment, the influence of offshore wave height on the wave height and run-up amplification ratio was analyzed by varying H_{off} for T_0 and T_1 period waves. Consequently, the resonant amplification ratios A_H and A_R were studied. Both experiments were carried out for two reef flat water depths, d_r = 0.8 m and d_r = 1.6 m.

4.1.1. Finding resonance for small amplitude regular long waves

In order to find resonance, SWASH runs (example in Appendix B) were carried out starting from the theoretical resonant modes T_0^* and T_1^* (Table 4.1), computed based on Equation 2.3, and continuing with neighboring periods. Through this methodology, the frequencies leading to the largest resonant amplifications were found. This maximum amplification was identified by comparing for every modeled period, the wave height at the beach toe ($H_{beachtoe}$), and the maximum run-up (R_{max}). These parameters, for d_r = 0.8 m, are

shown in Figure 4.1. $H_{beachtoe}$ was calculated with the zero down crossing technique, and R_{max} as the maximum value of the run-up series with the still water level as reference. For every period, both variables were computed with stationary water level time series. In this thesis, stationarity was considered when the slope of the signal envelope reaches values smaller $10^{-}6$. This condition was fulfilled at different times for the different surface elevations signals analyzed, with an average time needed to reach stationarity of around 5000 s.

Both parameters, $H_{beachtoe}$ and R_{max}, show two resonant amplification peaks in Figure 4.1, with a bandwidth of resonant periods around each peak. Within each of these resonant bandwidths, the wave height at the beach toe ($H_{beachtoe}$) and the maximum run-up (R_{max}) reach considerably higher values than the neighboring frequencies. The fundamental resonant bandwidth (right peak) is wider than the first mode (left peak) resonant bandwidth, which can be noted because the periods neighboring the fundamental mode experience a relatively lower resonant amplification reduction than periods close to the first mode. For example, a variation of five seconds from the resonant period reduces $H_{beachtoe}$ in 2.5% for the fundamental mode and 6.2% for the first resonant mode. Moreover, a 10 seconds variation from the resonant period reduces $H_{beachtoe}$ in 20% for the fundamental mode and 30% for the first resonant mode. Thus, the range of periods resonating around the fundamental mode is wider than the resonating bandwidth of periods neighboring the first mode.

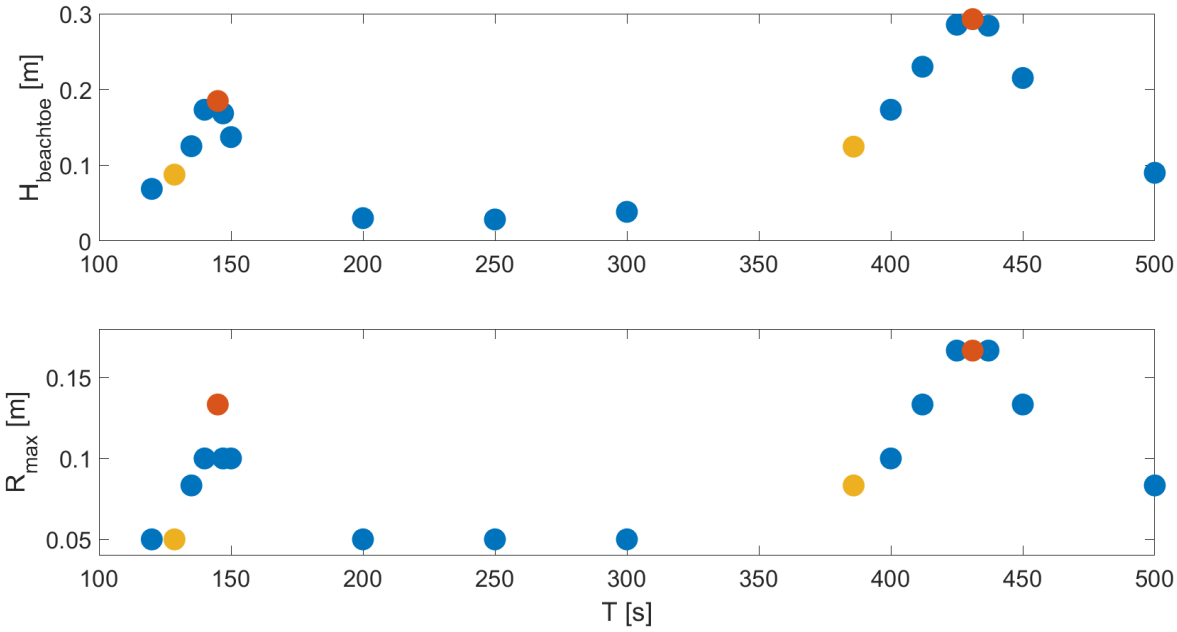

Figure 4.1: Stationary beach toe wave height $H_{beachtoe}$ (top figure) and maximum run-up R_{max} (bottom figure) for different wave periods. The offshore wave height is H_{off} = 0.01 m and d_r = 0.8 m. The yellow (orange) dots indicate the first two theoretical (modeled) resonant modes (Table 4.1).

The model setup implied shallow water conditions for the simulated long waves since the beginning of the domain. Hence, waves are expected to shoal at a similar rate independently of the wave period and not to show different $H_{beachtoe}$ and R_{max} values for the same H_{off}. As the amplification peaks occur on periods neighboring the theoretical resonant periods (yellow dots in Figure 4.1), the amplifications was associated with resonant waves over the reef. Inside the two resonant bandwidths, the maximum $H_{beachtoe}$ and R_{max} amplification occurs for the period located in the middle of each bandwidth. These two periods are defined as the modeled resonant periods T_0 and T_1 (orange dots from Figure 4.1), and they represent the first two reef natural frequencies. These periods were found to be T_0 = 431 s and T_1 = 145 s for d_r = 0.8 m, and T_0 = 325 s and T_1 = s for d_r =1.6 m (Table 4.1).

The first two modeled resonant modes (orange dots from Figure 4.1) are both longer than the corresponding theoretical ones (yellow dots from Figure 4.1). The same behavior was observed in d_r = 1.6 m results (Appendix C, Figure C.1). Moreover, the theoretical and modeled resonant periods are shorter for larger water

depths as expected from theory (Equation 2.3).

Table 4.1: Theoretical (Equation 2.3) and modeled fundamental and first resonant periods for different reef flat water depth (d_r). T^*_0 and T^*_1 corresponds to theory and T_0 and T_1 to SWASH results. Zero indicates fundamental resonant mode, and one the first resonant mode.

d_r (m)	$T^*{}_0$ (s)	$T^*{}_1$ (s)	T_0 (s)	T_1 (s)	H_{off} (cm)
0.8	385.9	128.6	431	145	1
1.6	273.3	91.1	325	105	1

As presented in Figure 4.1, both the beach toe wave height and the maximum run-up are larger for the fundamental mode than for the first resonant mode. Moreover, periods in the vicinity of T_0, such as T = 450 s can reach larger $H_{beachtoe}$ and R_{max} than T_1. For the maximum run-up, no difference can be observed between the closest periods to T_0, which is probably due to the grid resolution (Δx = 10 cm). However, the run-up grid resolution is sufficiently fine, ΔR = 1.67 cm (Δx = 10 cm over a 1/6 beach slope), to indicate that the impact of resonance on run-up is similar for T_0 and periods close to it.

4.1.2. Varying wave height of resonant regular long waves

In Subsection 4.1.1 the first two modeled resonant periods T_0 and T_1 were identified. These frequencies were found for the different d_r, assuming an incident wave height H_{off} = 1 cm (Table 4.1). In this subsection, H_{off} is varied for these two resonant modes to analyze its impact on the resonant amplification. In order to compare results with same period but different H_{off}, the ratios A_H (Equation 4.1) and A_R (Equation 4.2) are used.

Figure 4.2 shows that smaller waves undergo stronger resonant amplification for both beach toe wave height and maximum run-up. This behavior was observed for the fundamental and first resonant periods, for both reef flat water depth scenarios (results for d_r = 1.6 m are presented in Appendix C, Figure C.2). Thus, it could be said that higher resonant waves amplify less than smaller resonant waves. Furthermore, for the same H_{off}, the fundamental mode generates a larger amplification ratio than the first mode. This difference reduces with increasing offshore wave height.

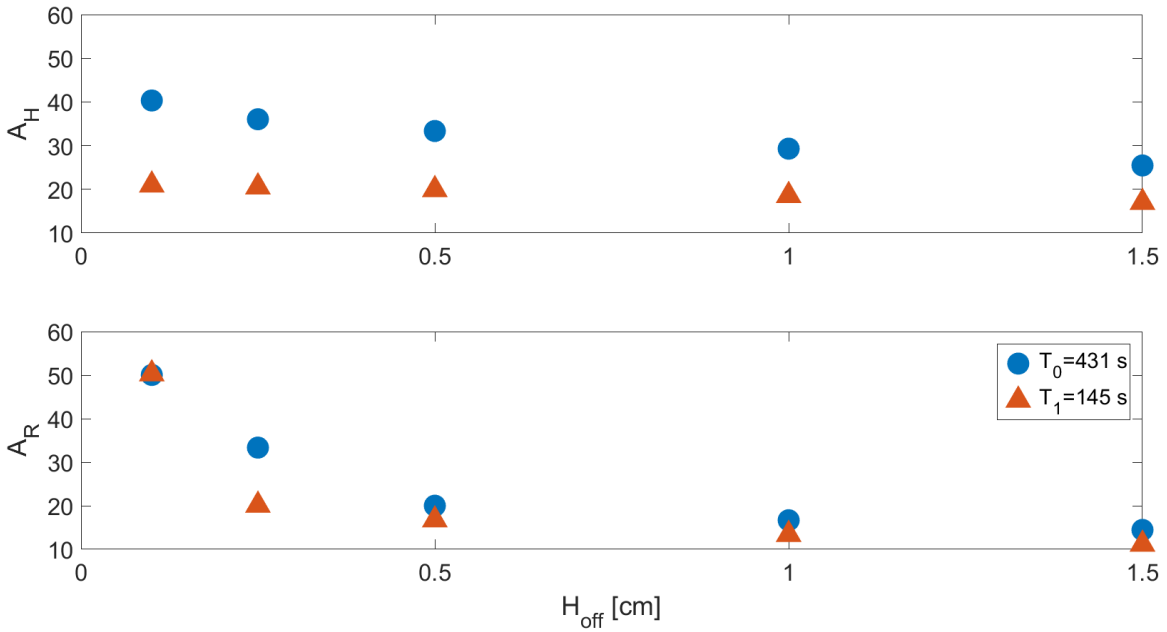

Figure 4.2: Stationary beach toe wave height ratio A_H (upper figure) and maximum run-up ratio A_R (lower figure) for different incident offshore wave heights H_{off}, and for the first two resonant mode T_O and T_1 (d_r = 0.8 m).

The maximum run-up ratio, considering the same H_{off}, is similar for T_0 and T_1 for most offshore wave

height input. This lack of variability between periods for R_{max} could be due to the grid resolution (Δx = 10 cm), and may improve with a finer grid. However, as the ΔR was taken smaller than 2 cm, it seems that, for a d_r of 0.8 m, the impact of resonance on R_{max}, is fairly constant for the first two resonant modes with the same H_{off}. For the larger reef water depth d_r = 1.6 m (Appendix C, Figure C.2), A_R showed stronger differences between both resonant periods than for d_r = 0.8 m. Thus, the results suggest that the influence of the resonant period on the resulting maximum run-up is lower for smaller water depths.

The amplification ratios A_H and A_R, are compared for different reef flat water depths and offshore wave heights with the same H_{off}/d_r relation (Figure 4.3). From this comparison, it is shown that smaller waves amplify more than larger ones, independently of the d_r. Moreover, these amplification ratios are stronger for smaller reef flat water depths. This behavior is more noticeable for a smaller H_{off}/d_r relation (smaller waves) than for a larger H_{off}/d_r relation (higher waves). The difference between the resonant amplification ratios for different d_r, decreases for larger wave heights. It can be note that with increasing H_{off}/d_r amplification ratios tend to the dashed blue lines in Figure 4.3, which symbolize equal resonant amplifications for the different water depths.

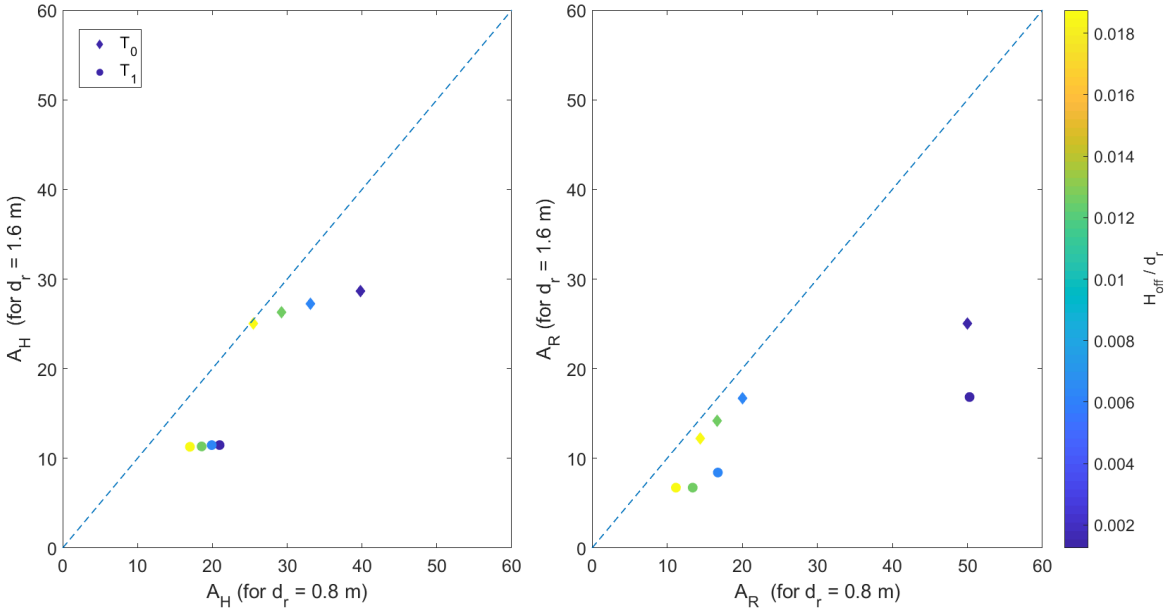

Figure 4.3: Stationary beach toe wave height ratio (left figure) and maximum run-up ratio (right figure) of different incident offshore wave heights and water depths. Each ratios is compared between d_r = 0.8 m (x axis) and d_r = 1.6 m (y axis) for the same H_{off}/d_r relation.

In general, for both d_r, the amplification ratios are larger for T_0 than for T_1, which is more perceptible for the wave height amplification ratio (A_H). Moreover, within the same reef flat water depth, this ratio shows stronger variation for the fundamental mode than for T_1. The first period A_H presents a shorter range of variation than the T_0, showing smoother A_H oscillations between different H_{off} and d_r scenarios. The maximum run-up amplification ratio presents a similar range and intensity of variation for different periods, water depths and wave heights scenarios.

Due to the d_r difference, between d_r = 0.8 m and d_r = 1.6 m, the linear wave theory shoaling coefficient ($K_{sh} = (d_{offshore}/d_r)^{1/4}$) for shallow water, where d_{off} corresponds to the offshore water depth) is expected to decrease in 15% for the deeper water depth, which could be the cause of stronger amplifications for the shallower water depth studied. However, by removing the shoaling influence, a comparison between the incident wave height resonant amplification of both d_r (Appendix C, Figure C.3) showed a similar tendency than Figure4.3. Smaller waves amplify more than higher waves, especially in the shallower water depth scenario (d_r = 0.8 m). Moreover, variations between waves with the smaller H_{off}/d_r relation and the larger H_{off}/d_r relation are stronger for T_0 than for T_1. Furthermore, the tendency to have similar resonant amplification

between different d_r is achieved with the fundamental period, for the largest values of H_{off}/d_r relation, in which d_r = 1.6 m can resonate between 5-9% more than d_r = 0.8 m. The first resonant period behavior remains unaltered when removing the wave shoaling influence, with the d_r = 0.8 m experiencing the stronger resonant amplifications, and without showing stronger resonant amplification differences whit H_{off} variations. Thus, the general tendency of stronger resonant amplifications for d_r = 0.8 m remains.

4.2. Influence of wave period on resonant amplification

Resonant waves behave like standing waves, with a node located close to the reef crest and an anti-node at the shoreline for the fundamental mode (top Figure 4.4). The first resonant mode has two nodes and two anti-nodes (bottom Figure 4.4). The nodes are located one close to the reef crest, and the other around two-thirds of the reef flat (x = 180 m). The position of the node closer to shore can vary depending on the reef flat water depth, while the second node remains close to the reef crest. Theoretical resonant periods, T_0^* = 385.9 s s and T_1^* = 128.6 s, and non-resonant periods, such as T = 300 s and T = 200 s, also present a standing wave pattern, but with a node shorewards and further of the reef crest than resonant periods. Thus, the node location condition needed for resonance to occur is not fulfilled for non-resonant periods.

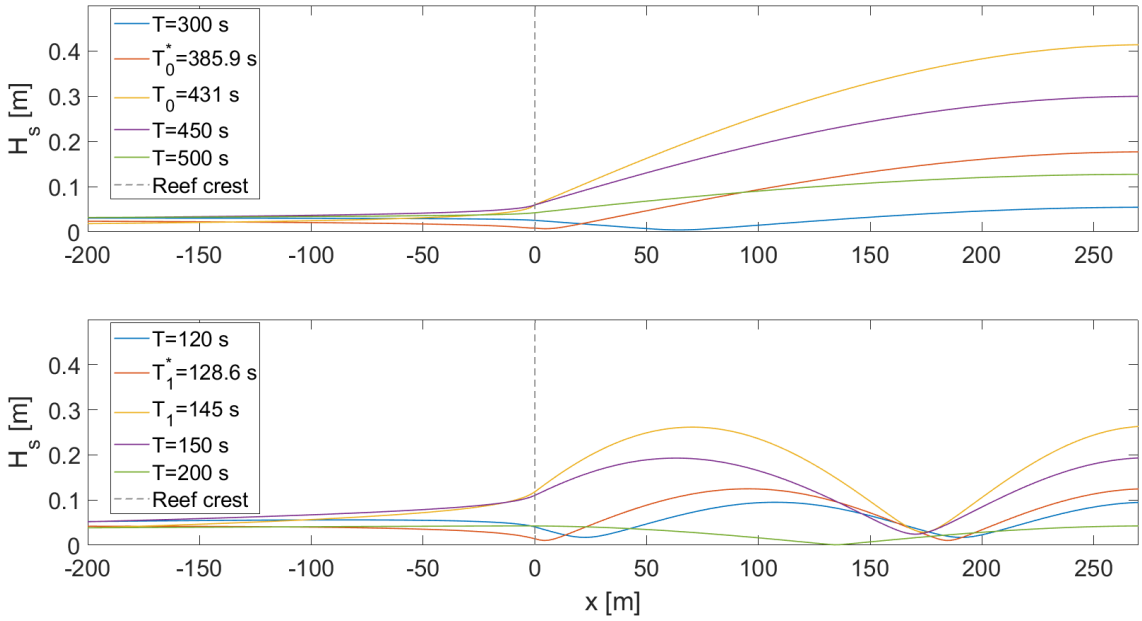

Figure 4.4: Stationary significant wave height (H_s) cross-shore evolution for different wave periods (x = 0 m indicates the reef crest and x = 270 m, right end of the figure, the beach toe). Top figure shows periods in the range of the theoretical and modeled fundamental resonant period. Bottom figure shows periods in the range of the theoretical and modeled first resonant period. In this analysis H_{off} = 1 cm and d_r = 0.8 m.

The cross-shore significant wave height (H_s) evolution, in shape and or magnitude, varies for waves with the same H_{off} and different periods. Remarkably, periods close to the resonant modes, T_0 and T_1 can show similar H_s values offshore the reef crest and differ considerably over the beach toe. A clear example can be seen by comparing T_0 = 431 s with T = 450 s, and T_1 = 145 s with T = 150 s, where in both cases waves show a standing wave pattern with a node close to the reef crest, and a similar significant wave height seawards of the reef crest. However, H_s at the beach toe can be approximately 40% larger for the modeled resonant period (T_0 = 431 s and T_1 = 145 s), which have the maxima resonant amplifications per mode, than for less amplify resonant period (T = 450 s and T = 150 s).

Also, there is a standing wave pattern transition from one to two nodes. This change is noticeable by comparing the H_s cross-shore evolution of intermediate periods between the fundamental and first resonant mode. For example, T = 300 s, T = 200 s and T = 150 s can be defined as intermediate periods. The first wave

period, T = 300 s, presents a standing wave pattern with only one node shoreward of the reef crest (around x = 70 m). Thus, when reducing the period starting from the fundamental one, the node position moves closer to the beach. This node shifting process is even more distinguishable for T = 200 s, where the node position is getting closer to two-thirds of the reef flat. For T = 150 s, the shifting node is almost at the position of the second node of a first mode standing wave, and the second anti-node is already observable. Thus, a two nodes behavior is almost fully developed, which is finally reached with T = 150 s.

The impact of resonance on wave height amplification can be better understood by normalizing the modeled incident significant wave height H_{s-in}, with the expected significant wave height due to wave shoaling $H_{s-shoal}$. The incident wave component was calculated following Guza et al. (1985) (Equation 3.3). $H_{s-shoal}$ was computed for each wave period by taking the offshore incident wave height (H_{off}) and multiplying it with the corresponding cross-shore shoaling coefficient. This coefficient was calculated with linear wave theory, and due to shallow water conditions it was the same for all the modeled periods. With this approach, the ratio A_{Shoal} was built as:

$$A_{Shoal} = H_{s-in} / H_{s-shoal} \tag{4.3}$$

A value of A_{Shoal} larger than one shows a wave height amplification stronger than the expected due to wave shoaling. This larger wave height amplification is likely due to wave resonance over the reef flat. For T_0 and T_1, for d_r = 0.8 m, the incident significant wave height over the reef flat is respectively 3 and 2 times larger than the expected wave height due to wave shoaling (Figure 4.5). Periods neighboring both resonant modes showed A_{Shoal} values larger than one, showing that they also experienced some wave resonance, and confirming the existence of bandwidth of resonant periods as shown in Figure 4.1.

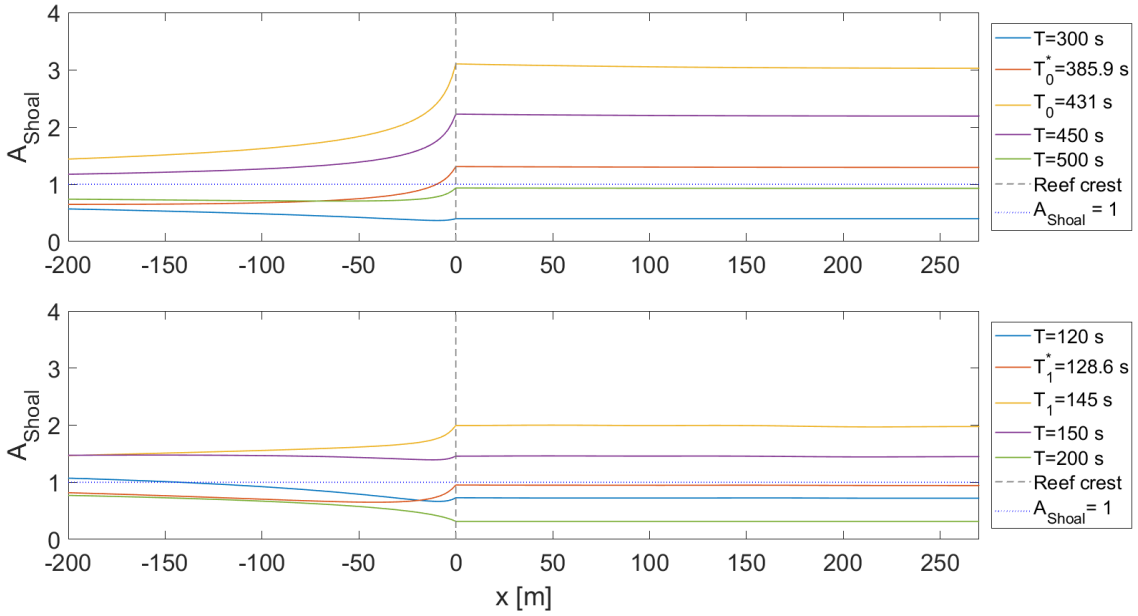

Figure 4.5: Stationary normalized incident significant wave height ($A_{Shoal} = H_{s-in}/H_{s-shoal}$) cross-shore evolution for different wave periods (x = 0 m indicates the reef crest and x = 270 m, right end of the figure, the beach toe). H_{s-in} represents the modeled incident wave height and $H_{s-shoal}$ the significant wave height related with the linear wave theory shoaling coefficient. In this analysis H_{off} = 1 cm and d_r = 0.8 m.

The reef profile has a constant value over the reef flat, which leads, without wave-setup, to a constant value of d_r over this area. The last implies that the incident significant wave height value is conserved over the reef flat. Thus, H_{s-in} variations occur between offshore locations and the reef crest. Furthermore, as the reef profile uniquely deepens offshore of the reef crest (Figure 3.6), only a wave height increase was expected for offshore waves propagating towards the reef. Nevertheless, some periods, such as T = 120 s and T = 300 s, showed a wave height decrease when approaching the reef crest. These wave height reductions could be

due to the effect of fore reef reflection or energy dissipation processes, such as bottom friction. For T =300 s, an extra run without friction was carried out to check this de-shoaling behavior, which showed no change in cross-shore H_s characteristics between models with and without friction. Thus, it could be said that dissipation due to bottom friction is likely not causing the wave height de-shoaling observed for some periods offshore the reef crest. Moreover, to understand if there was an influence of H_{off} in this de-shoaling behavior runs with period T =300 s and different wave heights between 0.1-2 cm were carried out. However, the wave height de-shoaling offshore of the reef crest remained on every wave climate scenario.

4.3. Influence of wave height on resonant amplification

The influence of the incident wave height on the resonant amplification can be better understood by analyzing the cross-shore evolution of the previously defined ratio $A_{Shoal} = H_{s-in} / H_{s-shoal}$, for each resonant mode and H_{off}. If this ratio is higher than one, it means that the wave height is increasing towards the coast with a proportion larger than the corresponding shoaling coefficient.

Figure 4.6 shows how smaller wave heights have a stronger amplification ratio, A_{Shoal}, than higher waves. This behavior is more distinguishable in the fundamental mode (top Figure 4.6) than on the first mode (bottom Figure 4.6). For T_1, the differences between A_{Shoal} for different H_{off} are considerably smaller than for T_0. The highest wave (H_{off} = 1.5 cm) with period T_1 (bottom Figure 4.6), shows peaks on the A_{Shoal} cross-shore evolution offshore of the reef crest. These instabilities were also present in the corresponding H_s cross-shore evolution, and cannot be explained at this stage.

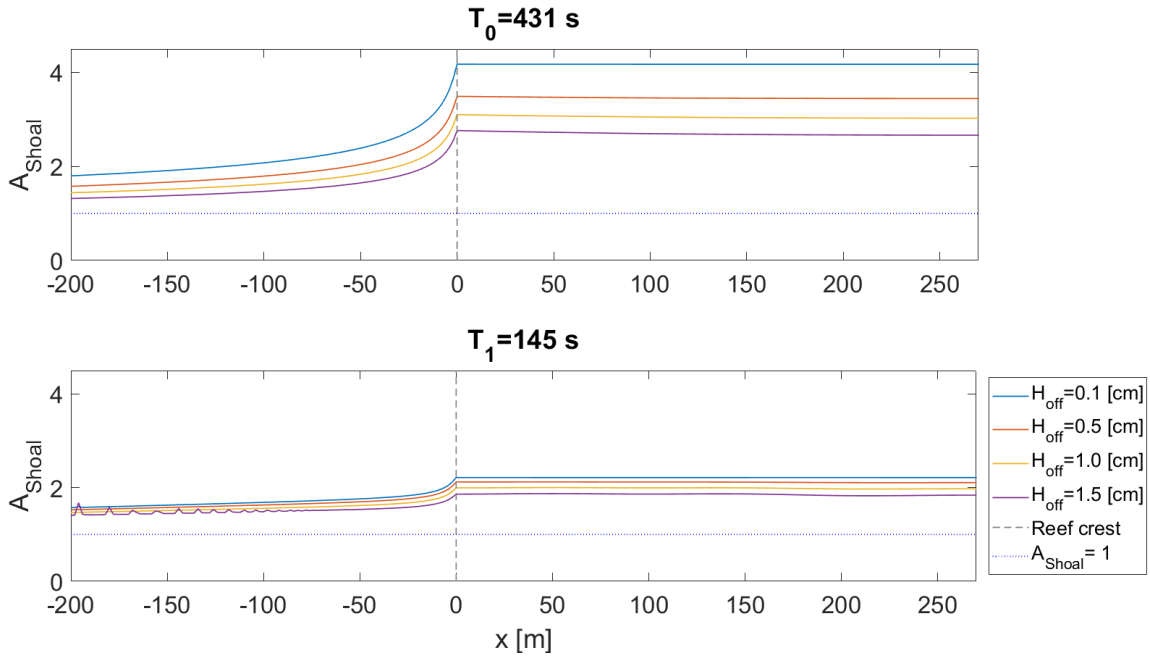

Figure 4.6: Stationary normalized significant wave height ($A_{Shoal} = H_{s-in} / H_{s-shoal}$) cross-shore evolution for different offshore wave heights for the first two resonant modes T_0 and T_1 (x = 0 m indicates the reef crest and x = 270 m, right end of the figure, the beach toe). In this analysis d_r = 0.8 m.

Non-linear wave shapes over the reef could explain the reduction of the amplification ratios with increasing wave height. Moreover, these non-linearities could be responsible for the amplification ratios variations between waves with the same H_{off} and different resonant modes (T_0 or T_1). Differences between the wave shapes of the incoming wave (η_{in}) and the outgoing wave (η_{out}) re-reflected at the reef crest are expected to determine the resonance effectiveness. This non-linear analysis is carried out based on wave skewness (Equation 3.5) and wave asymmetry (Equation 3.6) parameters.

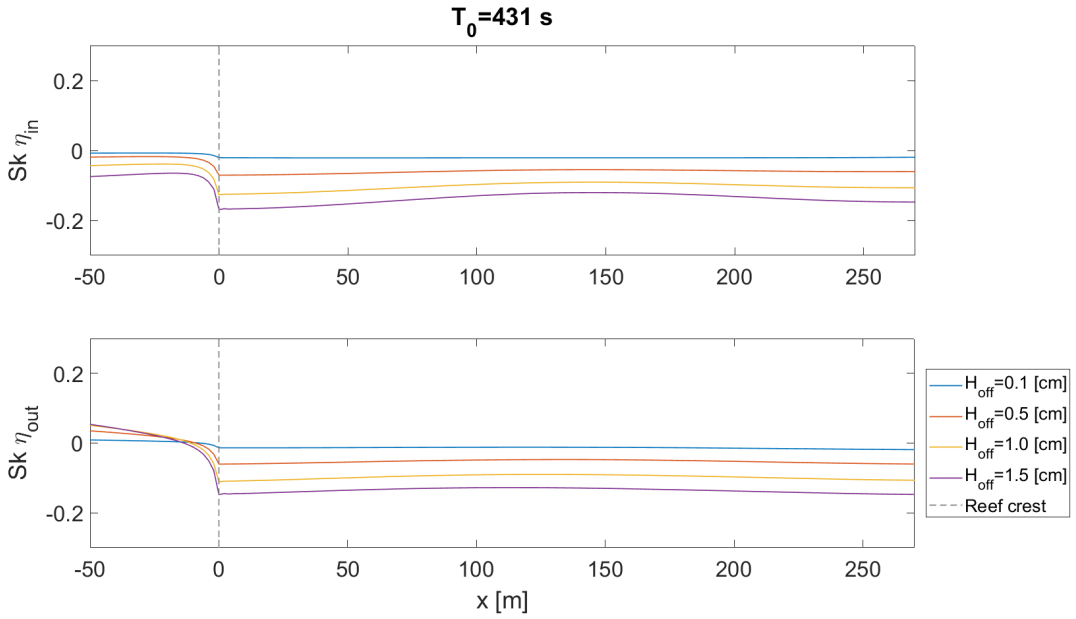

Figure 4.7: Wave skewness (Sk) of incident and reflected surface elevation for T_0 = 431 s ($x = 0m$ indicates the reef crest and $x = 270m$ the beach toe). The reef flat water depth is d_r = 0.8 m.

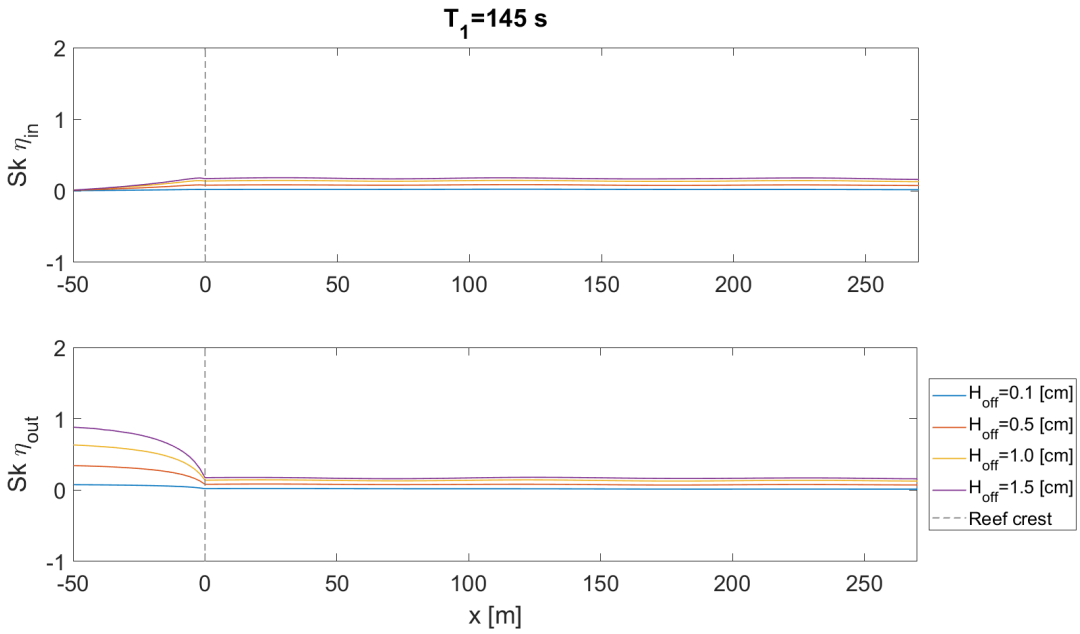

Figure 4.8: Wave skewness (Sk) of incident and reflected surface elevation for T_1 = 145 s ($x = 0m$ indicates the reef crest and $x = 270m$ the beach toe). The reef flat water depth is d_r = 0.8 m.

Skewness (Sk) is related to the wave asymmetry with respect to the horizontal axis. A positive value indicates that wave crests (the highest point of a wave) are bigger than troughs (the lowest point of a wave), and negative skewness defines the opposite. Figures 4.7 and 4.8 show skewness of η_{in} and η_{out} for T_0= 431 s and for T_1= 145 s respectively (resonant periods for d_r = 0.8 m). For the fundamental period, skewness persisted being negative for the incident and outgoing waves except for η_{out} seawards of the reef crest where it changes to a positive value. For T_1, skewness has a positive value for incoming and outgoing waves during the whole domain. The skewness magnitudes of waves with period T_0 are limited to the surroundings of zero, reaching a maximum negative value around -0.2 for the higher wave (H_{off} = 1.5 cm). Waves with period T_1 presented the largest values of skewness mainly offshore of the reef crest, reaching a maximum close to unity for H_{off}

= 1.5 cm. Summarizing, wave skewness increases with increasing wave height, and presents similar values of Sk_{in} and Sk_{out} within the same period and H_{off}. Thus, due to this similarity, the increase in wave skewness when increasing H_{off} is not expected to reduce the resonant amplification.

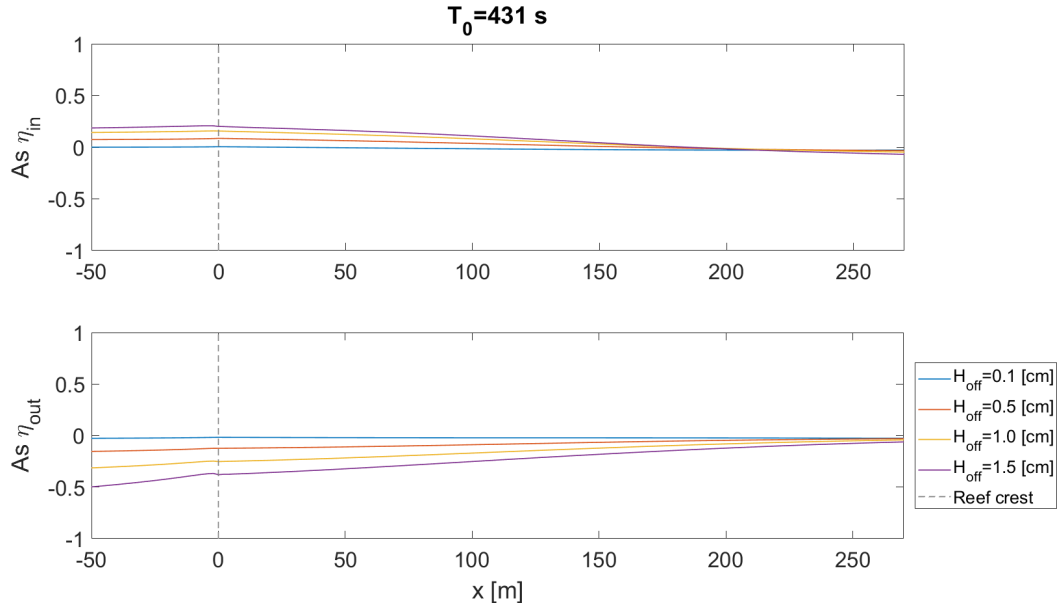

Figure 4.9: Wave asymmetry (As) of incident and reflected surface elevation for T_0 = 431 s ($x = 0m$ indicates the reef crest and $x = 270m$ the beach toe). The reef flat water depth is d_r = 0.8 m.

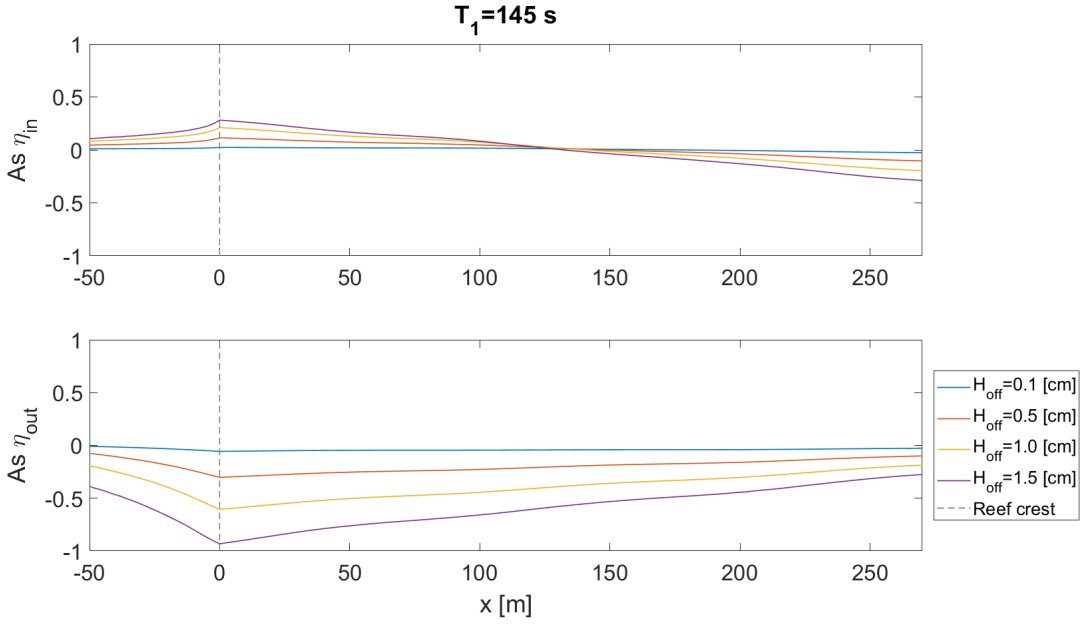

Figure 4.10: Wave asymmetry (As) of incident and reflected surface elevation for T_1 = 145 s ($x = 0m$ indicates the reef crest and $x = 270m$ the beach toe). The reef flat water depth is d_r = 0.8 m.

Asymmetry (As) is a wave shape comparison for the vertical axis and relates with the pitched-forward wave shape. A negative asymmetry indicates a rear face with a gentle slope and a steeper front face, also known as a sawtooth-like wave shape. Figures 4.9 and 4.10 show the computed asymmetry of η_{in} and η_{out} for T_0= 431 s and for T_1= 145 s respectively (resonant periods for d_r = 0.8 m). For the fundamental period, the incident wave has a small positive asymmetry that changes to negative values around x = 200 m (after the

middle reef flat x = 135 m). For this same period, the outgoing wave has negative asymmetry values, which increase seaward. T_1 asymmetry behaves similarly concerning the sign for both incoming and outgoing waves. The main difference between the two periods is that the first resonant period reaches larger asymmetry values. Also, for η_{in}, the change of sign occurs closer to reef crest (x = 100 m). Additionally, the asymmetry of η_{out} increases towards the sea until the reef crest, where it starts reducing.

Waves under the first resonant mode develop larger asymmetries than with the fundamental mode for the same H_{off}, which could explain the stronger amplifications experienced by the fundamental mode. For both resonant modes, the magnitude of asymmetry is larger for both incident and outgoing waves with larger wave heights. Also, for both resonant periods, η_{out} presents a stronger asymmetry than η_{in}, which shows that incident waves steepen across the reef flat, and keep steepening after being reflected at the beach.

Resonating waves start developing non-linear wave shapes with increasing H_{off} and showing stronger asymmetry differences (in magnitude and sign) between η_{in} and η_{out}, which could lead to smaller resonant amplification ratios. The difference in wave asymmetry between η_{in} and η_{out} could have an impact on the resonance effectiveness, which could explain the reduction of resonant amplification with increasing H_{off}, and consequently increasing wave non-linearities. A relation between incoming/outgoing wave shapes and resonant amplification is expected to happen because, outgoing waves will be (fully or partially) reflected at the reef crest, and likely resonate with incoming waves.

The difference in asymmetry (ΔAs) between η_{out} and η_{in} was studied at the reef crest ($\Delta As = As_{out} - As_{in}$), because is the location experiencing stronger absolute differences between As_{out} and As_{in}. This analysis was done for both modeled reef flat water depth, and the first two resonant modes (Figure 4.11). ΔAs showed that independently of the period and reef flat water depth, the asymmetry of the outgoing wave is negative and larger, in absolute value, than the asymmetry of the incoming wave. It also showed that, as already stated before, for the same d_r and H_{off}, waves with period T_1 steepen more over the reef flat than waves with the fundamental period. Additionally, when comparing the same resonant mode for different water depths, ΔAs is always larger in magnitude for smaller water depths. At the same time, the resonant amplification is stronger for smaller water depth (Figure 4.3). Thus, it could be said that for a given depth, the most amplified waves are those who have the most linear shape. However, it could not be proved that the magnitude of the resonant amplification is directly linked with the value of ΔAs. Because even when it has been shown that resonant amplification reduces with increasing ΔAs, waves under shallower reef flat water depths are, at the same time, more non-linear and more amplified than under larger water depths conditions.

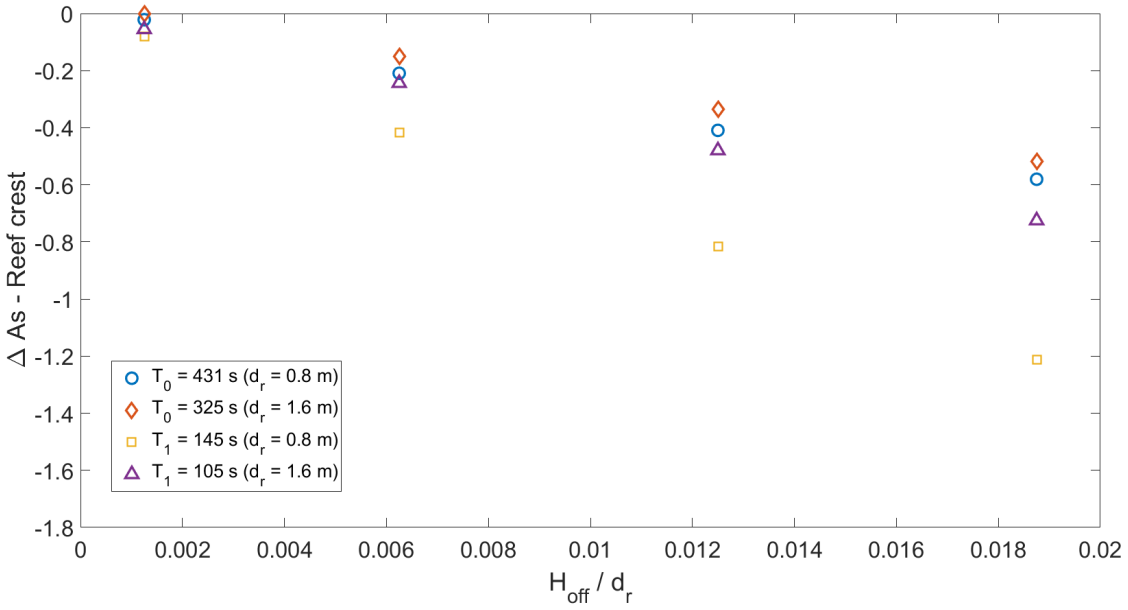

Figure 4.11: Variation of wave asymmetry between outgoing and incident surface elevation ($\Delta As = As_{out} - As_{in}$). ΔAs was computed at the reef crest (x = 0 m), for two different reef flat water depth (d_r) and their specific first two modeled resonant modes (T_0 and T_1).

The reduction of the resonant amplification with increasing H_{off} could also be influenced by a detuning from the most resonant wave period, which is defined as the wave period that leads to the largest wave height and run-up amplification computed respectively with ratios A_H and A_R. To understand if there is a shift of the modeled resonant period when varying wave height, A_H and A_R ratios were computed for waves with different H_{off}, and with periods neighboring the fundamental mode T_0 = 431 s (for d_r = 0.8 m). This analysis (Figure 4.12) showed that for small H_{off} the most resonant period slightly shifted inside the resonant bandwidth found in Figure 4.1. In this numerical experiment, slightly shorter resonant periods were observed for smaller waves, and slightly longer resonant periods for larger wave heights. This period shift can be observed when comparing the values of A_H for the same H_{off} and different periods, where for example H_{off} = 0.5 cm experiences the largest wave height amplification (A_H) with a wave period of T = 425 s, whereas H_{off} = 1.5 cm amplifies more with T = 437 s. The differences in resonant amplifications are not noticeable when comparing A_R values, because run-up variations due to resonant period detuning are smaller than the run-up resolution (ΔR = 1.6 cm). Thus, it could be said that the impact of period detuning on flooding due to resonant amplification, is considerable low under the scenario of small amplitude long waves.

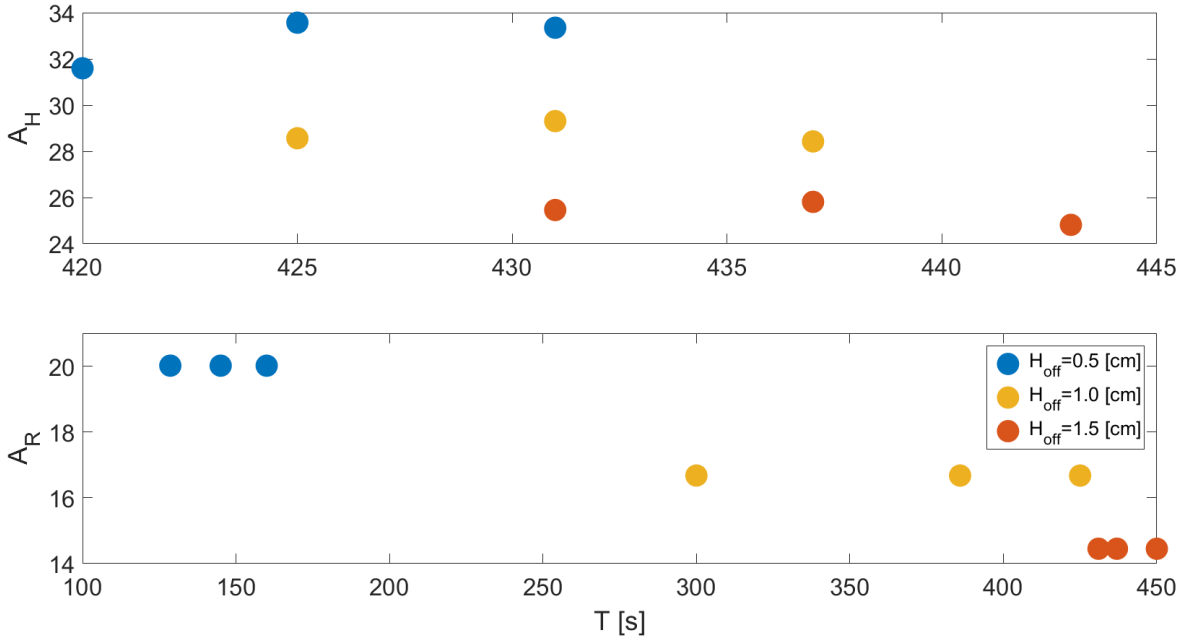

Figure 4.12: Variation of the fundamental resonant period due to offshore wave amplitude influence on A_H (upper figure) and A_R (bottom figure). For every case d_r = 0.8 m.

4.4. Resonant build-up behavior

According to literature, long waves over a reef flat can experience resonant amplification when their frequency matches one of the reef natural frequency, studied in the previous sections, and when there is sufficiently resonating wave energy trapped over the reef flat. The wave energy trapping process for a constant wave forcing starts with minimum energy, and gradually builds up until reaching a maximum resonant amplification or an equilibrium state (Nwogu and Demirbilek (2010), Guza and Bowen (1976)). The wave resonance build-up can be observed for resonant periods on the water level η (Figure 4.13) and run-up R (Figure 4.14) time series, where both resonant time-series become stationary after reaching a maximum resonant amplification. The run-up time series presents a staircase shape due to its resolution of ΔR = 1.67 cm. To have a more continuous run-up signal a finer grid resolution is needed, which implies a higher computational cost due to the lack of a locally refine grid option in a 1D SWASH model.

A resonant build-up behavior was present in this experiment for the first two resonant modes (T_0 = 431 s and T_1 = 145 s for d_r = 0.8 m). This behavior was observed to be faster in both η and R for the first resonant mode than for the fundamental period. However, the number of waves needed for both periods to become stationary is the same. Both modes need 14 waves for an H_{off} = 1 cm (Table 4.2). Waves with non-resonant

period (T = 120 s, T = 200 s,T = 300 s and T = 500 s), do not experience a build-up behavior neither in the η signal nor in the run-up signal. Moreover, the time needed to reach stable conditions was found to be longer for non-resonant periods than for resonant periods. For example, T_0 = 431 s reaches stationary conditions after 4920 s, T = 300 s after 6600 s, and T = 500 s after 7900 s.

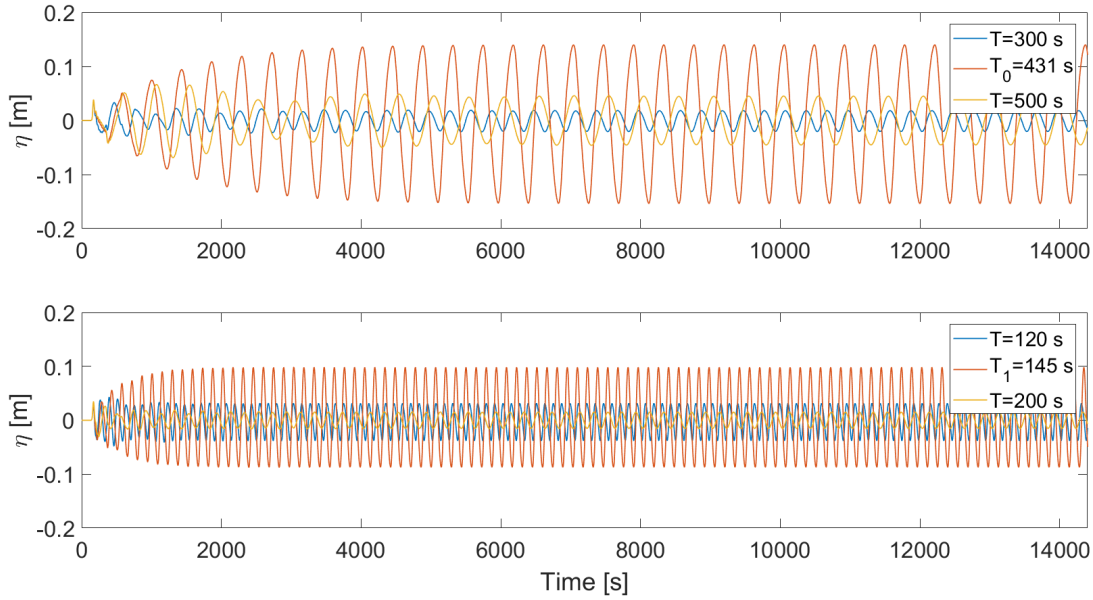

Figure 4.13: Resonant build-up behavior of the beach toe water level (η) time series for d_r = 0.8 m. Top figure includes the reef fundamental resonant period T_0 = 431 s and neighboring periods. Bottom figure includes the reef first resonant period T_1 = 145 s and neighboring periods.

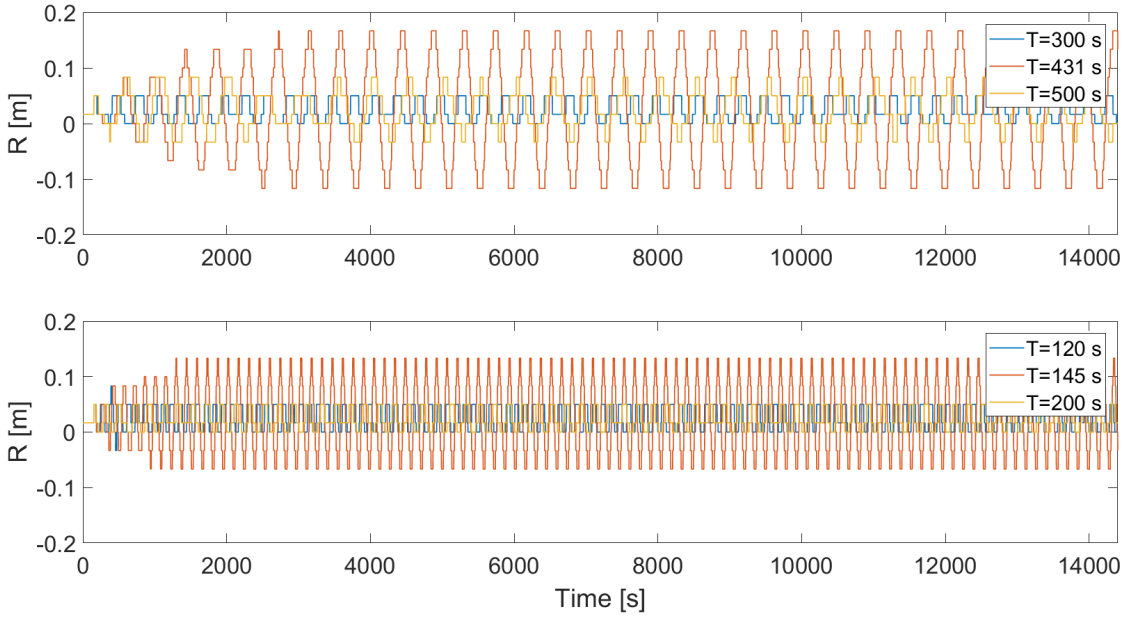

Figure 4.14: Resonant build up behavior of the run-up (R) time series for d_r = 0.8 m. Top figure includes the reef fundamental resonant period T_0 = 431 s and neighboring periods. Bottom figure includes the reef first resonant period T_1 = 145 s and neighboring periods

The resonant build-up behavior for different wave heights was analyzed by studying the wave height time evolution at the beach toe. To quantify how many waves are needed to build-up resonance until the maximum amplitude, a ratio ($A_{N°}$) was computed between the wave height of each wave reaching the beach toe, calculated through zero down crossing technique, and the maximum wave height by resonant period

reached under stationary conditions ($A_{N°}$ = $H_{beachtoe}$ / $H_{beachtoe-max}$). When this ratio $A_{N°}$ reaches the unity, it shows that the wave reached its maximum resonant wave height amplification and consequently an equilibrium state (dots Figure 4.15).

Figure 4.15 reflects how, for d_r = 0.8 m, smaller wave heights need more waves reaching the reef to build up resonance until an equilibrium state, whereas larger wave heights can reach a steady state with fewer waves. Similar results were found for d_r = 1.6 m, which can be seen in Appendix C (Figure C.1). The dependence between the number of waves needed to fully resonate and H_{off}, is stronger for the fundamental period (top Figure 4.15) than for the first mode (bottom Figure 4.15). This stronger dependence can be clearly noticed when comparing the number waves needed for the highest wave (purple dots Figure 4.15) and for the smaller wave (blue dots Figure 4.15) between both resonant periods, this comparison shows a larger difference between the minimum and maximum number of waves for T_0 than for T_1.

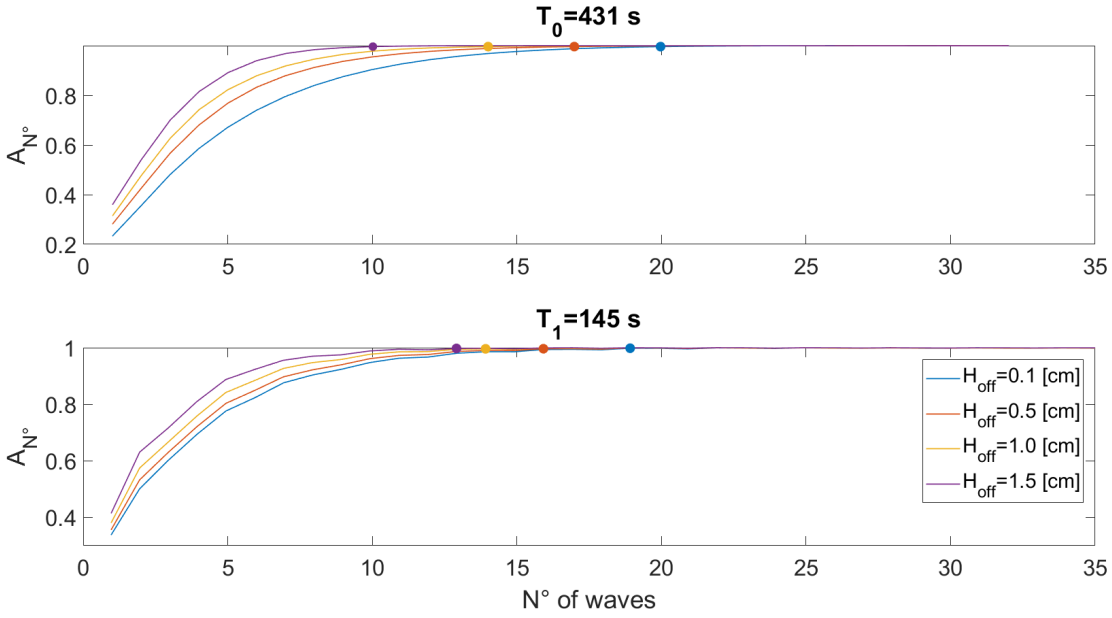

Figure 4.15: Number of waves needed to build-up a maximum wave height resonant amplification at the beach toe for different H_{off} and resonant modes. Top figure shows $A_{N°}$ per individual wave height for the fundamental mode T_0. Bottom figure shows $A_{N°}$ per individual wave height for the first mode T_1. This analysis was done for d_r= 0.8 m

The exact number of waves needed to reach a stationary resonant state for the different resonant modes, water depths, and incident offshore wave heights studied, can be seen in Table 4.2. The different H_{off} between d_r = 0.8 m and d_r = 1.6 m were chosen to maintain the H_{off}/d_r relation. For d_r = 0.8 m waves with the same height but different resonant modes reach a steady resonant state with a similar amount of waves. Hence, as the fundamental mode has a longer period, it needs more time to fully build up resonance (duration in Table 4.2) than T_1. Additionally, the number of waves needed to build up resonance, for the same H_{off} and different resonant modes, is similar but not equal. Higher waves reach maximum resonance with fewer waves for the fundamental mode, while smaller waves reach maximum resonance with fewer for the first mode. This difference, minimum with 1 cm of wave height, can be seen by comparing the different behavior of H_{off} = 0.1 cm and H_{off} = 1.5 cm for the first two resonant periods. The smallest wave rise to a ratio of $A_{N°}$ equals to one with fewer waves for T_1 and more waves for T_0, whereas the highest wave reaches $A_{N°}$ equals to one with fewer waves for T_0.

For the case of d_r = 1.6 m, waves with the same H_{off} reach a resonant equilibrium state with fewer waves with the first resonant period than with the fundamental one. Moreover, T_0 behaves similar to the resonant periods with d_r = 0.8 m, with a decreasing number of waves needed as the wave height increases. However, waves under the first mode build up resonance with the same number of waves independently of H_{off}. Thus, the results suggest that T_1 build-up time is less dependent on the offshore wave height than T_0, decreasing this dependence with increasing d_r.

Table 4.2: Number of waves needed to reach the maximum resonant wave height (dots Figure 4.15. Different wave heights are considered for the two modes T_0 and T_1 for d_r = 0.8 m

d_r (m)	H_{off} (cm)	Duration (T_0)	Duration (T_1)	$N°$ of waves (T_0)	$N°$ of waves (T_1)
0.8	0.1	2 h 23 min	46 min	20	19
	0.5	2 h	39 min	17	16
	1.0	1 h 41 min	34 min	14	14
	1.5	1 h 12 min	31 min	10	13
1.6	0.2	1 h 32 min	9 min	17	5
	1.0	1 h 26 min	9 min	16	5
	2.0	1 h 16 min	9 min	14	5
	3.0	1 h	9 min	11	5

The relation between the resonant build-up time, the reef flat water depth, and the H_{off} vary more for the fundamental mode than for the first resonant mode. Figure 4.16) present the number of waves needed to build-up resonance under the fundamental mode, for different d_r and the same H_{off}/d_r relation. As already stated before, smaller waves need more waves to resonate with a maximum resonant amplification than higher waves. Figure 4.16 also shows that smaller waves (small H_{off}/d_r) resonate with fewer waves for larger d_r, whereas higher waves reach full resonance with fewer waves for smaller reef flat water depths. However, the number of wave differences between both d_r for the fundamental mode, are not big enough to make a difference in the time needed to reach a maximum resonant amplification, being this time always shorter for increasing water depths (duration in Table 4.2).

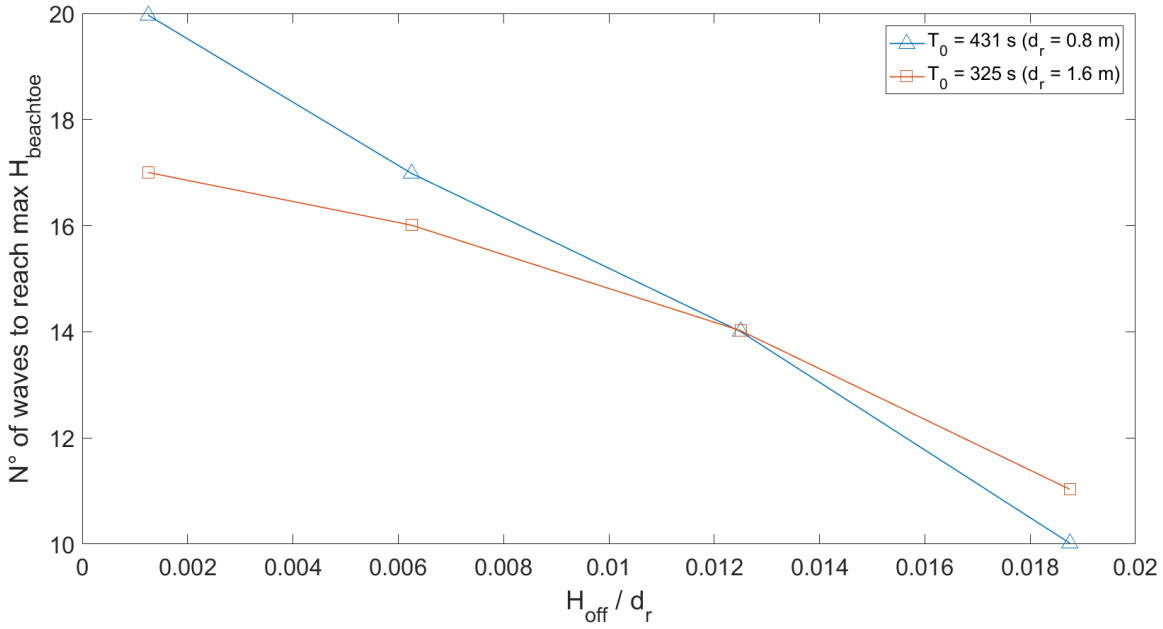

Figure 4.16: Number of waves needed to reach the maximum wave height at the beach toe. The waves are resonating with the respective fundamental mode, for two different reef flat water depth (d_r).

4.5. Influence of reef energy balance

The wave height and run-up resonant amplification are likely related to the amount of low-frequency energy trapped and dissipated over the reef. As the energy balance must be fulfilled, the wave energy trapped and or dissipated over the reef must be equal to the difference between the incoming and outgoing energy fluxes at the reef crest. The process of trapping wave energy over the reef is likely to have a build-up behavior, similar to the build-up behavior experienced by the surface elevation (Figure 4.13) and run-up (Figure 4.14) signals.

Thus, it is expected that the maximum amount of trapped wave energy over the reef occurs when reaching stationary conditions. In order to keep this maximum stationary energy value in time, with a constant forcing, is likely that the wave energy dissipated over the reef, due to for example bottom friction, is balanced by a continuous wave energy trapping process.

To understand if the reef energy balance influences the resonant amplification, energy fluxes were analyzed for cases with and without bottom friction for different wave periods and wave heights. Models including bottom friction were analyzed to understand the impact of bottom friction on the reef energy balance, and frictionless models were studied to understand the process of trapped wave energy.

4.5.1. Influence of friction on resonant amplification

The magnitude of the stationary dissipated wave energy, can be visualized through the cross-shore evolution of the ratio between the seaward (F_{out}) and shoreward (F_{in}) stationary energy flux (Figure 4.17), where a flux is taken as stationary after the surface elevation envelope slope is lower than $10^{-}6$. An energy flux ratio (F_{out}/F_{in}) smaller than one indicates a larger amount of energy coming in than going out.These energy fluxes were calculated based on Sheremet et al. (2002) (Equation 3.8).

Non-resonant periods in the range of the fundamental resonant one (top Figure 4.17) present a flux ratio close to one over the whole domain. The fundamental resonant period and close frequencies have values close to the unity only over the reef flat, reaching one at the beach toe. Offshore of the reef crest F_{out}/F_{in} decreases, reaching values between 0.6 and 0.8. The smallest energy flux ratio offshore of the reef corresponds to T_0. The periods in the range of the first resonant mode (bottom Figure 4.17) do not show a large cross-shore variation of energy flux ratios. These ratio values were limited between 0.9 and 1 for resonant and non-resonant periods, with the non-resonant periods close to one over the whole domain. The difference in the energy flux ratio values between the fundamental and first resonant mode could explain the largest amplification ratios experienced by waves with a period T_0, with larger resonant amplification leading to stronger frictional dissipation over the reef flat; thus, smaller F_{out}/F_{in} values.

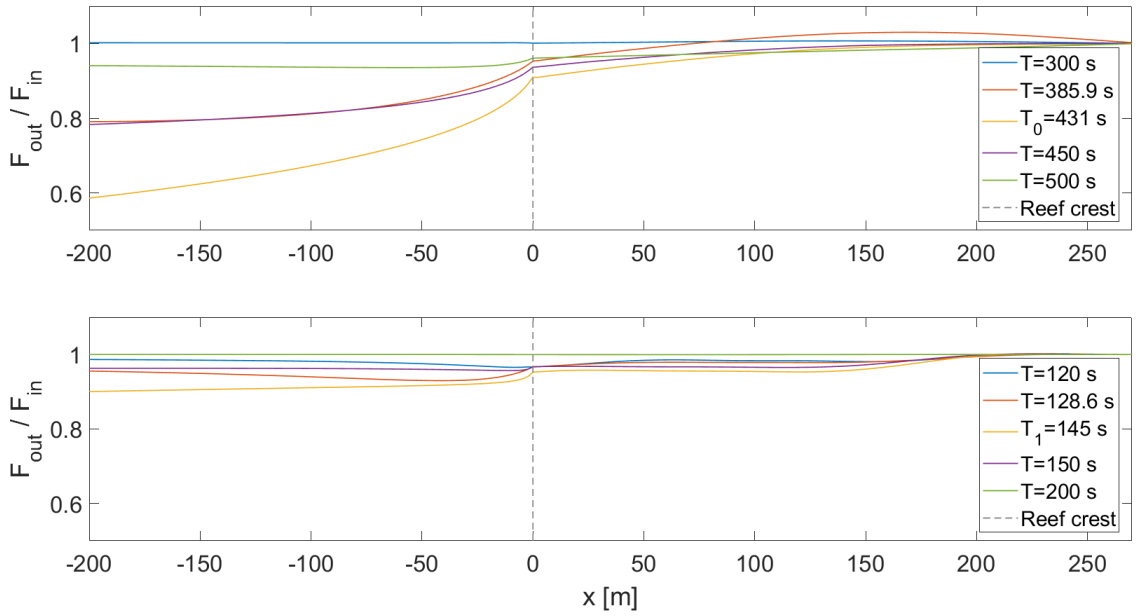

Figure 4.17: Stationary energy flux ratio F_{out}/F_{in} cross-shore evolution for different wave periods x = 0 m indicates the reef crest and x = 270 m, right end of the figure, the beach toe for the model with bottom friction.

The effect of friction on the wave height and maximum run-up resonant amplification was investigated by comparing the results of a frictionless and low friction bottom (Figure 4.18). The low friction bottom has a Manning friction coefficient of n = 0.01 $s/m^{1/3}$, which is similar to smooth plastic material. This analysis

showed that even low values of bottom friction could decrease the wave height and maximum run-up resonant amplification. The impact of this reduction was observed to be stronger for the fundamental mode than for the first resonant mode. The fundamental mode with frictional bottom can present a 26% smaller resonant wave height, and 23% smaller resonant maximum run-up than frictionless bottoms. The first mode experiences less than 5% reduction on the wave height, and no reduction was observed on the maximum run-up. For both resonant periods, the resonant amplification decreased without shifting the modeled resonant period. Thus, data suggest that bottom friction reduces resonance without changing the most resonant period. The frictional dissipation of non-resonant periods, like T = 200 s and T = 385.9 s, is insignificant (less than 0.05%), which can be seen in the almost unchanged values of $H_{beachtoe}$ and R_{max}.

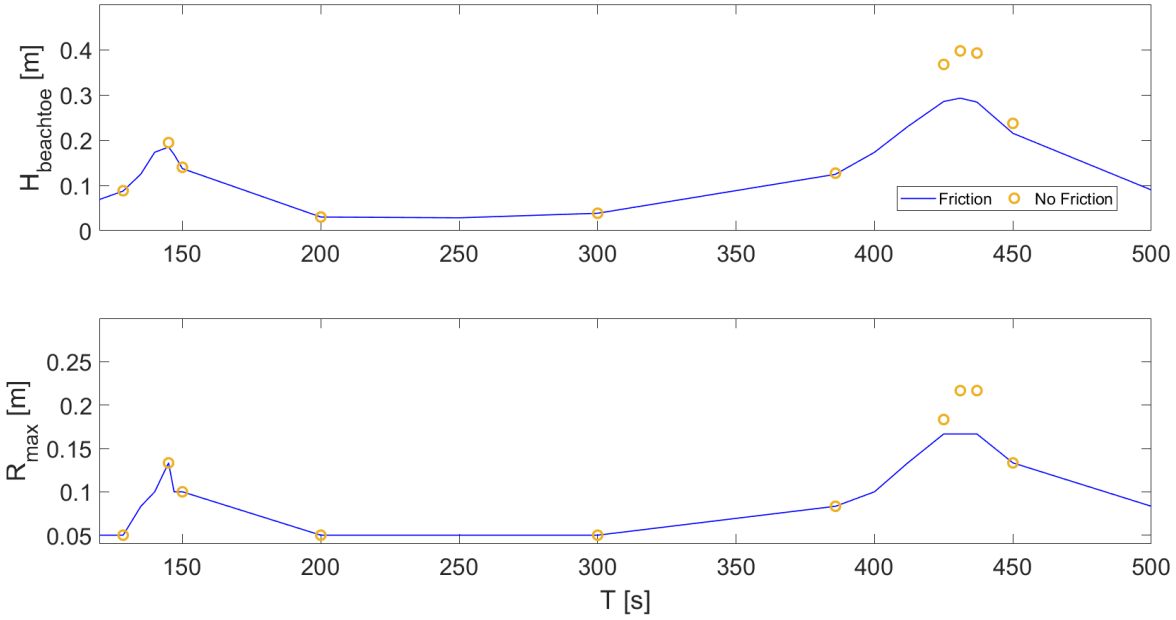

Figure 4.18: Beach toe wave height $H_{beachtoe}$ (top figure) and maximum run-up R_{max} (bottom figure) for different wave periods. The solid line indicates a model with friction, and the circles a model without friction. For every period H_{off} = 1 cm and d_r = 0.8 m.

The impact of friction on the resonant amplification can be better understood by comparing for the same H_{off} the incoming and outgoing energy flux between a resonant period (modeled fundamental period T_0), and a non-resonant period (fundamental theoretical period T_0^*). Figure 4.19 from (a) to (d) presents the incident and outgoing energy flux, respectively F_{in} and F_{out}, time evolution at the reef crest for frictionless bottoms,(a) and (c), and models considering low bottom friction, (b) and (d). These time evolution energy fluxes were calculated based on Madsen et al. (1997) (Equation 3.9), and the resulting signal was average with a moving window of size equal to the corresponding wave period. Figure 4.19 (e) shows the cross-shore evolution of F_{out} / F_{in} ratio for periods T_0^* and T_0 with and without friction, under stationary conditions (Figure 4.19 - e). These stationary energy fluxes were computed based on Sheremet et al. (2002) (Equation 3.8).

For frictional and frictionless bottoms, the outgoing energy flux time evolution (a-d) presents a time delay compared to the incoming flux, starting F_{out} to have values larger than zero around 200 seconds after F_{in}. This delay, which is similar for all the periods, is related to the time needed for the wave to travel onshore, get reflected at the beach, and travel back until the reef crest. At the beginning of the numerical modeling, incoming and outgoing energy fluxes experience an energy flux growth, which, when comparing per single wave is faster for the resonant period than for the non-resonant period (not shown). Moreover, T_0 energy fluxes keep increasing until reaching a maximum stationary value, whereas non-resonant period T_0^* energy fluxes start decreasing after approximately 2000 s. The stationary energy flux magnitudes are larger for resonant than non-resonant periods, which is especially noticeable when comparing the frictionless cases where T_0 energy fluxes are around ten times larger than T_0^* energy fluxes.

Models without friction present larger energy fluxes than models with friction for the same period. The

reduction of energy fluxes due to friction can be seen by comparing Figures 4.19 (c) and (d), where T_0 energy fluxes decrease around 50% when including friction in the model. Friction dissipation is lower for the non-resonant period T_0^*, with a 1.7% reduction of the stationary energy flux compared to the frictionless case (a). Furthermore, in every case (a-d) F_{in} is larger than F_{out} for at least a certain time. For T_0^*, the difference between the incoming and outgoing energy flux is more noticeable under non-stationary conditions (t = 0 - 6000 s). In contrast, for the modeled resonant period T_0, F_{in} is larger than F_{out} during the entire time. Stationary F_{in} and F_{out} for frictionless cases, are equal for the non-resonant period T_0^* and the resonant period T_0.When including friction, the difference between the incoming and outgoing fluxes increases. This difference, is roughly 4% for T_0^* (Figure 4.19 - b), and 9% for T_0 (Figure 4.19 - d) at the reef crest.

Thus, as already seen in Figure 4.18, resonant cases are more affected by friction, having a larger stationary flux magnitude reduction, and a larger difference between incoming and outgoing fluxes. The latter can be seen clearly in Figure 4.19 (e), which shows how the flux ratio is equal to one (or close to it) for frictionless cases, and smaller than one for models with friction. The non-resonant period reaches a minimum F_{out}/F_{in} of 0.8 offshore of the reef crest, approaching one seawards of this minimum point. On the contrary, for the resonant case F_{out}/F_{in} reduces seawards of the reef crest, reaching a minimum value of 0.16 at the end of the domain (x = -2000).

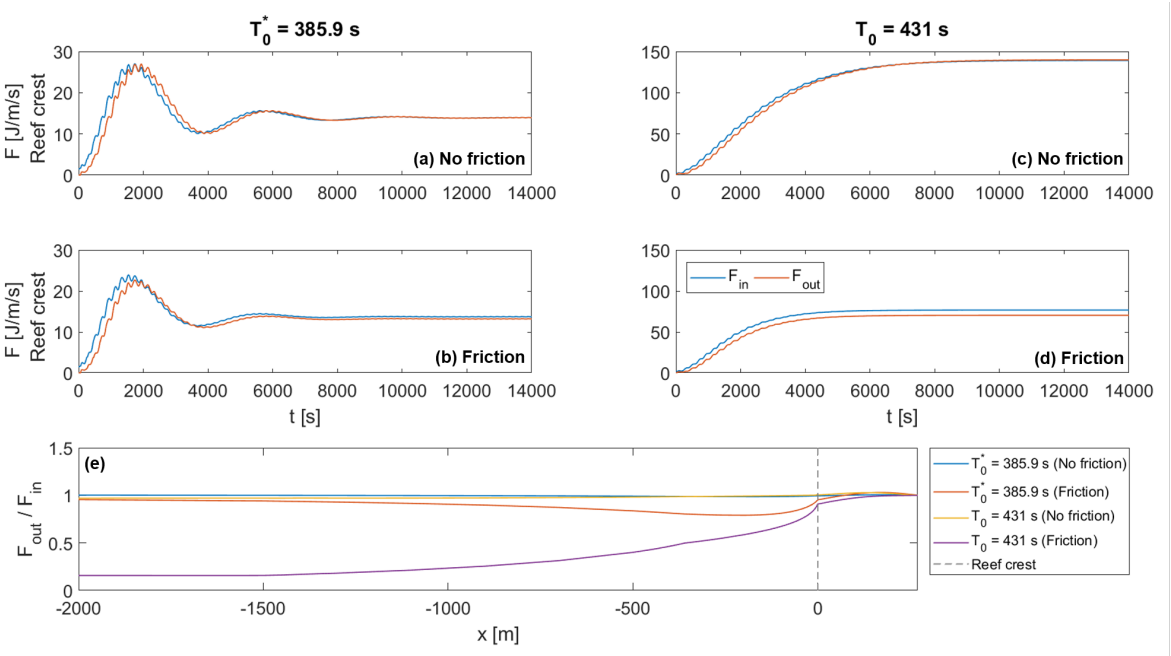

Figure 4.19: Energy flux time evolution at the reef crest, for incident and outgoing waves (a-d). This considers models without friction (a,b), and with friction (c,d). The cross-shore evolution of the reflection squared ratio (F_{out}/F_{in}), for stationary conditions, is shown in (e) for friction and no friction models. These figures compare the theoretical fundamental period T_0^* = 385.9 s (non-resonant) and the modeled fundamental period T_0 = 431 s (resonant). For every case H_{off} = 1 cm and d_r = 0.8 m.

4.5.2. Influence of trapped wave energy on resonant amplification for frictionless cases

The amount of trapped wave energy ($\Delta\mathscr{F}$) was computed as the integration in time of the difference between the incoming and outgoing energy flux of bottom frictionless cases ($\Delta\mathscr{F} = \int(F_{in}(t) - F_{out}(t))dt$). The energy fluxes were calculated based on Madsen et al. (1997) methodology (Equation 3.9), and an example can be observed in Figure 4.19 (a) and (b) (frictionless bottom). The variation of ΔF at the reef crest with wave periods can be seen in Figure 4.20, where the previously defined A_{Shoal} ratio (Equation 4.3) represents the resonant amplification. This analysis showed that larger $\Delta\mathscr{F}$ values lead to larger A_{Shoal} ratios. The correlation between the amount of trapped wave energy and the resonant amplification was found to be high and positive with a correlation coefficient of R^2 = 0.9897 (Appendix C, Figure C.8).

Figure 4.20, as Figure 4.1, presents a two peaks behavior where for each peak the maximum $\Delta\mathscr{F}$ occurs with the modeled resonant periods for d_r = 0.8 m (T_0 = 431 s, and T_1 = 145 s). Waves with these resonant periods also experience the maximum resonant amplification inside each resonant peak, which suggests that the modeled resonant periods are more efficient than neighboring periods in trapping wave energy over the reef for the same H_{off}. This larger energy wave trapping capacity is likely the cause that T_0 and T_1 experience stronger resonant amplifications than periods immediately close to them. Furthermore, it can be observed that the fundamental mode peak (right peak Figure 4.1) shows larger values of trapped wave energy than the first resonant mode peak (left peak Figure 4.1). This difference of energy trapped over the reef could explain the stronger resonant amplifications observed for T_0 and neighboring periods, than for the periods within the bandwidth of the first resonant mode.

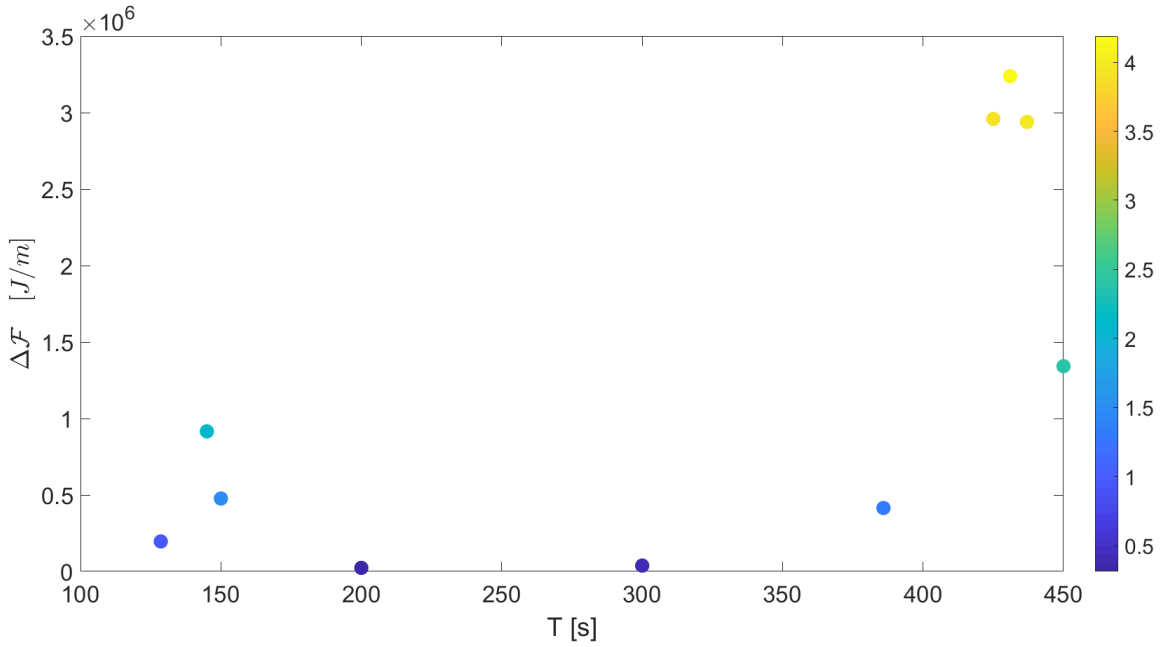

Figure 4.20: Relation between the amount of trapped wave energy ($\Delta\mathscr{F} = \int(F_{in}(t) - F_{out}(t))dt$) at the reef crest and the amplification ratio A_{Shoal} for different wave periods. The analysis was done with frictionless models, H_{off} = 1 cm, and d_r = 0.8 m.

The correlation between the amount of trapped wave energy and the corresponding resonant amplification was also studied for the fundamental resonant period under different d_r and H_{off} conditions. To remove the influence of the offshore wave height on the amount of trapped wave energy ($\Delta\mathscr{F}$), $\Delta\mathscr{F}$ was normalized by the time-integrated incoming energy flux ($\mathscr{F}_{in} = \int F_{in}(t)dt$). Figure 4.21 shows a similar tendency as Figure 4.20, where stronger resonant amplifications (A_{Shoal}) are related with a larger amount of trapped wave energy. However, the stronger resonant amplification is not necessarily the one with the larger relative amount of trapped wave energy, as it was seen in Figure 4.20. Thus, other processes must be playing a role, such as the influence of non-linear wave shape or a shift of the period from the natural frequency due to H_{off} influence (Figure 4.12). Also interesting is to note that $\Delta\mathscr{F}/\mathscr{F}_{in}$ can be understood as the percentage of the incoming energy that is trapped over the reef flat, which for every modeled case is smaller than 2%. Thus, the percentage of the incoming energy trapped over the reef is small, being the majority radiated to the far-field.

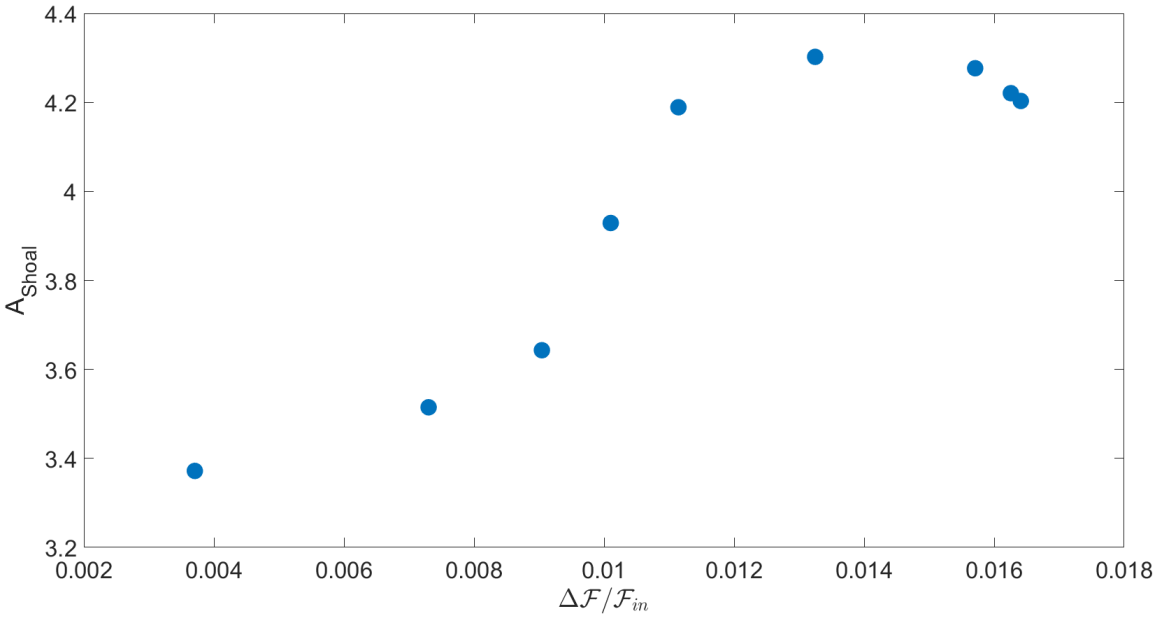

Figure 4.21: Relation between the normalized trapped wave energy ($\Delta\mathscr{F}/\mathscr{F}_{\backslash} = \int(F_{in}(t) - F_{out}(t))/\int(F_{in}(t))dt$) at the reef crest and the amplification ratio A_{Shoal}, for the fundamental resonant mode. The analysis was done with frictionless models, for different H_{off} and reef flat water depths (d_r = 0.8 m, and d_r = 1.6 m).

5

Discussion

In this chapter, the limitations of this thesis resonant experiments, the key findings, and possible future research topics are discussed. This resonance study was carried out over a fringing reef with SWASH numerical model. A cross-shore profile (1D model) of a schematized fringing coral reef was built, and wave resonance was forced over this bathymetry for the first two resonant modes.

In order to understand the most basic case of wave resonance on a reef, the offshore forcing was designed as a simplified wave climate with small amplitude regular low-frequency waves. The key findings of these numerical experiments are:

- The modeled natural resonant periods, T_0 and T_1, are longer than the theoretical periods T_0^* and T_1^*. The difference between the modeled and theoretical resonant period (ΔT) varied per resonant mode and d_r, with maximum differences found for both modes with d_r = 1.6 m. ΔT for T_0 was found to be 11.6% for d_r = 0.8 m, and 18.9% for d_r = 1.6 m. ΔT for T_1 showed smaller variations, being 12.8% for d_r = 0.8 m, and 15% for d_r = 1.6 m.

- For the cases studied, the shallower reef flat water depth had longer resonant periods, and larger resonant amplifications A_H and A_R than the deeper d_r. A_H was found to be up to 1.8 times larger and A_R up to 2 times larger for d_r = 0.8 m than for for d_r = 1.6 m.

- Resonance occurs inside a bandwidth of periods, with T_0 and T_1 the periods with the stronger amplification inside each resonant mode bandwidth. If considering the resonant bandwidth until a 25% reduction of the maximum amplification, the bandwidth around T_0 was found to be wider than the bandwidth around T_1 for d_r = 0.8 m. Because, a decrease of 25% of the resonant amplification was due to a period deviation of 4.4% for T_0 and 3.4% for T_1.

- The fundamental mode has larger $H_{beachtoe}$ and R_{max} amplifications than the first resonant mode, which respectively can reach 2.5 and 2 times larger values for the fundamental mode than the first mode.

- Smaller waves have a stronger relative amplification of $H_{beachtoe}$ and R_{max} than higher waves, with stronger differences for the fundamental mode. The smallest H_{off} can relative be amplified up to 1.6 times more on $H_{beachtoe}$, and up to 4.5 times more on R_{max} than the largest modeled H_{off} .

- Larger wave heights start developing non-linear wave shapes over the reef flat, increasing the differences between incoming and outgoing wave asymmetry (ΔAs). The maximum ΔAs difference between the minimum and maximum modeled H_{off} was found to be 24%, which corresponds to the scenario with T_1, H_{off} = 1.5 cm, and d_r= 0.8 m.

- Higher waves need fewer waves to reach a final steady resonant state than smaller waves. The maximum number of waves difference between the minimum and maximum H_{off} was found to be ten waves, which corresponds to the scenario with T_0 = 431 s, and d_r = 0.8 m.

- Stronger amplifications are related to more wave energy trapped over the reef flat, which relation was found to be 98.97% correlated within a comparison between different periods and the same H_{off}.

- Low bottom friction values can reduce $H_{beachtoe}$ and R_{max} resonant amplifications up to 26% and 23% respectively, when increasing friction from a smooth reef (frictionless) to a material similar to a smooth plastic ($n = 0.01\ s/m^{1/3}$).

5.1. Study limitations

A SWASH validation was carried out for a fringing coral reef based on laboratory experiments performed by Demirbilek et al. (2007). This validation showed the capability of SWASH to model coral reef hydrodynamics with an acceptable error using a 1D model. Moreover, SWASH was also effective in modeling resonance over coral reefs for different wave climate and water level scenarios.

The numerical experiments of this thesis are based on a simplified 1D bathymetry of a fringing coral reef. This cross-shore profile does not take into account processes such as 2D effects and directional wave spreading, which can give conservative predictions of run-up (Veldt 2019). Thus, according to literature (Van Dongeren et al. 2013), it is expected that the results of this thesis are overestimating the impact of resonance, and being more in the conservative side of a coastal safety assessment.

To fulfill the SWASH requirement of linear wave theory at the wavemaker, the reef profile (Figure 3.6) had to be deepened and extended. Offshore of the fore reef slope end (x = -360), the modeled profile was extended until x = -2000 m to reach a depth of 440 m below the reef platform, and to ensure 500 m of a flat bottom before the wavemaker. With these changes, the domain ended up having 2360 m of extension, which added to the chosen grid resolution of Δx = 10 cm lead to a high computational cost, and consequently a limited amount of simulations that could be carried out to answer the research questions.

The fine grid resolution was needed to understand variations of beach run-up between different periods and wave heights; because coarser grids did not show run-up signals differences for different wave climates. The large dimensional difference between Δx and the offshore water depth (minimum of 440.8 m for d_r = 0.8 m) made SWASH runs unstable for more than one vertical layer, which implied that all the results had to be computed with a depth-averaged model. Thus, differences of velocities directions and magnitudes for different locations in the water column, such as an undertow current, are not taken into account. However, differences between the results of depth-averaged models and higher vertical resolution models are not likely to be relevant under a small amplitude regular long wave scenario. A higher vertical resolution could be achieved if instead of a 1D model (in x and z direction), a 2D model (in x, y, and z direction) was built by repeating the cross-shore profile in the y direction at least two times. This 2D model will allow working with a non-uniform grid using onshore higher resolution and offshore lower resolution, which likely will make the deepest part of the model stable for more than one vertical layer.

The wave climate of this thesis is limited to regular low-frequency waves with small wave heights (0.1 cm to 3 cm). Thus, the interaction between short and long waves observed in nature is not considered. Moreover, typical reef hydrodynamic processes such as long wave generation and wave breaking are likely not present in this thesis. Long wave generation is not expected due to the absence of short waves, needed for the bound long waves generation mechanism, and the lack of incident wave height variation needed for generating waves through wave breakpoint oscillations. Low-frequency wave breaking over the reef is not expected to occur because a 1:6 beach slope sets a fully reflective regime for low-frequency waves (Cheriton et al. 2016). Moreover, for the frictional bottom case, wave breaking was not observed under the chosen resonant wave climates, which can be noted by analyzing the cross-shore evolution of the incident significant wave height. Figure 4.6 shows that the incident resonant wave height increases offshore of the reef crest and remains almost constant over the reef flat. Thus, even though the wave steepens while propagating over the reef flat, this steepening (Figures 4.9 and 4.10) did not reach the almost vertical wall needed for wave breaking in SWASH. For the case without bottom friction, larger wave asymmetries were observed than with the corresponding model, including bottom friction. These wave asymmetries were especially large for the outgoing wave, where the formation of undular bores could be observed close to the reef crest for the highest waves. However, even for the larger wave heights, the cross-shore evolution of the outgoing wave did not show a decrease. Thus,

wave breaking is likely not present over the reef under both frictionless and frictional cases.

The wave climate characterized by regular long waves with small wave amplitude was chosen to understand pure resonant amplification with a controlled forcing environment and to reduce as much as possible the development of non-linear wave shapes. Even though this simplified wave climate cannot be found by itself in nature, and the results cannot be directly applied to the real world, it gives an insight into the reef resonance behavior and the processes influencing it. For example, by modeling with this simplified wave climate, a resonant bandwidth of periods for different reef flat water depths could be identified, and the amplification for different wave heights could be estimated. This knowledge can help to predict possible resonant scenarios for a certain measured offshore wave group signal, which is correlated with the low-frequency energy over the reef (Gawehn et al. 2016), and to develop flooding early warning systems further. However, to reach this more research applied state further resonance studies with more realistic hydrodynamic conditions must be carried out, by forcing wave resonance on a reef for different d_r, and scaling in complexity from bi-chromatic waves to wave spectrum climates.

The range of H_{off} in this study was limited by the requirement of linear wave theory at the wavemaker in SWASH, which under long wave scenarios only allowed wave heights of a few centimeters. Even when fulfilling this linear condition, higher waves starting showing instabilities on the wave height cross-shore evolution. These instabilities appeared immediately offshore of the reef crest, but also around x = -1450. This unstable behavior was analyzed with a different number of parallel runs and changing the calculations methods; however, the results of these new runs did not allow to explain this behavior. To cope with this problem, the SWASH offshore boundary should be deeper, to be as far as possible from non-linear wave theory. Additionally, other programs without the requirement of linear wave theory at the wavemaker could be tested for modeling higher regular long waves, for example, programs that can generate cnoidal waves could be a more suitable option for this regular low-frequency wave numerical experiment.

Finally, the numerical experiments were modeled considering low friction similar to smooth plastic. Thus, the influence of a rougher bed, more similar to a real coral reef, was not taken into account. According to Pomeroy et al. (2012), high frictional values, like a healthy coral reef, could suppress higher resonant modes, which was also concluded by Gawehn et al. (2016). Thus, under a more realistic coral reef roughness scenario, experiencing first mode resonance should be less probable than experiencing fundamental resonance (Gawehn et al. 2016). Also, it is expected that a stronger forcing is needed for T_1 to resonate than for T_0 in order to counteract the resonant amplification reduction due to friction. This behavior was not observed in the results of this thesis, where both T_0 and T_1 showed resonant amplifications even for an offshore wave height of 1 mm probably because of the low friction coefficient.

5.2. Results discussion

Resonance over coral reefs can be forced with small amplitude regular long waves. Moreover, modeled wave resonance can generate amplifications on the wave height at the beach toe, and in wave run-up. The wave height at the beach toe can be amplified between 10 to 40 times the incident offshore wave height, and wave run-up can be amplified between 5 to 50 times the incident offshore wave height. This amplified behavior also has been observed in several experiments and fieldwork data analysis, with Nwogu and Demirbilek (2010) and Gawehn et al. (2016) as corresponding examples. In this thesis, resonance was found to be possible to occur for the first two resonant modes and two different reef flat water depths. The main topics to be discussed can be divided into two main topics (1) differences between resonant and non-resonant periods and (2) causes of different resonant amplifications. The discussion in (1) focuses in trying to understand which processes could be responsible for the difference between theoretical and modeled resonant periods, and discussion (2) focuses in trying to understand why smaller waves amplify relatively more than higher waves, and why shallower waters are more efficient in resonating.

5.2.1. Differences between resonant and non-resonant periods

A bandwidth of resonant periods was found for each resonant mode, with the respective modeled natural frequency as the maximum amplification located at the center of each resonant bandwidth mode. These resonant bandwidths with a maximum at their middle have also been observed on edge waves resonance

over sloping beaches Guza and Bowen (1976), which suggest similarities between edge waves resonance over beaches and low-frequency resonance over reef flats. As resonance can occur for a range of frequencies (resonant bandwidth), waves with periods neighboring the natural frequencies can also experience wave height and run-up amplifications. The resonant amplification of periods close to the natural frequencies diminishes with increasing distance from T_0 and T_1. This reduction is more efficient for the first mode, which on average decreases two times faster than the fundamental mode for the same period difference. The resonant amplification experienced by waves with periods neighboring the natural frequencies, even when being smaller than the amplification of the natural resonant period, can have a significant impact on coastal flooding, being an example of this the tsunami-like wave studied by Roeber and Bricker (2015). In this study, it was found that the wave setup over the reef oscillated with the incident wave group leading to several damages, which would have been larger if the incident wave group period would have been closer to the reef natural period.

Resonating waves form standing wave patterns with a node located close to the reef crest, as expected due to previous research (Buckley et al. 2018). However, the exact position of this node is difficult to identify likely due to the influence of the steep fore reef slope (1:6), which generates an abrupt water depth change between the area offshore and onshore of the reef crest. Non-resonating waves were also observed to form standing wave patterns, with a distinguishable node located onshore of the reef crest, and over the reef flat (Figure 4.4). For example, the node closest to the reef crest of both theoretical periods, T_0^* and T_1^*, can be seen mismatching the reef crest location. This presence of resonating and non-resonating standing wave patterns can be related to Gawehn et al. (2016) findings, which analysis of field data also showed the presence of these two low-frequency waves behavior over the reef flat. Thus, as the schematized reef profile of this thesis is based on the real reef profile studied by Gawehn et al. (2016), modeled simplified low-frequency waves behavior can relate at a certain extent to the expected real behavior over the reef flat.

The modeled natural periods were found to be in every case longer than the theoretical ones, which was also observed in Pearson et al. (2017). This difference could be related to the influence of the fore reef slope, which is not considered in Equation 2.3. The beach slope is also not considered in this equation, but should not play an important role in this case because theoretical periods were calculated considering the reef flat width from the reef crest until the shoreline. Moreover, Pearson (2016) found beach slope to have a small relatively influence in the run-up, and thus in wave resonance. The only impact that beach slope could have is in run-up resonance over the beach, which was observed in reef environments by Shimozono et al. (2015). However, run-up beach resonance is out of the scope of this thesis.

The fore reef slope can be partially responsible for the difference between theoretical and modeled resonant periods due to its effect on reflecting incoming and outgoing waves with different periods, and wave heights are not taken into account. According to Dekkers (2018), the reflection coefficient increases for increasing offshore wave period and wave height. The reflection at the reef crest of incoming waves relates to the amount of wave energy entering the reef, and the reflection of outgoing waves relates to the amount of energy being trapped over the reef, which are important parameters for wave resonance. The energy flux ratio F_{out}/F_{in} (Figure 4.17), which can be seen as a reflection coefficient, agreed with Dekkers (2018) findings related to the periods, except for resonant periods or periods neighboring natural frequencies, which showed lower reflection coefficient than longer neighboring periods. Thus, the results suggest that resonance should be able to counteract reflection at some level.

Additionally, resonant wave periods were found to be amplitude-dependent, slightly shifting the modeled natural frequency to longer periods with an increase of 50% the incident wave height, and to shorter periods with a 50% reduction of the incident wave height (Figure 4.12). The shift of the modeled resonant period due to changes in the incident wave height was found to be 1.4% of the base case fundamental resonant period found for H_{off} = 1 cm and d_r = 0.8 m, remaining inside the resonant bandwidth. This shift of the period cannot be explained by a deviation from the linear dispersion relation, because according to Guza and Bowen (1976), higher waves lead to longer wavelengths that propagate faster than shorter wavelengths, which would imply a decrease on the resonant period. Furthermore, this shift of the natural resonant period is not related to an increase or decrease of the reef flat water depth because its variation is minimum over the reef compared to the total water depth and wave height (less than 1%). Moreover, larger water depth, as seen for increasing incident wave height, will lead to shorter resonant periods, according to Equation 2.1, which is the opposite of what it was observed.

Even though the amplitude-dependence analysis was carried out for different H_{off}, it can also apply for one particular H_{off}, because it has been seen that the individual wave height varies in time until reaching an equilibrium (Figure 4.15). As the wave period does not change in time, the individual wave height time variation can lead to a change in the wavelength (L) in time due to a possible deviation from the linear dispersion relation. A deviation from the linear dispersion relation will lead to variations of the location of the node, due to the L changes in time caused by wave height alterations. In order to understand if time variations in L can be related to the wave height variations in time, the variation in time of the location of the node closest to the shoreline for the first resonating mode was studied. The node closest to the shoreline was studied instead of the node closer to the reef crest because its location can be more easily identified for resonating and non-resonating waves. The changes in time of this node location can be seen as wavelength variations because the distance between the shoreline and the node ($x_{shoreline}$ - x_{node}) can be related to a quarter of a wavelength ($L/4$). The node location variations, and consequently L variations, were studied during the resonance build-up time and were compared with the respective wave height evolution at the beach toe for the theoretical (T_1^*) and modeled (T_1) first resonant mode (Figure 5.1). The node location variations were investigated by dividing the surface elevation time series in sub-series with a duration of two wave periods (not taking into account the first two waves of the time series), and by studying the cross-shore variation of the surface elevation variance ($var(\eta)$) to find the node or minimum value of $var(\eta)$. To visualize deviations from the linear dispersion relation the expected upper and lower boundary of L are shown, which were computed as the corresponding period T by the wave celerity c ($L = Tc$). The lower value corresponds to the L computed with the shallow water linear wave celerity as $c = \sqrt{(}gd_r)$, and the upper value was calculated with the shallow water non-linear wave celerity of a solitary wave as $c = \sqrt{(}g(d_r + H))$ (Catálan and Haller 2008, Tissier et al. 2011), with g the gravitational acceleration, d_r the reef flat water depth and H the (maximum) individual wave height at the beach toe.

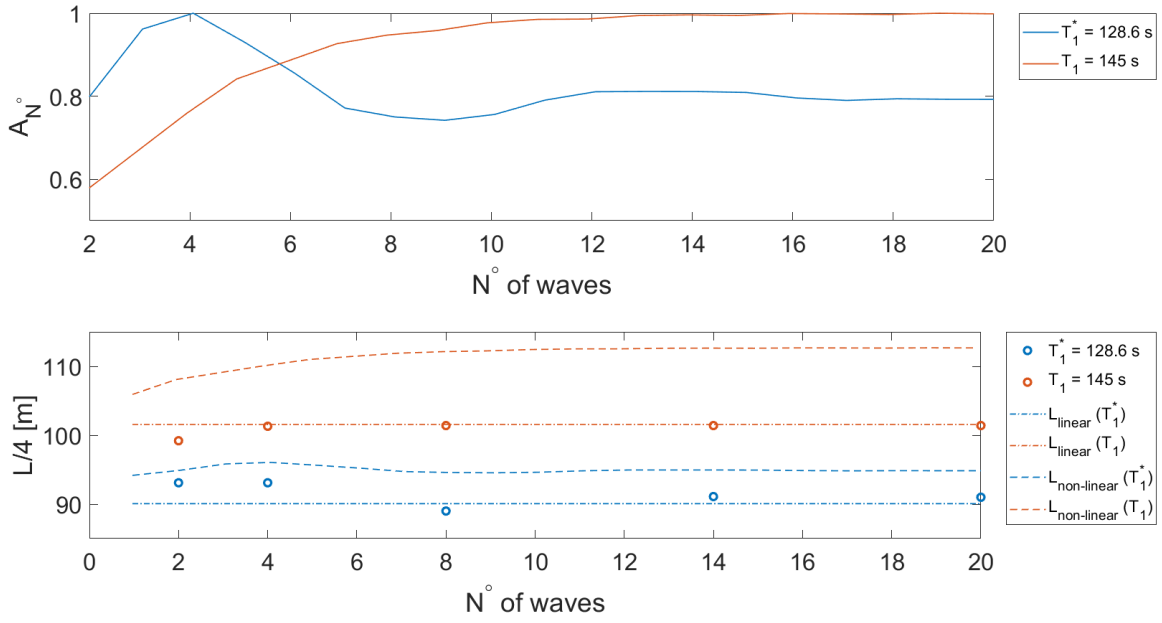

Figure 5.1: First resonant mode wavelength variation due to beach toe wave height changes in time. Top figure shows the individual wave height evolution at the beach toe as a ratio of the maximum wave height ($A_{N°} = H_{beachtoe}$ / $H_{beachtoe-max}$). Bottom figure presents the quarter of wavelength evolution ($L/4$) corresponding to the individual wave showed in the top figure. The dashed lines represent the theoretical linear wavelength, and the dashed-point lines represent the solitary non-linear wavelength.The analysis was done for d_r = 0.8 m, for the theoretical and modeled first resonant mode, respectively T_1^* = 128.6 s and T_1 = 145 s.

This analysis showed that the theoretical (T_1^*) and modeled (T_1) resonant periods experience variations of the wavelength that can be related to wave height variations, especially for (T_1^*). The wavelength variations are larger for T_1^* than T_1, oscillating L_1^* (corresponding T_1^* wavelength) between the non-linear upper boundary and the linear lower boundary, while L_1 (corresponding T_1 wavelength) tends to the linear disper-

sion relation since the first waves, and reaches a constant linear L even before reaching a stationary wave height. Therefore, results suggest that the theoretical first mode L_1^* is more prone to be affected by non-linear effects due to wave height variations than L_1, which could be due to the more abrupt wave height variations, and the larger amount of waves needed to reach stationary conditions for T_1^* than T_1.

According to Equation 2.1, the first mode resonance over an open-ended basin can occur when $L/4$ matches one third of the reef width (W), counted from the reef crest until the shoreline, which in this case is in the range of $W/3$ = 91.6 - 91.8 m due to variations on the shoreline location. The oscillations of L_1^* in time are always closer to $W/3$ than L_1 values, but the other node, further from the shoreline, is located onshore of the reef crest, which likely does not allow resonance to occur. The wavelength of the modeled resonant period T_1 corresponds to 3/2 W, which is between the value of L for the first mode resonance (n = 1 in Figure 2.4) of an open-end basin (L = 4/3 W) and a closed basin (L = 2 W). Thus, it seems that the reef natural resonant modes are in between the open-ended basin and close basin theoretical resonant modes, likely due to the influence of the fore reef slope.

5.2.2. Causes of different resonant amplifications

The fundamental mode was found to generate larger wave height and run-up amplifications than the first mode, which has also been observed in other resonance studies such as Guza and Bowen (1977), Pomeroy et al. (2012) and Nwogu and Demirbilek (2010). The resonating efficiency difference between the first two modes can also be seen when comparing the amount of trapped wave energy over the reef, which for the same H_{off} was found to be 2.5 times larger for the fundamental mode than for the first mode (Figure 4.20). Moreover, the amount of trapped wave energy was found to be highly correlated with the wave height resonant amplification (R^2= 0.9897). Thus, for the same offshore wave height, T_0 traps a larger amount of low-frequency energy, which reflects in more energy available to resonate over the reef, and consequently in a stronger resonant amplifications than for T_1.

The highest efficiency of the fundamental mode to resonate could also be related to the wave shapes interacting over the reef for each mode. The comparison between the asymmetries of the incoming and outgoing wave at the reef crest could help to understand the interactions between the incoming wave and the reflected outgoing wave (first at the beach and after at the reef crest). The efficiency of the coupling of these two waves will likely have an impact on the resonant amplification. Similar wave shapes are expected to interact more efficiently than waves with large wave asymmetries differences. This coupling could explain the stronger resonant amplification experienced by waves with period T_0 since the first resonant mode presents for every H_{off} a more significant difference between η_{out} and η_{in} asymmetry at the reef crest. However, to the knowledge of the author, this topic has not been studied before and could not be proved in this thesis.

In every resonant mode and water depth scenario, smaller offshore wave heights were found to amplify relatively more than higher waves. This stronger amplification is expected to be related to smaller waves being relatively more efficient in trapping low-frequency wave energy over the reef flat and in being less dissipated due to, for example, bottom friction. Gathering the information from Figure 4.21, and Figure 4.6 it can be noted that stronger resonant amplifications A_{Shoal} are related with a relatively larger amount of trapped wave energy $\Delta F/F_{in}$, and resonant amplifications A_{Shoal} are stronger for smaller wave heights. Thus, smaller wave heights can trap a relatively larger amount of wave energy over the reef than higher waves and consequently, are more efficient in resonating (larger A_{Shoal}). Moreover, Figure 5.2 shows the influence of friction on the fundamental resonant amplification for different H_{off} by comparing the respective A_{Shoal} ratio for models with and without friction. This analysis shows that smaller waves are less affected by friction than higher waves, which can be seen by comparing the difference between the friction and no friction values of A_{Shoal} for H_{off} = 0.1 cm and H_{off} = 1.5 cm. The smallest wave is almost not affected by friction (reduction of 0.6%), whereas the highest wave resonant amplification reduces roughly from 3.6 times the expected wave shoaling to 2.8 times the expected shoaling (reduction of 22 %).

Additionally, it can be observed that the model with friction shows similar behavior in decreasing resonant amplification when increasing H_{off} for the whole range of wave heights studied, while the model without friction presents two patterns. The first pattern goes from H_{off} = 0.1 cm to H_{off} = 0.75 cm, and shows an increase of the resonant amplification when increasing H_{off}. On the contrary, the second pattern (H_{off} >

0.75 cm) shows that wave heights larger than H_{off} = 0.75 cm experience a decrease of A_{Shoal} when increasing H_{off}, similar to the behavior of the frictional model. When analyzing the ratio F_{out}/F_{in} for wave heights from the second pattern, it was found to be less than 3% larger than for smaller wave heights; thus, it cannot explain the different behavior found between the two A_{Shoal} patterns of the frictionless case. However, when comparing the difference in asymmetry between the outgoing and incoming wave ($\Delta As = As_{out} - Asin$) between the frictionless and frictional models, it was found that by removing friction ΔAs increases 4.4 % for the smaller wave height (H_{off} = 0.1 cm), and 74.7% for the higher wave (H_{off} = 1.5 cm). Thus, the results suggest that ΔAs increases with frictionless bottoms, and that this rising is stronger for larger wave heights. This larger ΔAs, found for larger wave heights, will likely lead to a less efficient coupling between incoming and outgoing waves. This less efficient coupling could explain why after certain H_{off} threshold (0.75 m in this case) waves start being less efficient in keeping wave energy over the reef, and consequently start amplifying relatively less than smaller waves.

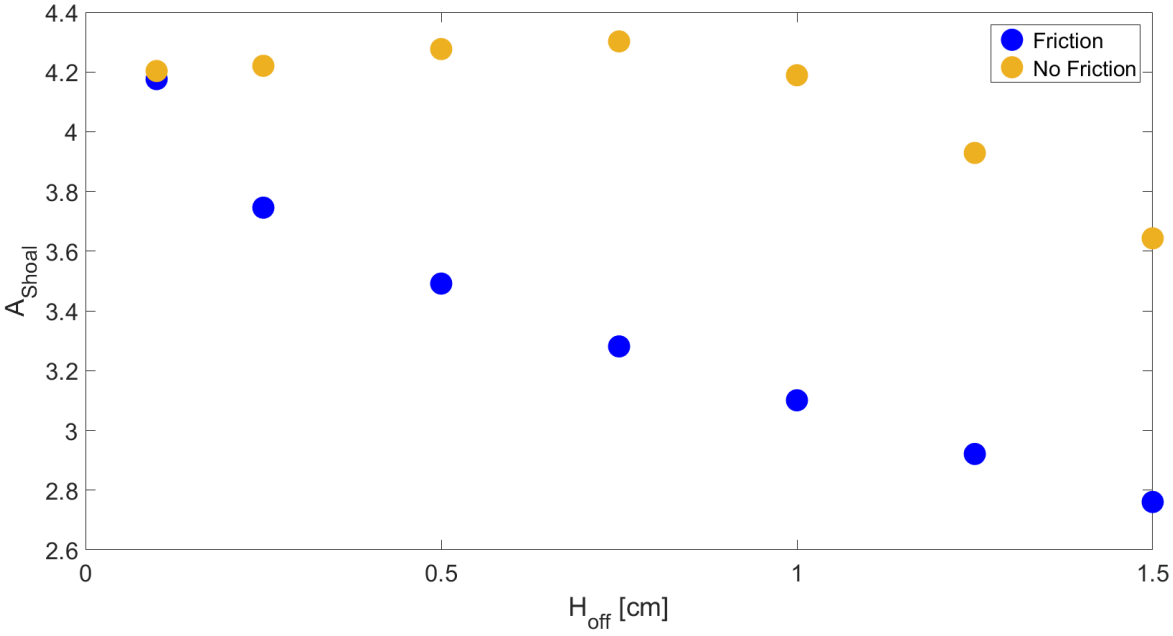

Figure 5.2: Fundamental resonant amplification factor (A_{Shoal}) at the reef crest for different $Hoff$ under models without and with friction. The analysis was done for d_r = 0.8 m and T_0 = 431 s, with a Manning friction coefficient of n = 0.01 $s/m^{1/3}$ for the model considering friction.

Another phenomenon that could explain the relatively larger amplification of smaller waves is the resonant period amplitude dependence found in Figure 4.12. This analysis showed that the period leading to the maximum wave height resonance slightly changes depending on H_{off}, with a wave height increase (decrease) of 50% leading to a 1.4% longer (shorter) periods. However, the variations of A_H due to a shift of the most resonant period are not large enough to completely explain the difference between smaller and higher resonant amplification. The shift of the most resonant period, or also called period detuning, is likely caused by a deviation from the linear dispersion relation due to a H_{off} increase. This deviation leads to changes of the wavelength, with a lower boundary set by the linear dispersion relation ($c = \sqrt{(g d_r)}$), and an upper boundary set by the solitary wave non-linear dispersion relation ($c = \sqrt{(g(d_r + H))}$). Figure 5.3 presents these two boundaries for the fundamental mode $T = 431s$ (for d_r = 0.8 m) wavelength (L). Under linear dispersion relation, L remains almost constant for different H_{off}, showing small variations only due to small changes of d_r over the reef. On the contrary, when assuming solitary wave non-linear dispersion, the wavelength difference between the minimum and maximum H_{off} can reach values around 150 m, which corresponds to 44% of the reef width. The increasing values of L due to increasing H_{off} could lead to a detuning from the most resonant period. However, this detuning cannot explain the found amplitude dependence where higher waves lead to longer periods, because according to theory, non-linear waves travel faster than linear waves ($c_{linear} < c_{non-linear}$). Consequently, by estimating the fundamental resonant period as $T_0 = 4W/c$

(Equation 2.1) it can be concluded that $T_{0-non-linear} < T_{0-linear}$, which would lead to higher waves shifting the natural frequency to shorter periods. Moreover, in Figure 5.1, it was shown that the resonant wavelength is almost not varying with wave height variations. Thus, a deviation from the linear dispersion cannot explain the resonant period amplitude dependence.

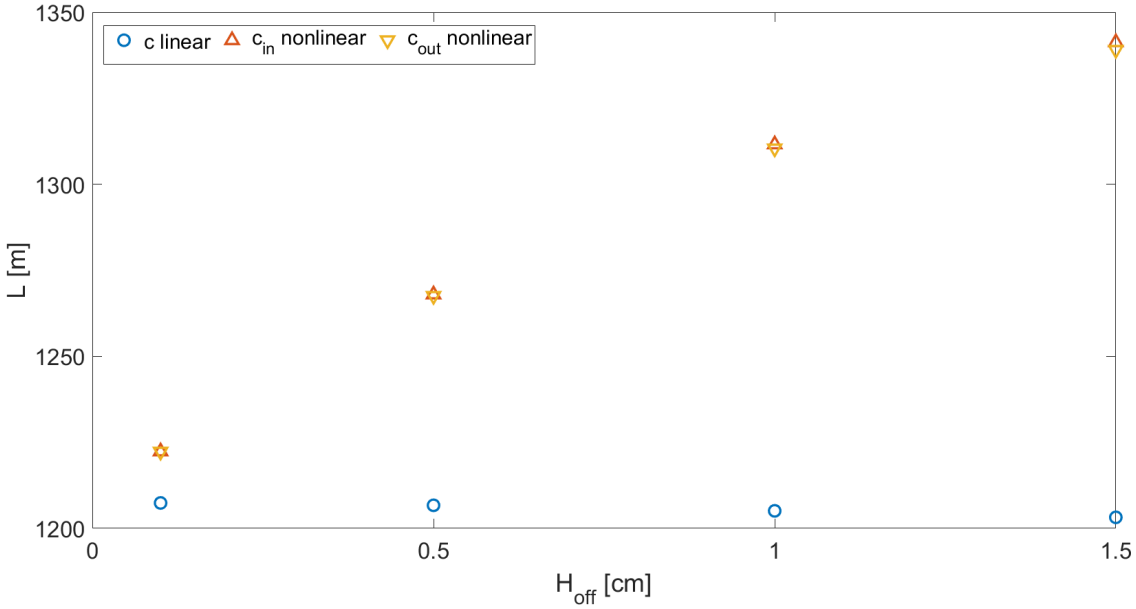

Figure 5.3: Fundamental resonant wavelength (L) variation for different H_off when deviating from linear theory dispersion relation.c_linear corresponds to $\sqrt{(gd_r)}$ and $c_nonlinear$ to $\sqrt{(g(d_r + H))}$ (solitary wave equation). The analysis was done for d_r = 0.8 m and T_0 = 431 s.

Larger water depths developed shorter resonant periods than smaller water depths, which was expected according to theory (Equation 2.1). Additionally, the wave height and run-up amplification for the same relation H_{off}/d_r is stronger for shallower water depths. The effect of more non-linear wave shape was not able to explain this difference in resonant amplification for different d_r because the ΔAs between incoming and outgoing waves at the reef crest was found to be smaller for deeper d_r. The reduction of non-linearities with increasing water depth over the reef flat was also observed by Cheriton et al. (2016).

The reduction of resonant amplification with increasing d_r could be due to a reduction of the reef efficiency to trap wave energy as the reef flat water depth increases. Figure 5.4 presents the relation between the relative amount of trapped wave energy ($\Delta F/F_{in}$), the relative offshore wave height (H_{off}/d_r) and the resonant amplification (A_{Shoal}). This analysis was carried out with the fundamental resonant period for two different water depth (d_r = 0.8 m and d_r = 1.6 m). This analysis showed that the shallower reef flat water depth is more efficient in trapping wave energy than the deeper d_r, which, as already observed before, leads to stronger resonant amplifications. Thus, it seems that small amplitude long waves experience stronger resonant amplification for equivalent H_{off}/d_r relations under the shallower water depth scenario, because the smaller d_r is more efficient in trapping wave energy, and consequently in having more energy available to resonate.

According to Nwogu and Demirbilek (2010) experiments, under irregular wave conditions, low-frequency wave energy over the reef was seen to increase with increasing water depths. Moreover, resonance has been found to be more likely to occur with deeper d_r and more energetic wave conditions in field measurements analysis (Cheriton et al. 2016), and numerical experiments (Pearson et al. 2017). These findings are expected because larger water depths reduce the wave dissipation due to bottom friction and lead to shorter periods, which are located in a more energetic area of the spectrum. Thus, even though the shallower water depth showed to be more efficient in resonating than the deeper d_r, under a more realistic wave climate, this higher efficiency is not able to counteract the more energetic resonant wave conditions available under deeper d_r

conditions. Thus, under a sea-level rise scenario reef resonance occurrence is expected to increase even if deeper d_r are less efficient in trapping low-frequency wave energy over the reef (Péquignet et al. (2009), Pearson et al. (2017)).

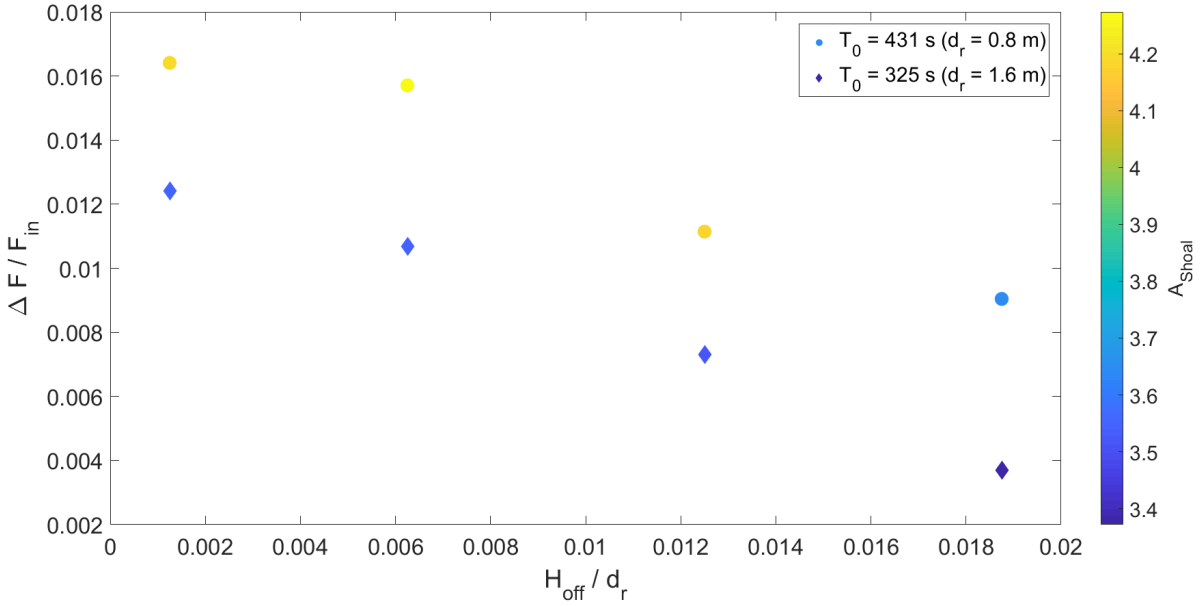

Figure 5.4: Relative amount of trapped wave energy ($\Delta F/F_{in}$) for the fundamental resonant mode under different water depth (d_r) and offshore wave height conditions (H_{off}). The circle marker represents the fundamental mode for d_r = 0.8 m, and the diamond marker represents the fundamental mode for d_r = 1.6 m.

Resonance was found to be characterized by a build-up behavior, needing a certain number of waves to grow and reach a maximum and finite stationary resonant amplification, which remained constant under this experiment, likely due to the permanent forcing. Guza and Bowen (1976) also found an initial growth followed by a maximum and finite resonant amplification in resonating edge waves over a beach; thus, again, reef resonance and beach resonance were found to behave similarly. The number of waves needed for resonant waves to reach a maximum amplification and a steady state varies depending on the resonant mode, d_r, and H_{off}. Tor the scenarios evaluated, the minimum number of waves needed to build-up resonance was five waves (T_1 for d_r = 1.6 m), and the maximum was twenty waves (T_0 for d_r = 0.8 m). Moreover, the deeper modeled water depth needed fewer waves to develop a fully resonant state than the shallower water depth, and consequently, the duration of the forcing also decreases, because resonant periods are shorter for larger water depths. The reduction of the number of waves and forcing duration is especially noticeable for the first resonant mode, where independently of H_{off} five waves are sufficient to reach a maximum amplification for d_r = 1.6 m. Moreover, for both studied d_r, the first resonant period was found less dependent on H_{off} than the fundamental mode. T_1 experienced fewer variations in the number of waves, and also in the resonant amplification with increasing or decreasing offshore wave height. However, for both resonant modes, wave resonance developed independently of the wave height when matching the incident wave period with one of the reef natural frequency. Thus, the results suggest that the period is more important than the wave height for resonance to occur, which was also found by Gawehn et al. (2016). This study identified a 3.6% of resonance over five months of measurement, and the presence of brief resonant conditions over the reef. These brief duration of resonance can be related to a matching resonant forcing shorter than the duration needed to reach a stationary resonant state. Thus, under a regular forcing like the characteristic swell wave climate that dominates in low lying islands, resonance can develop without needing the full duration computed in Table 4.2. Nevertheless, under brief resonance scenarios, the resonant amplification likely will be lower than the corresponding finite maximum resonant amplification. Furthermore, as a general tendency, larger wave heights were found to need fewer waves to reach a maximum resonant steady state than smaller waves. These findings on real coastal safety imply that larger waves are more likely to resonate with a maximum amplification than smaller waves. However, the wave amplitudes studied in this thesis are very small, and at this state

cannot be directly linked with real swell or storm wave conditions resonant behaviors.

The impact of friction in resonance was found to be related to a reduction of the resonant wave height amplification without changing the natural resonant periods. The influence of friction over the resonant amplification was found to be stronger for the fundamental mode than for the first resonant mode, which was also observed by Pomeroy et al. (2012) with low bottom friction. The implication of this finding is also related to coastal safety because it proved that small variations on the coral roughness could have a significant impact on the resonant amplification. A minimal frictional increase, from a frictionless case to smooth plastic friction, reduced the wave height at the beach toe, and the run-up until respectively 26% and 23%. Moreover, according to Gawehn et al. (2016), coral reefs roughness dissipates too much energy, and reefs are not able to develop higher resonant modes, which was possible in this study likely due to low frictional values. Thus, the fundamental mode is the most expected to resonate, and as it is also the mode more affected by bottom friction dissipation, coral preservation, coral restoration, or other methods to increase reef frictional dissipation are essential to counteract reef resonant amplification.

5.3. Future research

This thesis contributes to the understanding of long wave resonance over fringing reefs, by forcing resonance with a simple wave climate of small amplitude regular long waves. However, it also opened more questions regarding the influence over resonance of different processes, and the resonant behavior under more complex wave climates. These new questions could be answered by deepening and extending this research. Some future studies could be related to topics such as:

- **Differences between theoretical and modeled resonant periods:** the differences between the theoretical and modeled resonant period were found in this thesis to be likely related to the influence of the fore reef slope. Thus, it would be interesting to understand if this parameter is causing this difference or if other factors could be playing a role. The influence of the fore reef can be studied by varying this parameter and trying to find the scenario resonating with a period as close as possible to the theoretical period. Also interesting would be to force resonance with at least the first three or four modes, and try to understand if the assumption of a closed-end basin is the most appropriate for a reef, or if another type of basin could lead to a better fit between theoretical and modeled resonant periods.

- **Wave de-shoaling:** waves with non-resonant periods, between the first two resonant modes, showed an incident wave height decrease immediately offshore of the reef crest(discussed in Section 4.2, Figure 4.5). This reduction was not expected due to the constant decrease of the water depth when approaching the reef. Moreover, frictional dissipation has an insignificant effect on non-resonant periods. Thus, other phenomena must be forcing this wave height reduction. One phenomenon influencing the wave de-shoaling could be the fore reef reflection, which may be more effective for non-resonant periods, and counteracted by resonant periods. This theory could be tested by comparing/analyzing the results of models with and without a beach slope. The design of a reef with a flat beach can be achieved by using a Sommerfeld boundary condition, which is recommended for long waves modeled in SWASH.

- **Model larger amplitude long waves:** modeling larger wave heights could help to understand better the influence of incident offshore wave height on resonant amplification. This research could also help to relate the results with more realistic wave height values closer to swell and wind waves wave heights. Moreover, it would be interesting to investigate further the resonant period - wave amplitude dependence, and check if it is possible to find a wave amplitude that shifts the resonant period enough to reach periods outside the resonant bandwidth. Thus, passing from resonant to non-resonant conditions.

- **Bi-chromatic waves:** the same experiments carried out in this thesis could be done with bi-chromatic waves. This type of wave should be built with the bound long wave period matching one natural reef frequency. This wave climate will probably generate more realistic results than regular long waves, by taking into account the influence of short waves on resonance. Including high-frequency waves into the numerical model, will likely lead to wave breaking and non-linear transfer of energy. Moreover,

wave set-up will start playing a role by changing the natural frequencies due to its impact in increasing the water depth.
Under bi-chromatic wave conditions, some further experimental data analysis could be done. For example, the effect of wave groupiness on resonant amplification can be studied by comparing runs with the same long bound wave (same wave height an period), but with a different ΔT between the periods of both short monochromatic waves. Another analysis could be carried out to understand the impact of the two different low-frequency wave generation processes on the resonant amplification ratio. The dominant generation process is dependent on the fore reef slope. Thus runs with varying fore reef slope should be carried out, and results could lead to understanding which type of generation could lead to a more efficient resonance. Finally, to add more variability to the wave conditions, a wave signal with a transition from non-resonant to resonant conditions could be modeled. This transitional wave climate could help to understand more realistic the phenomenon of resonance build-up, and the time needed to reach a finite maximum resonant amplification. Additionally, the build - down of resonance could be studied by changing the transition of the wave signal, from resonant to non-resonant. Both the resonance build-up and build-down are essential to assess coastal flooding better.

- **Impact of run-up on coastal flooding:** in this topic, two main analyses/experiments could be carried out. The first analysis relates to understanding the impact of the wave shape on coastal flooding. This thesis results showed how, for a specific d_r, larger wave heights become more non-linear, and also experience a smaller amplification. According to literature, the impact of non-linear wave shapes could be larger due to the impact on structures as a shock force (Shimozono et al. 2015). Thus, it could be worth studying the damages that run-up can generate over a certain structure. Because it may be possible that a smaller non-linear run-up could generate more significant damage than a larger regular run-up. Moreover,Gawehn et al. (2016) found that resonant bores can grow much larger than progressive-growing bores, and can be more dangerous for coastal flooding. Thus, resonant coastal flooding should be assessed, taking into account the resonant amplification, and if there is an extra impact caused by non-linear waves. Another interesting experiment related to run-up would be to force beach run-up resonance by reducing the beach slope. Run-up resonance is expected to occur on milder slopes, and it can amplify run-up over the beach. Thus, it could be relevant to assess the impact on coastal flooding of a scenario with both wave resonance and beach run-up resonance.

- **Rougher reef influence on resonance:** friction dissipation was shown to be an essential parameter to reduce resonant amplification. Thus, new analyses should be done for larger friction coefficients, closer to real values, to understand how probable is reef resonance to occur, and if it can be seen only with the fundamental mode or also with higher modes. According to Pomeroy et al. (2012), low frictional values have a larger impact on the fundamental mode amplification, whereas higher frictional values lead to a reduction of all resonant modes amplifications. Moreover, other experiments can be carried out; for example, a frictional grid could be built varying the friction coefficient for the different reef areas. This approach could help to understand where to focus the efforts of coral restoration, depending on their effectiveness to counteract resonant amplification. Roelvink (2019) studied the effects and efficiency of coral restoration to protect coasts against flooding; however, their impact on resonance was not assessed.

6

Conclusions and Recommendations

6.1. Conclusions

In this thesis, resonance was forced over a schematized fringing coral reef for the first two resonant modes and two different reef flat water depths. This numerical experiment was successfully achieved using the SWASH computational tool with small amplitude regular low-frequency waves. Based on these results the questions posed at the beginning of this study will be answered.

Research sub-questions

For a certain water level, what are the characteristics (period and wave height) of a regular long wave leading to a maximum wave height/run-up amplification?

For the first two resonant modes, resonance can develop within a range of periods neighboring the natural resonant period. Inside these bandwidths, the modeled natural periods T_0 and T_1 were found to be the most resonant, and the ones located in the center of the resonant bandwidth of each mode. Modeled resonant periods were found to be longer than the theoretical ones, which is likely due to the influence of the fore reef slope in reflecting incoming and outgoing waves. Wavelength variations due to a deviation from the linear wave dispersion were not found to be the cause of the difference between the theoretical and modeled periods.

Coral reef resonance can generate waves between 10 and 40 times the incident offshore wave height, and run-ups between 5 and 50 times the incident offshore wave height. Resonant amplification is larger for the fundamental mode (T_0) than the first mode (T_1) and decreases for both modes with increasing water depth over the reef (d_r). The resonant amplification was found to be correlated to the amount of wave energy trapped over the reef, with a larger amount of trapped wave energy leading to stronger resonant amplifications. For the case with d_r=0.8 m and H_{off} = 1 cm, a correlation coefficient of R^2 = 0.9897 was found between the amount of energy trapped over the reef and the wave resonant amplification.

Smaller waves experience a larger relative resonant amplification than higher waves. This behavior can be seen in both wave height and run-up resonant amplification, independently of the wave period and the reef flat water depth. Smaller waves were found to be more efficient in trapping wave energy over the reef than higher waves, which could explain their stronger resonant amplification.

How do long waves transform over the reef flat under resonant conditions? Which non-linear wave shapes are present under resonance? Does this have a significant impact on wave height/run-up amplification?

Resonant waves behave like standing waves with a node close to the reef crest. The incoming and outgoing waves forming this standing pattern start developing non-linear wave shapes over the reef flat. This wave non-linearity becomes larger with increasing offshore incident wave height. The non-linear wave shapes can be analyzed through wave skewness and wave asymmetry. Over the reef, skewness is similar for the incoming

and outgoing waves, whereas asymmetry is larger and opposite in sign for the outgoing wave. This difference in asymmetry, ΔAs, between the incoming and outgoing wave is larger at the reef crest, which shows that waves steepen while approaching the beach and keep steepening after being reflected towards the reef crest. ΔAs is more significant for higher waves, for smaller water depths, and the first resonant period.

Independently of the reef flat water depth, smaller waves are more linear and experience stronger amplifications than higher waves over the reef. Thus, for a specific d_r, non-linear waves resonate less effectively than regular waves. However, when comparing between different d_r, the effect of amplification reduction due to non-linear wave shape was not found. Because resonant amplification was found to be stronger for smaller water depths than larger water depths, even though smaller water depths present more non-linear wave shapes than larger water depths.

How long does it take for resonant behavior to be built up in order to generate a maximum wave height/run-up amplification over the reef?

Resonance was found to need a certain number of waves to reach a maximum wave height/run-up amplification. This number of waves varies for different resonant modes, reef flat water depths, and incident offshore wave heights. For the ranges of wave conditions and depth considered, the number of waves needed to reach a maximum resonant amplification varies between 5 and 20 waves. Higher waves were found to need fewer waves than smaller wave heights for every studied scenario, with the exception of the first mode under d_r = 1.6. Within this scenario, wave resonance reached a maximum resonant amplification with the same number of waves independently of the incident offshore wave height, which also corresponded to the minimum number of waves of all the scenarios. The maximum resonance was in every scenario reached under a steady state, which implied that resonant amplification has a finite wave amplitude that remains constant for an invariant offshore wave forcing.

What is the effect of friction on wave height/run-up resonant amplification over the reef?

Even low friction values can reduce the resonant amplification of both wave height and run-up resonant amplification. This reduction of the resonant amplification is stronger for the fundamental mode (around 26% of the wave height and 23% of the run-up) than for the first resonant mode (less than 5% of the wave height and no observable run-up reduction).

The effect of friction on reducing resonant amplification is stronger for larger water depths than for smaller water depths. Low values of frictions can reduce 22% the wave height resonant amplification for the highest offshore wave height, whereas the smallest wave is barely affected with a 0.6% of reduction.

Research question

What are the main processes limiting the resonant amplification of long waves and the associated run-up over a schematized fringing coral reef?

Hypotheses: Resonant amplification is expected to be more effective when energetic long waves reach the reef flat. However, non-linear wave shapes and energy dissipation are more likely to develop for the largest long waves, which could limit the amplification factor. Thus, perhaps the highest wave will not result in the maximum wave height and run-up amplification.

Wave resonance of small amplitude regular long waves was found to be more efficient for smaller water depths, smaller wave heights, and for the fundamental mode. Stronger amplifications for different resonant modes and reef flat water depths were found to be correlated with a larger amount of trapped wave energy over the reef. Stronger amplifications for different offshore wave heights were found for larger amounts of wave energy trapped over the reef, and lower wave resonant amplification reduction due to frictional dissipation.

Higher waves started developing non-linear wave shapes over the reef, which could be influential in reducing their resonant amplification. However, this behavior was only found when comparing results for a

specific reef flat water depth. A comparison between the amplification of the same H_{off}/d_r relation for two water depths, gave the opposite relation between non-linearity and resonant amplification, with stronger resonant amplification for more non-linear waves. Thus, wave steepening could not be generalized as a process counteracting resonance.

Frictional dissipation was found to be essential for counteracting wave resonance, especially on the fundamental resonant mode and for increasing incident offshore wave height. Thus, increasing coral reef bottom friction, through coral reef preservation, coral reef restoration, or other methods is essential for enhancing low-lying island coastal safety.

In conclusion, the underlying hypotheses were partially supported because for all the resonant scenarios analyzed larger wave heights amplified relatively less than smaller wave heights. The reason for the relatively smaller amplification was due to a relatively smaller amount of wave energy trapped on the reef, and a larger resonant amplification reduction due to bottom friction for higher than smaller waves. However, a possible reduction of resonant amplification due to stronger non-linearity for large wave heights could not be proven in this study.

6.2. Recommendations

This research marks a step forward in understanding low-frequency waves resonance over coral reefs. Based on the results of this study, some recommendations are made for broadening and deepening the knowledge on this topic:

- Understanding the mechanism/processes responsible for the difference between the theoretical and modeled resonant period could help to have better predictions of the offshore conditions leading to resonance.
- Carry out numerical modeling of regular low-frequency waves with larger wave amplitudes could lead to a better understanding of the impact of incoming offshore wave height on resonant amplification, and the resonant wave period - wave amplitude dependence.
- Analyzing the mechanism inducing waves to shoal or de-shoal before the reef crest could be relevant for reducing or suppressing resonance impact.
- Forcing resonance over coral reefs with bi-chromatic waves will put this research in a more realistic perspective by including the interaction between high and low-frequency waves. The results of this study are expected to be more applicable to real conditions.
- The impact of run-up on coastal flooding should be analyzed by including run-up amplification due to wave resonance over the reef flat, run-up resonance over the beach, and the level of damage depending on the wave shape.
- The friction dissipation process and efficiency should be studied thoroughly in terms of the space variation of friction coefficients. This approach would help to understand the most effective areas to develop coral reef restoration.

A

Reef profile

This appendix shows the full bathymetry over which resonance was forced (Figure A.1). The reef cross-shore profile had to be extended in 1740 m with a slope of 1/3 to fulfill SWASH requirement of linear wave theory at the wavemaker. This requirement is fulfilled with an Ursell number $U = a/d/(kd)^3 < 0.2$, where U represents the Ursell number, a the wave height, d the water depth, and k the wavenumber. Thus, as low-frequency waves are very long waves of with more than a few km wavelengths, the profile had to be deepened (until 440 m below the reef flat level) and extended (total length of 2360 m .) considerable, and small wave amplitude variations were allowed to remain stable.

The full modeled cross-shore profile consists in an offshore area (x = -2000 to x = -360, including a flat area and a 1/3 slope), fore reef slope (x = -360 to x = -0, with a 1/6 slope), the reef flat (x = 0 to x = 270), and the beach slope (x = 270 to x = 360, with a 1/6 slope).

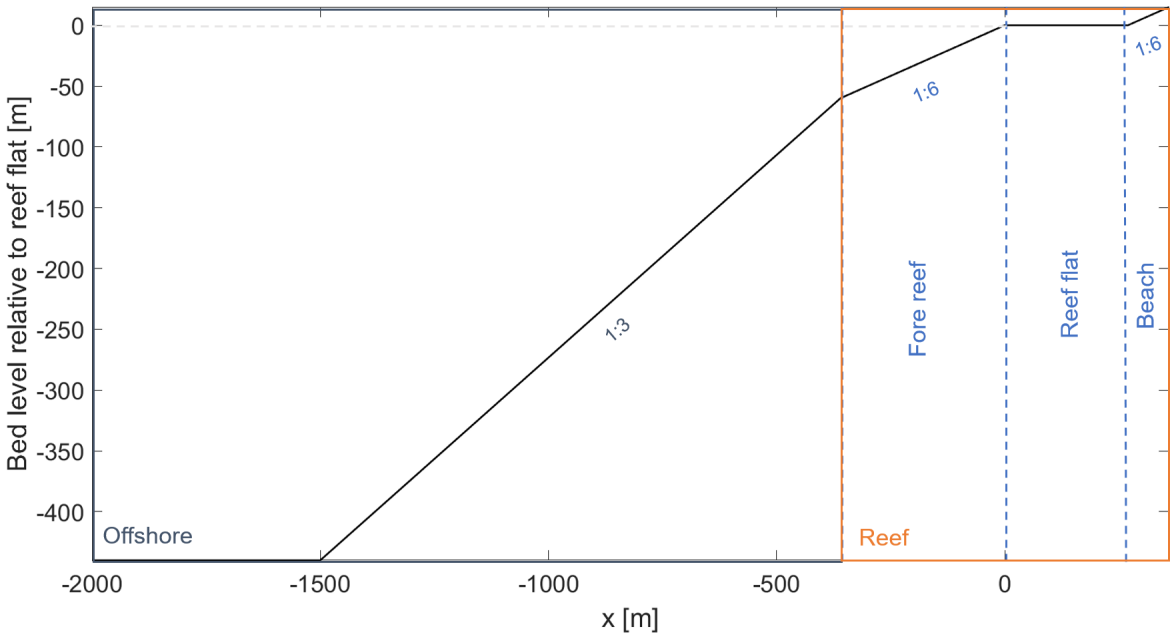

Figure A.1: Complete modeled bathymetry, including an offshore area and the reef profile (Figure 3.6).

B

SWASH code

This appendix shows the base SWASH code used for every numerical experiment. Variations were done to the water depth, wave height, wave period, and friction coefficient depending on the modeled scenario.

```
    $************HEADING*************************************
$
PROJ 'Reef' 'FR'
$
$ Finding resonance
$**********MODEL INPUT*********************************
$
SET LEVEL=0.8
$
MODE NONSTATIONARY ONED
$
CGRID REG -2000 0. 0. 2360 0. 23600 0
$
INPGRID BOTTOM REGULAR -2000 0. 0. 2360 0 1 0.
READ BOTTOM 1. 'Profile1md440.bot' 1 0 FREE
$
INIT ZERO
$
BOUN SIDE W BTYPE WEAK CON REG 0.01 385.9
FRIC MANNING 0.01
BREAK
NONHYDROSTATIC
$
DISCRET UPW MOM
DISCRET UPW UMOM H NONE
DISCRET UPW WMOM H NONE
$
TIMEI METH EXPL 0.1 0.5
$
$************ OUTPUT REQUESTS ************************
POINTS 'points' FILE 'reef-01.loc'
$
TABLE 'points' NOHEAD 'reef-385.9-0.01.tab' TSEC XP DEPTH BOTL WATL VEL OUTPUT 000000.000 1 SEC
$
COMPUTE 000000.000 0.005 SEC 040000.000
STOP
```

C

Complementary results

This appendix presents results complementary to the results and analysis showed in the main text. These results include most of the analysis carried out for the water depth d_r = 1.6 m.

C.1. Finding resonance with d_r = 1.6 m

In order to find resonance, SWASH runs (example in Appendix B) were carried out starting from the theoretical resonant modes T_0^* and T_1^* (Table 4.1), computed based on Equation 2.3, and continuing with neighboring periods. Through this methodology, the frequencies leading to the largest resonant amplifications were found. This maximum amplification was identified by comparing for every modeled period, the wave height at the beach toe ($H_{beachtoe}$), and the maximum run-up (R_{max}). These parameters, for d_r = 1.6 m, are shown in Figure C.1. $H_{beachtoe}$ was calculated with the zero down crossing technique, and R_{max} as the maximum value of the run-up series with the still water level as reference. For every period, both variables were computed with stationary water level time series. In this thesis, stationarity was considered when the slope of the signal envelope reaches values smaller 10^-6.

Both parameters, $H_{beachtoe}$ and R_{max}, show two amplification peaks in Figure C.1, which could be defined as a a bandwidth of resonant periods. Inside each of these resonant bandwidths, the wave height at the beach toe ($H_{beachtoe}$) and the maximum run-up (R_{max}) reach considerably higher values than the neighboring frequencies.

The model setup implied shallow water conditions for the simulated long waves since the beginning of the domain. Hence, waves are expected to shoal at a similar rate independently of the wave period and not to show different $H_{beachtoe}$ and R_{max} values for the same H_{off}. As the amplification peaks occur on periods neighboring the theoretical resonant periods (yellow dots in Figure 4.1), the amplification could be associated with resonant waves over the reef. Inside the two resonant bandwidths, the maximum $H_{beachtoe}$ and R_{max} amplification occurs for the period located in the middle of each peak. These two periods are defined as the modeled resonant periods T_0 and T_1 (orange dots from Figure C.1), and they represent the first two reef natural frequencies. These periods were found to be T_0 = 325 s and T_1 = s for d_r =1.6 m (Table 4.1).The first two modeled resonant modes (orange dots from Figure C.1) are both longer than the corresponding theoretical ones (yellow dots from Figure C.1).

As presented in Figure C.1, both the beach toe wave height and the maximum run-up are larger for the fundamental mode than for the first resonant mode. Moreover, periods in the vicinity of T_0, such as T = 450 s can reach larger $H_{beachtoe}$ and R_{max} than T_1. For the maximum run-up, no difference can be observed between the closest periods to T_0, which is probably due to the grid resolution (Δx = 10 cm). However, the run-up grid resolution is sufficiently fine, ΔR = 1.67 cm (Δx = 10 cm over a 1/6 beach slope), to indicate that the impact of resonance on run-up is similar for T_0 and periods close to it.

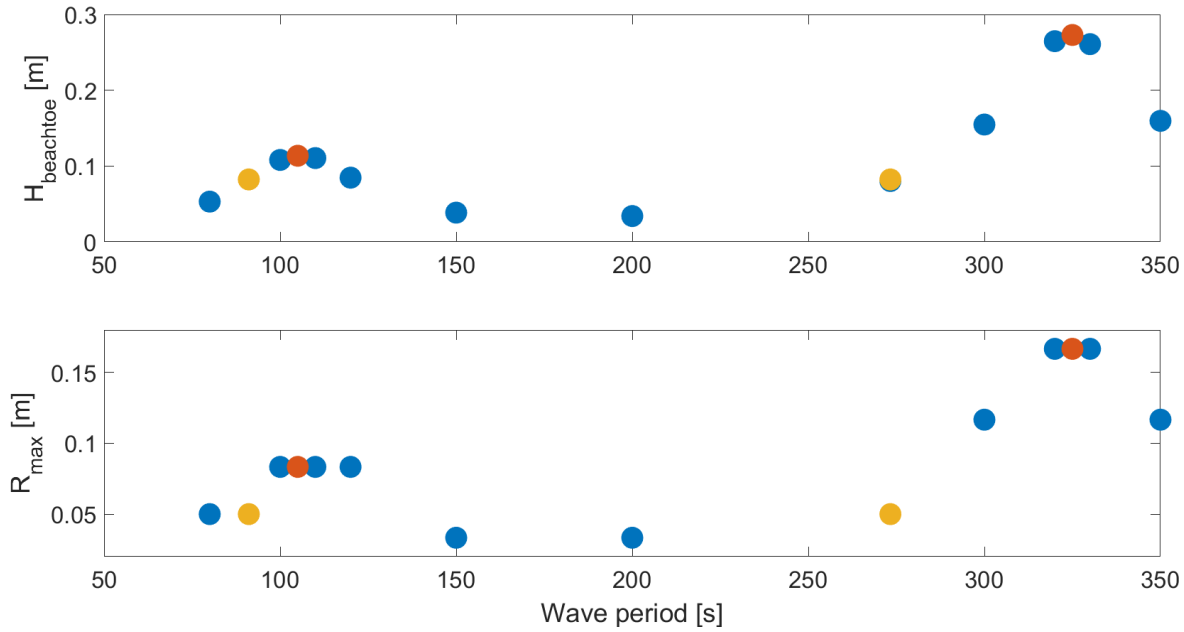

Figure C.1: Stationary beach toe wave height $H_{beachtoe}$ (top figure) and maximum run-up R_{max} (bottom figure) for different wave periods. The offshore wave height is H_{off} = 0.01 m and d_r = 1.6 m. The yellow (orange) dots indicate the first two theoretical (modeled) resonant modes (Table 4.1).

C.2. Varying wave height for resonant waves with d_r = 1.6 m

In Subsection C.1 the first two modeled resonant periods T_0 and T_1 were identified. These frequencies were found assuming an incident wave height H_{off} = 1 cm (Table 4.1). In this subsection, H_{off} is varied for these two resonant modes to analyze its impact on the resonant amplification. In order to compare results with same period but different H_{off}, the ratios A_H (Equation 4.1) and A_R (Equation 4.2) are used. Moreover H_{off} varies between 0.2 cm and 3 cm to keep the same ratio H_{off}/d_r than with d_r = 0.8 m.

Figure C.2 shows that smaller waves undergo stronger resonant amplification for both beach toe wave height and maximum run-up. This behavior was observed for the fundamental and first resonant periods. Thus, it could be said that higher resonant waves amplify less than smaller resonant waves. Furthermore, for the same H_{off}, the fundamental mode generates a larger amplification ratio than the first mode. This difference reduces with increasing offshore wave height.

The impact of resonance on wave height amplification can be analyzed by building the ratio $A_{Shoal} = H_{s-in}/H_{s-shoal}$, which normalizes the modeled incident significant wave height H_{s-in} with the expected significant wave height due to wave shoaling $H_{s-shoal}$. The incident wave component was calculated following Guza et al. (1985) (Equation 3.3). $H_{s-shoal}$ was computed for each wave period by taking the offshore incident wave height (H_{off}) and multiplying it with the corresponding cross-shore shoaling coefficient. This coefficient was calculated with linear wave theory, and due to shallow water conditions, it was the same for all the modeled periods. A A_{Shoal} value larger than one shows a wave height amplification stronger than the expected due to wave shoaling, which is likely due to resonant amplification.

The shoaling coefficient ($K_{sh} = (d_{offshore}/d_r)^(1/4)$ for shallow water, where d_{off} corresponds to the offshore water depth) is expected to decrease in 15% for the deeper water depth. However, by removing the shoaling influence, a comparison between the incident wave height resonant amplification of both d_r (Figure C.3) showed that smaller waves amplify more than higher waves, especially in the shallower water depth scenario (d_r = 0.8 m). Moreover, variations between waves with the smaller H_{off}/d_r relation and the larger H_{off}/d_r relation are stronger for T_0 than for T_1. Furthermore,a stronger resonant amplification for the deeper d_r is achieved with the fundamental period for the largest values of H_{off}/d_r relation, where d_r = 1.6 m can resonate between 5-9% more than d_r = 0.8 m. The first resonant period experienced stronger resonant amplifications for d_r = 0.8 m, in every modeled H_{off}/d_r scenario . Thus, within the modeled conditions results

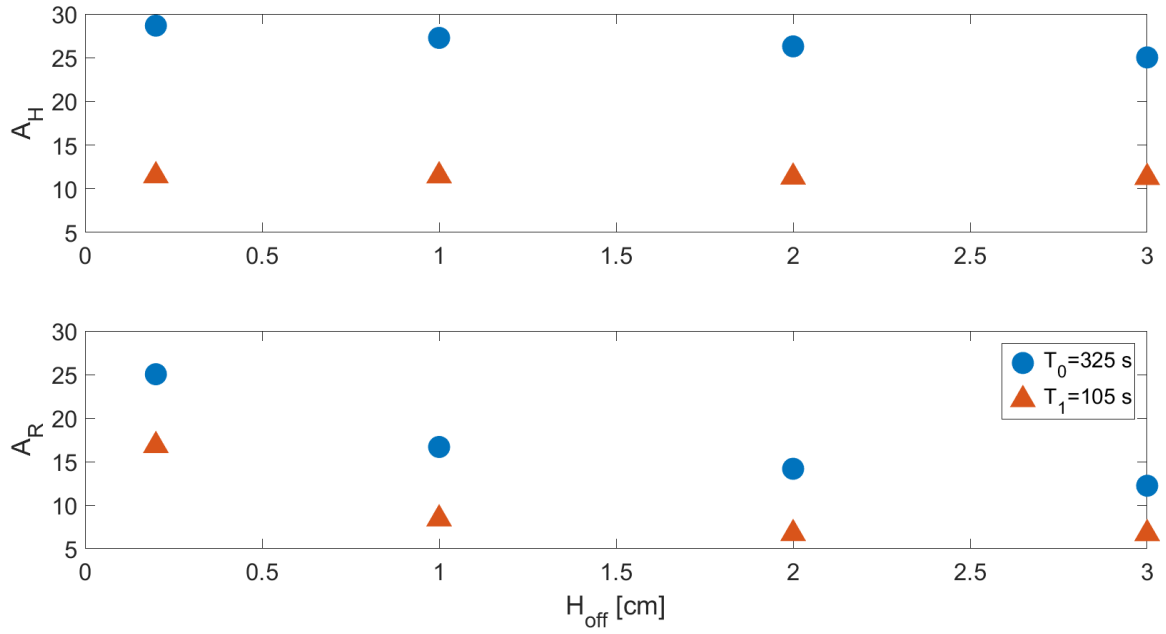

Figure C.2: Stationary beach toe wave height ratio A_H (upper figure) and maximum run-up ratio A_R (lower figure) for different incident offshore wave heights H_{off}, and for the first two resonant mode T_O and T_1 (d_r = 1.6 m).

suggest that the resonant waves amplify more for d_r = 0.8 m than for d_r = 1.6 m.

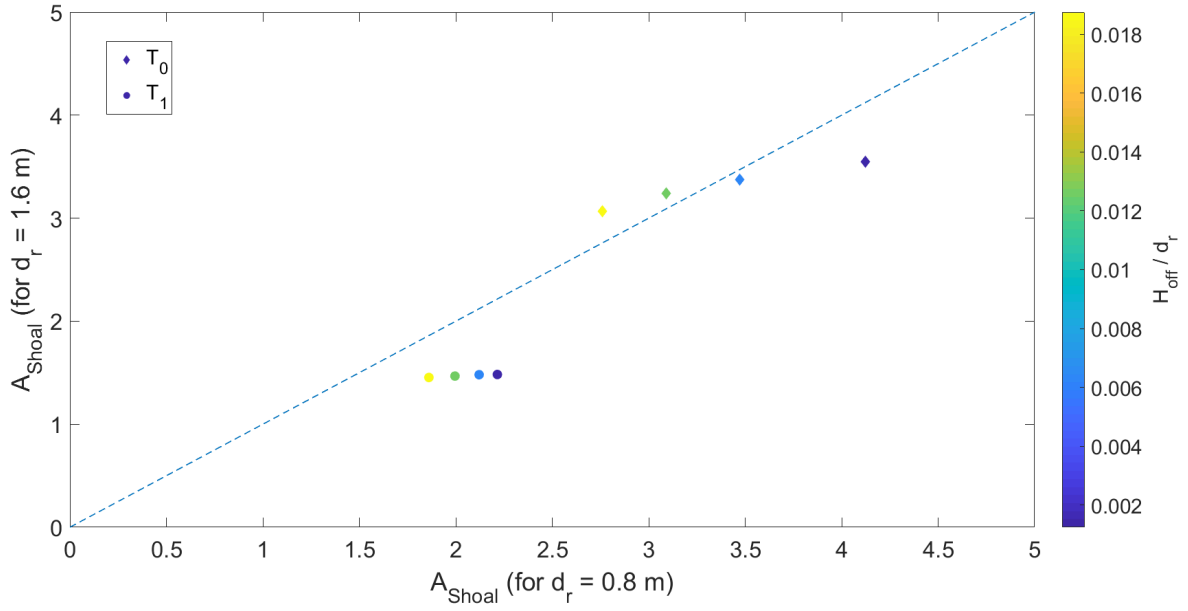

Figure C.3: Stationary A_{Shoal} ratio for different resonant modes, incident offshore wave heights and water depths. A_{Shoal} is compared between d_r = 0.8 m (x axis) and d_r = 1.6 m (y axis) for the same H_{off}/d_r relation.

C.3. Influence of wave period on resonant amplification for d_r = 1.6 m

Resonant waves behave like standing waves, with a node located close to the reef crest and an anti-node at the shoreline for the fundamental mode (top Figure C.4). The first resonant mode has two nodes and two anti-nodes (bottom Figure C.4). Theoretical resonant periods, T_0^* = 273.3 s s and T_1^* = 91.1 s, and non-resonant periods, such as T = 200 s and T = 80 s, also present a standing wave pattern, but with a node shorewards and further of the reef crest than resonant periods. Thus, the node location condition needed for resonance to occur is not fulfilled for non-resonant periods.

The cross-shore significant wave height (H_s) evolution, in shape and or magnitude, varies for waves with the same H_{off} and different periods. Nevertheless, the maximum H_s, with respect to neighboring periods, is achieved by the fundamental period T_0 (top Figure C.4) and by the first resonant period T_1 (bottom Figure C.4). This stronger resonant amplification for the first two resonant modes, in comparison with neighboring periods, can also be seen in Figure C.5), where the incident significant wave height over the reef flat is respectively 3.4 and 1.5 times larger than the expected wave height due to wave shoaling for T_0 and T_1.

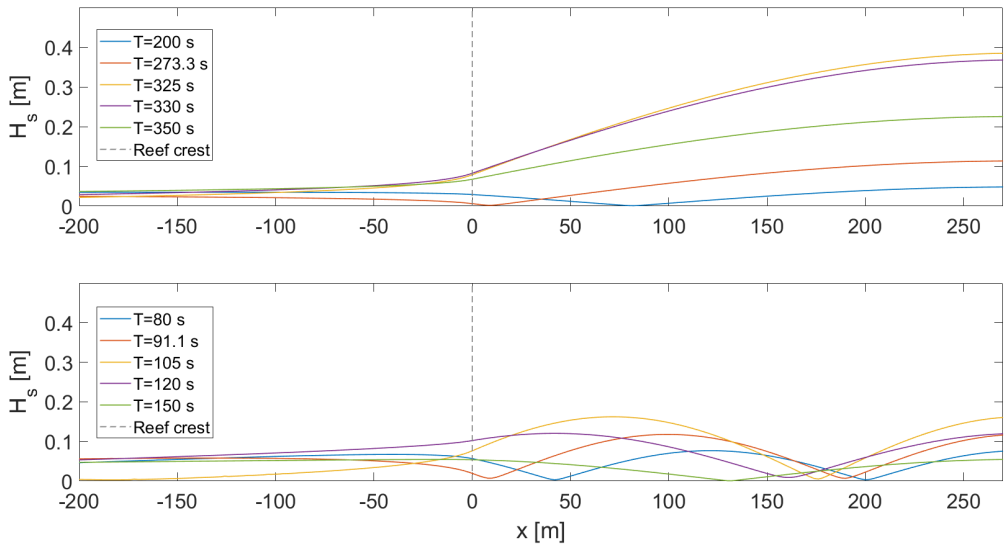

Figure C.4: Stationary significant wave height (H_s) cross-shore evolution for different wave periods (x = 0 m indicates the reef crest and x = 270 m, right end of the figure, the beach toe). Top figure shows periods in the range of the theoretical and modeled fundamental resonant period. Bottom figure shows periods in the range of the theoretical and modeled first resonant period. In this analysis H_{off} = 1 cm and d_r = 1.6 m.

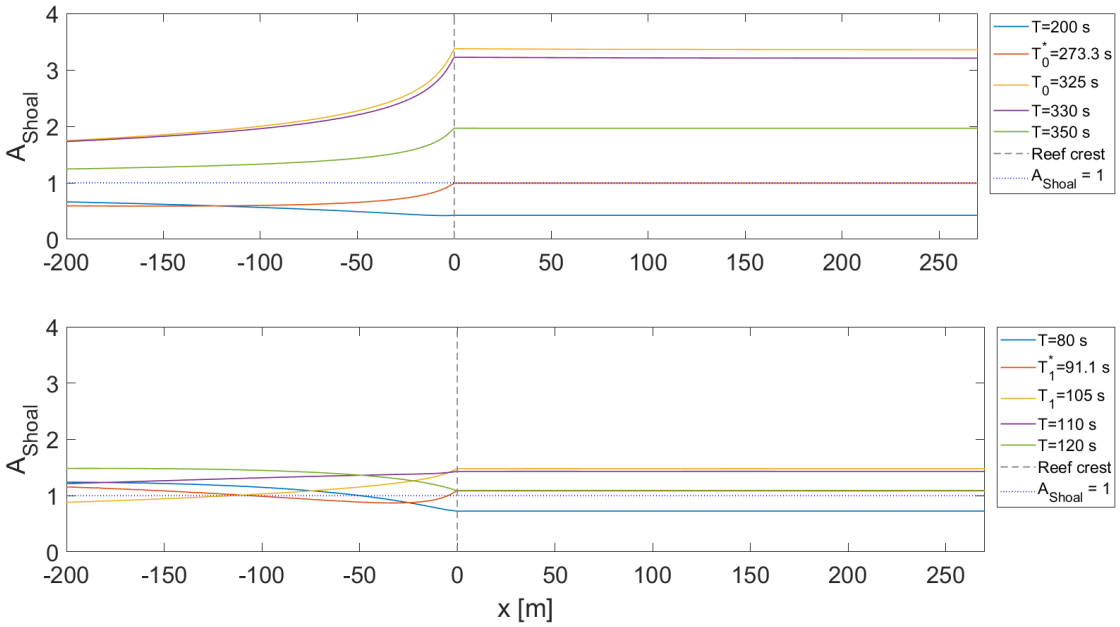

Figure C.5: Stationary normalized incident significant wave height ($A_{Shoal} = H_{s-in}/H_{s-shoal}$) cross-shore evolution for different wave periods (x = 0 m indicates the reef crest and x = 270 m, right end of the figure, the beach toe). H_{s-in} represents the modeled incident wave height and $H_{s-shoal}$ the significant wave height related with the linear wave theory shoaling coefficient. In this analysis H_{off} = 1 cm and d_r = 1.6 m.

C.4. Influence of wave height on resonant amplification for d_r = 1.6 m

Resonant larger wave heights amplify relatively more than smaller wave heights (Figure C.6), which is especially noticeable for the fundamental mode T_0 = 325 s. The first mode resonant amplification showed to be still stronger for smaller wave heights, but with fewer variations between different wave heights. Thus, it could be said that the first mode resonant amplification for d_r = 1.6 m is less dependent on the incident offshore wave height.

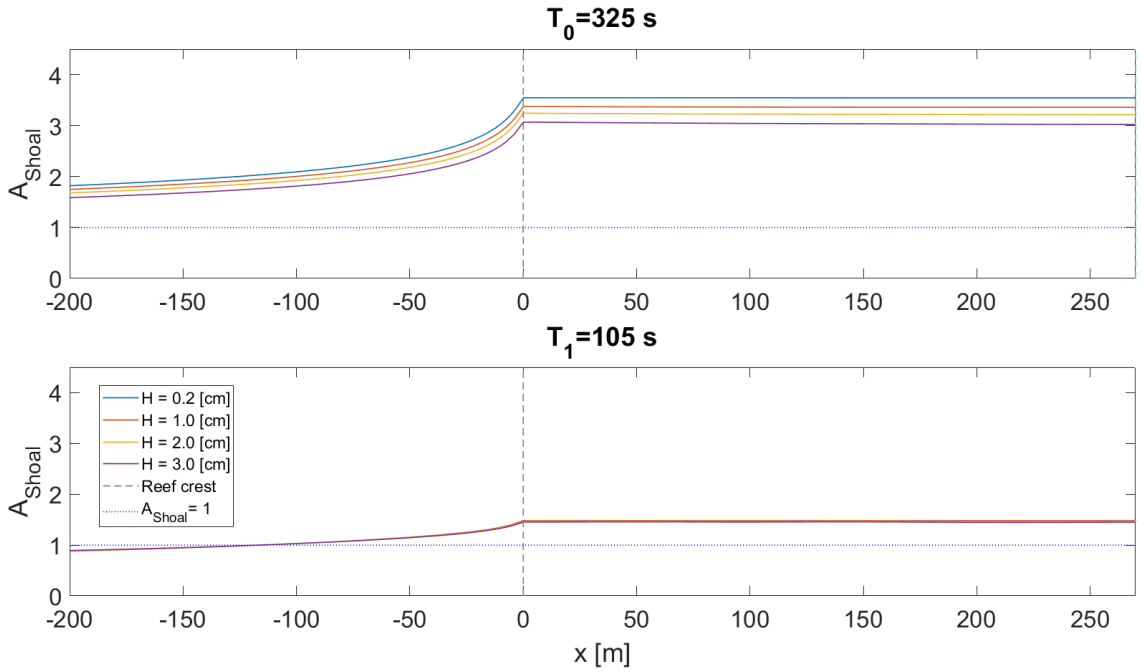

Figure C.6: Stationary normalized significant wave height ($A_{Shoal} = H_{s-in} / H_{s-shoal}$) cross-shore evolution for different offshore wave heights for the first two resonant modes T_0 and T_1 (x = 0 m indicates the reef crest and x = 270 m, right end of the figure, the beach toe). In this analysis d_r = 1.6 m.

C.5. Resonant build-up behavior for d_r = 1.6 m

The resonant build-up behavior for different wave heights was analyzed by studying the wave height time evolution at the beach toe. To quantify how many waves are needed to build-up resonance until the maximum amplitude, a ratio (A_{N°) was computed between the wave height of each wave reaching the beach toe, calculated through zero down crossing technique, and the maximum wave height by resonant period reached under stationary conditions ($A_{N^\circ} = H_{beachtoe} \ / \ H_{beachtoe-max}$). When this ratio A_{N° reaches the unity, it shows that the wave reached its maximum resonant wave height amplification and consequently an equilibrium state (dots Figure C.7).

Figure C.7 reflects how, for the fundamental mode, smaller wave heights need more waves to reach a maximum resonant amplification than higher waves. The first resonant mode needs five waves to reach a maximum resonant amplification independently of the H_{off}. Thus, the results suggest that the behavior of the first resonant period is less dependent on H_{off} than the fundamental mode.

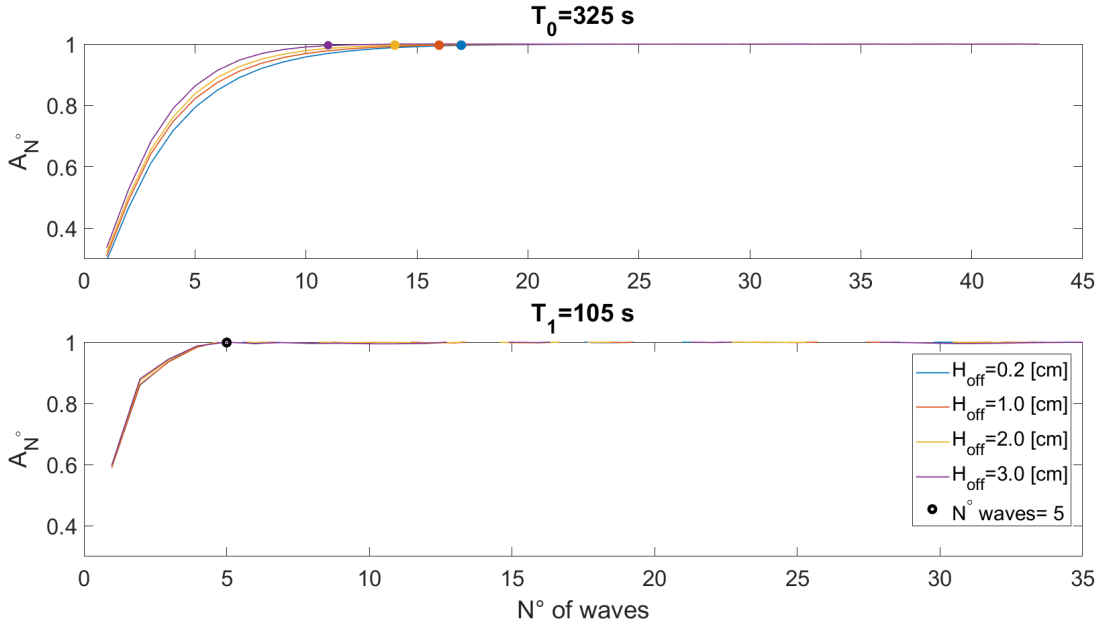

Figure C.7: Number of waves needed to build-up a maximum wave height resonant amplification at the beach toe for different H_{off} and resonant modes. Top figure shows A_{N° per individual wave height for the fundamental mode T_0. Bottom figure shows A_{N° per individual wave height for the first mode T_1. This analysis was done for d_r= 1.6 m

C.6. Influence of reef energy balance

The relation between the resonant amplification A_{Shoal} and the amount of energy trapped ($\Delta\mathcal{F}$) was studied at the reef crest for different wave periods and H_{off} = 1 cm (Figure C.8). A strong and positive correlation was found between A_{Shoal} and $\Delta\mathcal{F}$, with a correlation coefficient of R^2 = 0.9897, showing that larger $\Delta\mathcal{F}$ values lead to larger A_{Shoal} ratios.

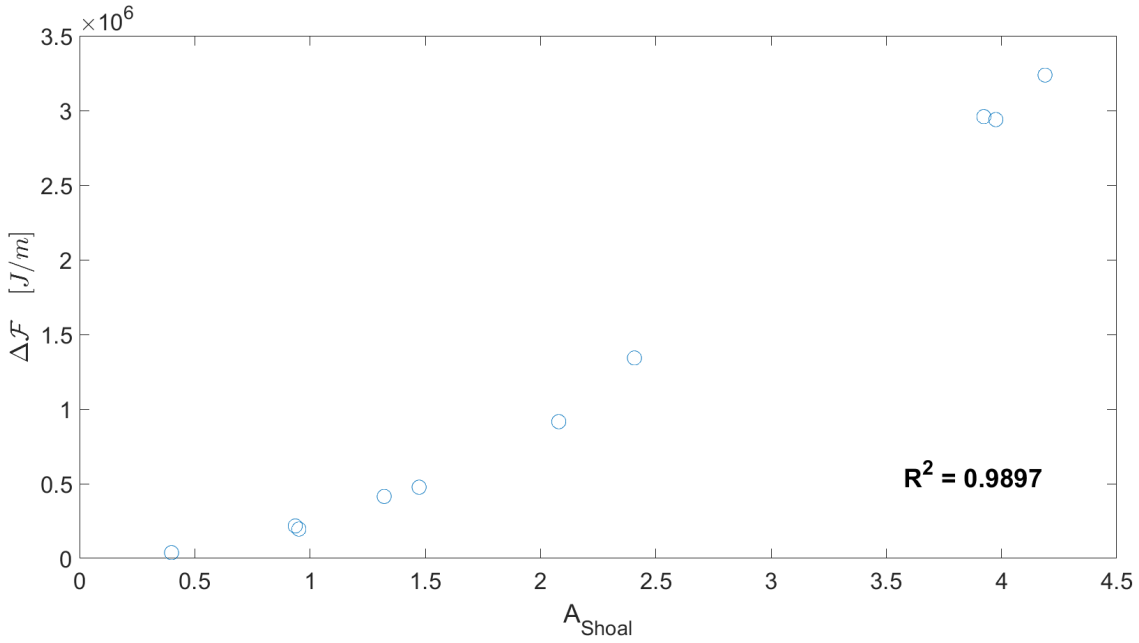

Figure C.8: Correlation between the amount of trapped wave energy ($\Delta\mathcal{F} = \int(F_{in} - F_{out})dt$) at the reef crest and the amplification ratio A_{Shoal} for different wave periods. The analysis was done with frictionless models, H_{off} = 1 cm, and d_r = 0.8 m.

Bibliography

Mark L Buckley, Ryan J Lowe, Jeff E Hansen, Ap R van Dongeren, and CD Storlazzi. Mechanisms of wave-driven water level variability on reef-fringed coastlines. *Journal of Geophysical Research: Oceans*, 123(5): 3811–3831, 2018.

Patricio A Catálan and Merrick C Haller. Remote sensing of breaking wave phase speeds with application to non-linear depth inversions. *Coastal Engineering*, 55(1):93–111, 2008.

Olivia M Cheriton, Curt D Storlazzi, and Kurt J Rosenberger. Observations of wave transformation over a fringing coral reef and the importance of low-frequency waves and offshore water levels to runup, overwash, and coastal flooding. *Journal of Geophysical Research: Oceans*, 121(5):3121–3140, 2016.

Jochem M. Dekkers. Undular bore development over coral reefs. an experimental study, 2018.

Zeki Demirbilek, Okey G Nwogu, and Donald L Ward. Laboratory study of wind effect on runup over fringing reefs. report 1. data report. Technical report, ENGINEER RESEARCH AND DEVELOPMENT CENTER CHAMPAIGN IL CONSTRUCTION . . . , 2007.

Irina Didenkulova, Efim Pelinovsky, Tarmo Soomere, and Narcisse Zahibo. Runup of nonlinear asymmetric waves on a plane beach. In *Tsunami and nonlinear waves*, pages 175–190. Springer, 2007.

Filippo Ferrario, Michael W Beck, Curt D Storlazzi, Fiorenza Micheli, Christine C Shepard, and Laura Airoldi. The effectiveness of coral reefs for coastal hazard risk reduction and adaptation. *Nature communications*, 5:3794, 2014.

Matthijs Gawehn, Ap van Dongeren, Arnold van Rooijen, Curt D Storlazzi, Olivia M Cheriton, and Ad Reniers. Identification and classification of very low frequency waves on a coral reef flat. *Journal of Geophysical Research: Oceans*, 121(10):7560–7574, 2016.

Robert T Guza and Anthony J Bowen. Resonant interactions for waves breaking on a beach. In *Coastal Engineering 1976*, pages 560–579. 1977.

Robert T Guza and Russ E Davis. Excitation of edge waves by waves incident on a beach. *Journal of Geophysical Research*, 79(9):1285–1291, 1974.

RT Guza and AJ Bowen. Finite amplitude edge waves. *J. Mar. Res*, 34(1):269–293, 1976.

RT Guza, EB Thornton, and RA Holman. Swash on steep and shallow beaches. In *Coastal Engineering 1984*, pages 708–723. 1985.

Thomas A Hardy and Ian R Young. Field study of wave attenuation on an offshore coral reef. *Journal of Geophysical Research: Oceans*, 101(C6):14311–14326, 1996.

Per A Madsen, OR Sørensen, and HA Schäffer. Surf zone dynamics simulated by a boussinesq type model. part i. model description and cross-shore motion of regular waves. *Coastal Engineering*, 32(4):255–287, 1997.

Gerd Masselink, Megan Tuck, Robert McCall, Ap van Dongeren, Murray Ford, and Paul Kench. Physical and numerical modelling of infragravity wave generation and transformation on coral reef platforms. *Journal of Geophysical Research: Oceans*, 2019.

Okey Nwogu and Zeki Demirbilek. Infragravity wave motions and runup over shallow fringing reefs. *Journal of waterway, port, coastal, and ocean engineering*, 136(6):295–305, 2010.

SG Pearson, CD Storlazzi, AR van Dongeren, MFS Tissier, and AJHM Reniers. A bayesian-based system to assess wave-driven flooding hazards on coral reef-lined coasts. *Journal of Geophysical Research: Oceans*, 122(12):10099–10117, 2017.

Stuart Grant Pearson. Predicting wave-induced flooding on low-lying tropical islands using a bayesian network, 2016.

A-C Péquignet, JM Becker, MA Merrifield, and SJ Boc. The dissipation of wind wave energy across a fringing reef at ipan, guam. *Coral Reefs*, 30(1):71–82, 2011.

A Christine N Péquignet, Janet M Becker, Mark A Merrifield, and Jérome Aucan. Forcing of resonant modes on a fringing reef during tropical storm man-yi. *Geophysical Research Letters*, 36(3), 2009.

Andrew William Mackay Pomeroy, Ap Van Dongeren, Ryan Lowe, Jaap van Thiel de Vries, and Jan Roelvink. Low frequency wave resonance in fringing reef environments. *Coastal Engineering Proceedings*, 1(33):25, 2012.

Ellen Quataert, Curt Storlazzi, Arnold Rooijen, Olivia Cheriton, and Ap Dongeren. The influence of coral reefs and climate change on wave-driven flooding of tropical coastlines. *Geophysical Research Letters*, 42(15): 6407–6415, 2015.

Alexander B Rabinovich. Seiches and harbor oscillations, chapter 9, handbook of coastal and ocean engineering, edited by: Kim, yc, 2009.

Volker Roeber and Jeremy D Bricker. Destructive tsunami-like wave generated by surf beat over a coral reef during typhoon haiyan. *Nature Communications*, 6:7854, 2015.

Floortje E. Roelvink. Coral restoration for coastal hazard risk reduction: The effect of coral restoration on wave transformation over various reef morphologies and the resulting runup, 2019.

A Sheremet, RT Guza, Steve Elgar, and THC Herbers. Observations of nearshore infragravity waves: Seaward and shoreward propagating components. *Journal of Geophysical Research: Oceans*, 107(C8):10–1, 2002.

Takenori Shimozono, Yoshimitsu Tajima, Andrew B Kennedy, Hisamichi Nobuoka, Jun Sasaki, and Shinji Sato. Combined infragravity wave and sea-swell runup over fringing reefs by super typhoon haiyan. *Journal of Geophysical Research: Oceans*, 120(6):4463–4486, 2015.

Pieter Smit, Tim Janssen, Leo Holthuijsen, and Jane Smith. Non-hydrostatic modeling of surf zone wave dynamics. *Coastal Engineering*, 83:36–48, 2014.

Curt D Storlazzi, Stephen B Gingerich, Ap van Dongeren, Olivia M Cheriton, Peter W Swarzenski, Ellen Quataert, Clifford I Voss, Donald W Field, Hariharasubramanian Annamalai, Greg A Piniak, et al. Most atolls will be uninhabitable by the mid-21st century because of sea-level rise exacerbating wave-driven flooding. *Science advances*, 4(4):eaap9741, 2018.

Graham Symonds, David A Huntley, and Anthony J Bowen. Two-dimensional surf beat: Long wave generation by a time-varying breakpoint. *Journal of Geophysical Research: Oceans*, 87(C1):492–498, 1982.

M Tissier, P Bonneton, R Almar, B Castelle, N Bonneton, and A Nahon. Field measurements and non-linear prediction of wave celerity in the surf zone. *European Journal of Mechanics-B/Fluids*, 30(6):635–641, 2011.

AP Van Dongeren, Ryan Lowe, Andrew Pomeroy, Duong Minh Trang, Dano Roelvink, Graham Symonds, and Roshanka Ranasinghe. Numerical modeling of low-frequency wave dynamics over a fringing coral reef. *Coastal Engineering*, 73:178–190, 2013.

Timo Veldt. The effect of wave directional spread on coastal hazards at coastlines fronted by a coral reef, 2019.

Colin D Woodroffe. Reef-island topography and the vulnerability of atolls to sea-level rise. *Global and Planetary Change*, 62(1-2):77–96, 2008.

Marcel Zijlema. Modelling wave transformation across a fringing reef using swash. *Coastal Engineering Proceedings*, 1(33):26, 2012.

Marcel Zijlema, Guus Stelling, and Pieter Smit. Swash: An operational public domain code for simulating wave fields and rapidly varied flows in coastal waters. *Coastal Engineering*, 58(10):992–1012, 2011.